LBL-20201
UC-13

Lawrence Berkeley Laboratory
UNIVERSITY OF CALIFORNIA

APPLIED SCIENCE DIVISION

FY 1985 Annual Report

CHEMICAL PROCESS RESEARCH AND DEVELOPMENT PROGRAM

August 1986

APPLIED SCIENCE DIVISION

Prepared for the U.S. Department of Energy under Contract DE-AC03-76SF00098

DISCLAIMER

LBL-20201

APPLIED SCIENCE DIVISION ANNUAL REPORT

CHEMICAL PROCESS RESEARCH & DEVELOPMENT PROGRAM

FY 1985

Elton J. Cairns
Program Leader
Head, Applied Science Division

and

Associate Director, LBL

Applied Science Division
Lawrence Berkeley Laboratory
University of California
Berkeley, California 94720

Prepared for the U.S. Department of Energy under Contract No. DE-AC03-76SF00098

CONTENTS

CHEMICAL PROCESS RESEARCH AND DEVELOPMENT PROGRAM STAFF

Elton Cairns, Program Leader
Harvey Blanch, Deputy Program Leader

Thomas Adler
Daniel Arenson
Jacki Ayer
Myra Baker
Vincent Battaglia
Wyn Bennett
Paul Berdahl
Douglas Bousfield
Garth Burns
Van Carey
Yew Khoy Chuah
Thomas Colson
Daniel Crean
Ayesha Daniels
Morton Denn
Minh Do
Jesse Dobson
Gregory Dow
Jean Dupon
Rachelle Edmond
Richard Fish
John Fitch
Gad Friedman*
Terry Grant
Edward Grens
Donald Hanson
Richard Hix
Arlon Hunt
Mark Isaacson
Alejandro Izquierdo
Rajiv Jain
Aviezer Kertes
Tae-Jeong Kim
C. Judson King
Kim Kinoshita
John Komlenic
Susan Lauer
Phillip Lessner
Scott Lynn
Giuseppe Marrucci
Frank McLarnon
Kenneth Miller
Riley Moore
Curtis Munson
Stewart Naftel
Joann Nakamura
Dan Neumann
Rollie Otto
Loree Pool
Mark Prausnitz
Robert Price
William Rixey
Ricardo San Martin
Michael Schuh
Aldo Sciamanna
Steve Sciamanna
John Senetar
Michael Smith
Craig Stevens
Kathy Striebel
Jon Sundquist
Janet Tamada
Raja Tannous
Rodney Thompson
Arne Thormodsen
Kent Udell†
Dale Wiley
Charles Wilke
Richard Williams
Jack Winnick*

*Participating guest.
†Earth Sciences Division.

CHEMICAL PROCESS RESEARCH AND DEVELOPMENT PROGRAM

INTRODUCTION

The Chemical Process Research and Development Program has five main projects applying chemistry and chemical engineering to problems in the production of new fuels, their environmental impact, and energy storage. These projects are:

(1) Energy-related organometallic chemistry
(2) Processing of effluent gases and liquids resulting from synthetic-fuel production, to provide acceptable waste or recycle streams
(3) Production of liquid fuels from biomass
(4) Electrochemical energy storage
(5) Thermal energy storage

Each of these projects focuses on transport-process principles, chemical kinetics, thermodynamics, separation processes, and organic and physical chemistry.

The first project involves studies on the use of heterogeneous metal cataysts to remove nitrogen from model coal compounds and to synthesize organometallic compounds that are models for metal mediated carbon-nitrogen bond cleavage reactions. Another aspect involves the use of alkali metals and crown ethers to study the cleavage reactions of compounds such as ethers and esters that have carbon-oxygen bonds and that model the linkages in coal. In addition, the isolation and molecular characterization of trace metal compounds in fossil materials is being studied, and innovative methods of removing these trace metal compounds are being developed. This includes the use of polymer-pendant catechol ligands to remove characterized arsenic, vanadium, and nickel compounds from solution and eventually from complex matrices.

The second project involves the development of novel and improved methods for processing synfuel condensate waters to make them suitable for recycle, thereby minimizing process-water requirements. The main emphasis is on physiochemical methods, particularly solvent extraction and stripping, to remove organics. Identification of the contaminating organics is difficult, but necessary to permit development of appropriate solvents for their removal. LBL studies have successfully examined simultaneous solvent extraction in removal of ammonia and acid gases by stripping.

The conversion of biomass to liquid fuels has been an area of considerable research and development within the Chemical Process Program over the past several years. The biological conversion of wood and agricultural residues to ethanol has been examined. An enzymatic hydrolysis of these cellulosic materials has been developed to yield monomeric hexose and pentose sugars. These can be subsequently fermented to produce ethanol. Various high-rate fermentation processes have been developed, and novel processes for ethanol recovery that are less energy intensive than conventional processes are being studied.

The electrochemical energy storage program provides research to develop advanced battery systems for electric vehicle and stationary energy storage applications. Topics include identification of new electrochemical couples for advanced batteries, improvements in battery components and materials, establishment of engineering principles applicable to electrochemical energy storage and conversion, and the development of metal/air cells and fuel cells for transportation. Major emphasis is on applied research that will lead to superior performance and lower life-cycle costs.

The fifth project is a series of research and development efforts in thermal energy storage. This project focuses on new and innovative approaches that have a broad range of applications and on the utilization of solar energy.

Synthesis of Dimetalla-azacyclobutenes via Reaction of Polynuclear Heteroaromatic Nitrogen Compounds with Triruthenium Dodecacarbonyl: Reactivity and Structural Elucidation*

Richard H. Fish, Tae-Jeong Kim, Joanne L. Stewart, John H. Bushweller, Robert K. Rosen, and Jean Wisner Dupon

We, as well as others, have found that a wide variety of transition metal compounds[1a-g] catalyze the homogeneous, regiospecific hydrogenation of polynuclear heteroaromatic nitrogen and sulfur compounds. The mechanism of hydrogenation of the nitrogen heterocyclic ring encompasses a prior coordination of the nitrogen compound to the catalytic metal center using either rhodium or ruthenium complexes.[1b,d] These rhodium and ruthenium complexes were either mono or tetranuclear, and thus it would be of interest to more clearly define the coordination of the polynuclear heteroaromatic nitrogen compounds to catalyst metal centers. We chose to study a ruthenium cluster, $Ru_3(CO)_{12}$, where several ruthenium metal centers were available for bonding to the nitrogen ring. Recently, several groups have reported on the reactions of polynuclear heteroaromatic nitrogen compounds with metal clusters. These include the studies of Yin and Deeming[2] with the triosmium cluster, $Os_3(CO)_{12}$, and polynuclear heteroaromatic compounds such as pyridines and quinolines. The resultant substituted clusters have been characterized spectroscopically as a triangle of osmium atoms with the nitrogen and the 2-carbon atoms. More recently, Laine *et al.*[3] substantiated the structure of both mono- and disubstituted quinoline-triosmium clusters by x-ray analysis and extended the examples to saturated nitrogen heterocyclic compounds such as piperidines and 1,2,3,4-tetrahydroquinoline. An excellent review of cyclometallated complexes with heterocyclic ligands, covering many other examples, was recently published by Constable.[4]

While our present study on the triruthenium cluster, $Ru_3(CO)_{12}$, reactions with quinoline, 1,2,3,4-tetrahydroquinoline, phenanthridine, and 9,10-dihydrophenanthridine was under way, Laine *et al.*[3] and Lewis *et al.*[5] both reported the quinoline-triruthenium complex. Our present results extend the knowledge in the synthesis and reactivity of dimetalla-azacyclobutene compounds of ruthenium with the above-mentioned nitrogen ligands. In addition, we also report the x-ray crystal structure of the phenanthridine-triruthenium derivative, $Ru_3(\mu\text{-}H)(\mu\text{-}C_{13}H_8N)(CO)_{10}$, **5**, as well as the reactions of the quinoline and phenanthridine-triruthenium complexes, **1**, **5**, with hydrogen gas, hydride reagents, and trifluoroacetic acid.

ACCOMPLISHMENTS DURING FY 1985

The Reaction of Quinoline with Triruthenium Dodecacarbonyl ($Ru_3(CO)_{12}$)

The reaction of triruthenium dodecacarbonyl ($Ru_3(CO)_{12}$) with excess quinoline only provided the mono-substituted four membered ring dimetalla-azacyclobutene complex, **1**, (Eq. 1).

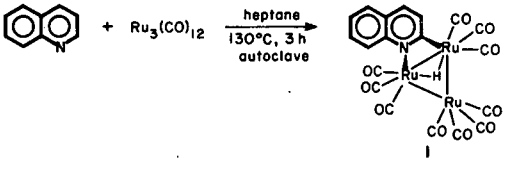

(1)

The reaction was performed in a sealed autoclave, in order to prevent decomposition from loss of CO, in heptane solvent at 130°C for 2–3 hours under argon. This result is in contrast to the recently reported result of Laine *et al.*[3] where they obtain the mono and bis quinoline-ruthenium complex in a 1:2 ratio under similar conditions, but using methylcyclohexane as the solvent. The orange to red complex has been formulated from its ^1H, ^{13}C, and IR spectra as well as by elemental and mass spectral analysis and was consistent with the reported parameters.[3] The 200 MHz ^1H NMR spectrum of **1** showed the

*This work was supported by the Assistant Secretary for Fossil Energy, Office of Technical Coordination of the U.S. Department of Energy through the Pittsburgh Energy Technology Center under Contract No. DE-AC03-76SF00098.

absence of the 2-carbon proton, which appears as a doublet of doublets in the spectrum of free quinoline at 8.81 ppm. The proton of the 8-carbon atom remains evident in the spectrum of the quinoline derivative. As expected, all of the signals due to the remaining aromatic protons shift upfield upon coordination to the triruthenium cluster. The bridging hydride signal of the quinoline complex, a singlet, occurs at −14.01 ppm. This value is normal for hydrides bridging one face of a triruthenium cluster, e.g., $Ru_3(\mu\text{-}H)(\mu\text{-}0{=}C(Me))(CO)_{10}$ at −13.88 ppm and $NEt_4Ru_3(\mu\text{-}H)(\mu\text{-}CO)(CO)_{10}$ at −12.76 ppm.

The Reaction of Complex 1 with Hydrogen Gas

In order to determine the utility of the dimetalla-azacyclobutenes as potential model intermediates in catalytic hydrogenation reactions, we studied complex **1** with hydrogen gas (500 psi at 85°C in toluene) and found that quinoline was formed along with $H_4Ru_4(CO)_{12}$ (Eq. 2).

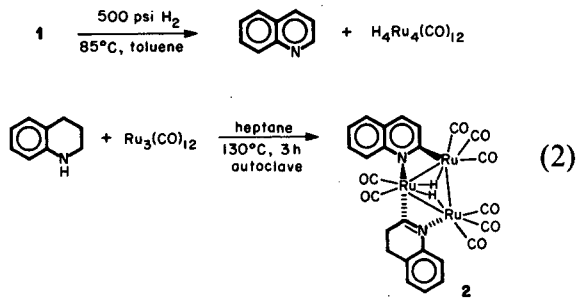

(2)

Apparently, the ligand is released as the cluster reacts with H_2 to form $H_4Ru_4(CO)_{12}$, a catalyst we studied in the hydrogenation of polynuclear heteroaromatic nitrogen compounds including quinoline.[1a,c]

The Reaction of Complex 1 with Hydride Reagents

Complex **1** was reacted with both $LiAlH_4$ and $LiBEt_3H$; however, **1** does appear to react even under forcing conditions, i.e., 60°C for several hrs in THF. Apparently, the carbon-nitrogen double bond is not reduced in the complex, while in the free ligand it is readily reduced. These results infer that the nitrogen ligand is not the site of reaction with hydride or H_2 reactants for reasons that are not clear as yet.

The Reaction of 1,2,3,4-Tetrahydroquinoline with $Ru_3(CO)_{12}$

$Ru_3(CO)_{12}$ reacts with 1,2,3,4-tetrahydroquinoline, under similar conditions as described above in the synthesis of the quinoline derivative, to form several different products. The major product was a novel triruthenium cluster[2] containing one molecule of quinoline and one of 3,4-dihydroquinoline. The proposed structure (Eq. 3) is based on ^1H, ^{13}C NMR, and infrared and mass spectroscopic evidence.

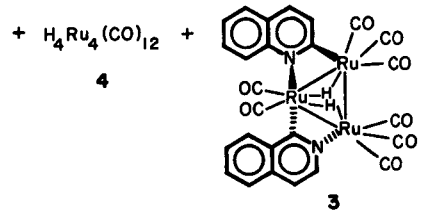

(3)

In the 200 MHz ^1H NMR spectrum, the region from 7.4 to 8.0 ppm strongly resembles that of the monosubstituted quinoline derivative, complex **1**. The 6.9 to 7.3 ppm region of the same NMR spectrum can therefore be interpreted as signals due to the 3,4-dihydroquinoline aromatic protons. Two triplets due to the methylene protons are located at 3.18 and 2.62 ppm. Signals for the two bridging hydrides were found at −14.01 and −17.64 ppm. The EIMS had prominent fragment ions at m/e 687 ($M^{+\cdot}-Ru$), 658 ($M^{+\cdot}-$quinoline), 657 ($M^{+\cdot}-$3,4-dihydroquinoline), and a sequence of ions that show a loss of CO from the m/e 658 and 657 ions to eventually give the ions at m/e 433 and 432 ($M^{+\cdot}-8CO$-quinoline or 3,4-dihydroquinoline). Additionally, the solution IR spectrum shows twelve CO stretches from 2104 to 1970 cm^{-1}. Complex **2** appears to disproportionate readily in cold (−30°C) acetone over several days to afford $H_4Ru_4(CO)_{12}$ and quinoline. The other minor products in the THQ reaction with $Ru_3(CO)_{12}$ are the bis quinoline complex, **3** (Ref. 3), and $H_4Ru_4(CO)_{12}$, **4**.

The Reaction of Phenanthridine and Dihydrophenanthridine $Ru_3(CO)_{12}$

The reaction of either phenanthridine or 9,10-dihydrophenanthridine with $Ru_3(CO)_{12}$ provided the same compound, **5** (Eq. 4). The NMR spectrum was conclusive for **5** with the absence of the C-9 proton at ~ 9.3 ppm, while the other signals were found between 8.4 and 7.61 ppm in the correct ratios and the bridging hydride at −13.73 ppm. The solution

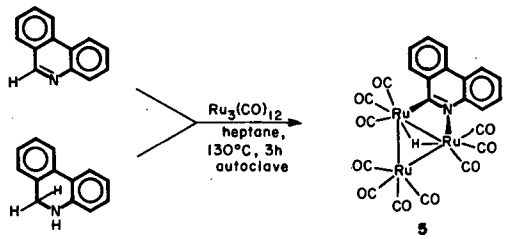

(4)

IR showed eight CO stretches between 2106 and 1991 cm, while the EIMS had prominent ions at m/e 706 ($M^{+\cdot}-2CO$), 594 ($M^{+\cdot}-6CO$), and 482 ($M^{+\cdot}-10CO$).

The X-Ray Crystal Structure of $Ru_3(\mu\text{-}H)(\mu\text{-}C_{13}H_8N)(CO)_{10}$, 5

In order to more clearly define the structure of **5** and compare the results to the recently reported x-ray crystal data of the quinoline-triosmium complex,[3] we obtained the single crystal x-ray analysis of **5**, as shown in Fig. 1. The molecule contains an isosceles triangle of ruthenium atoms with a hydride atom and the phenanthridine ligand bridging one edge. The Ru(2)-Ru(3) bond (2.866(1) Å), spanned by the two bridging ligands, is significantly longer than the other two Ru-Ru bonds (2.851(1), 2.844(1) Å). In fact, this bond is longer than the average Ru-Ru bond length in $Ru_3(CO)_{12}$ (2.854(7) Å).[6] It has been noted previously, by Churchill, DeBoer, and Rotella, that a single, unsupported hydride bridging two or more metal atoms causes a lengthening of the metal-metal bond.[7] However, those metal-metal bonds bridged by a hydride and another ligand generally shortened relative to the metal-metal bond in the unsubstituted compound. Bruce has suggested that the metal-metal bond length is a measure of the donor and pi-acceptor capacity of the bridging ligand.[8] For example, if the bridging group is a good pi-acceptor, a counterbalancing shortening effect on the metal-metal bond is noted: e.g., $HRu_3(CO)_{10}(COCH_3)$, 2.803 Å;[9] $HRu_3(CO)_{10}(C_2But)$, 2.792 Å.[10] In this case, because the bond is lengthened, we conclude that the phenanthridine is only weakly bound to the cluster and does not seem to be involved in any sort of delocalized backbonding with the metals.

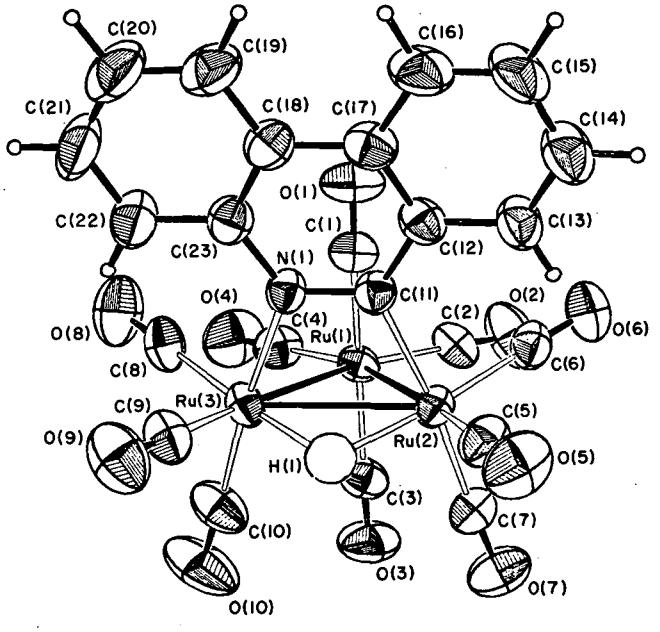

Figure 1. ORTEP diagram of $Ru_3(\mu\text{-}H)(N\text{-}C_{13}H_8N)(CO)_{10}$, **5** showing 50% probability ellipsoids. (XBL 859-4023)

The phenanthridine ligand is nearly planar; the maximum deviations being those of atom C(14), 0.024 Å and C(22) −0.043 Å, from the best weighted least-squares plane. The heterocyclic ligand is nearly perpendicular to the triangle of ruthenium atoms, with a dihedral angle of 106.7° between the two planes. The angle between the plane of metal atoms and the plane consisting of Ru(2), Ru(3), and H(1) is 32.5°. The dihedral angle between the plane of the phenanthridine ligand and the Ru(2)-Ru(3)-H(1) plane is 74.2°, probably due to the steric congestion of the carbonyl ligands and the bulk of the phenanthridine. In comparison with the bond parameters of free phenanthridine, the C(11)-N bond is lengthened by 0.021 Å (1.312 Å vs 1.291 Å).[11] This type of effect has been noted previously in the case of coordination of alkenes and alkynes to Pt(II) and Pt(0) where the C-C bond lengthens by 0.015−0.02 Å.[12] The length of the C(11)-N bond of this study is somewhat shorter than those reported for similar osmium clusters with coordinated heterocycles, e.g., $HOs_3(C_9H_6N)(CO)_{10}$, 1.329(35) Å; $H_2Os_3(C_9H_6N)_2(CO)_8$, 1.367−1.383 Å.[3] Other osmium clusters with bridging C-N bonds have bond lengths in the range 1.21 Å to 1.403 Å.[13] Nubel, Wilson, and Brown have reported a dinuclear bridged pyridine complex, $(\mu\text{-}H)Re_2(CO)_8(\mu\text{-}NC_5H_4)$, with a C-N bond length of 1.372(9)Å.[14]

The Reaction of Complex 5 with Hydrogen Gas

The hydrogenation of complex **5**, under longer reaction times than studied for complex **1**, again provided the ligand and $H_4Ru_4(CO)_{12}$ as well as some of the reduced ligand 9,10-dihydrophenanthridine. This result is not to surprising, since the hydride, **4**,

was active as a catalyst in the hydrogenation of polynuclear heteroaromatic nitrogen compounds.[1a,c]

PLANNED ACTIVITIES FOR FY 1986

We carried out several reactions with complexes **1** and **5** with the theme that they would allow insight in the interaction of reagents such H_2 gas, hydrides, and protons with the nitrogen ligands bonded to the triangle of ruthenium atoms. The hydrogenation reaction with complex **1** gave quinoline and $H_4Ru_4(CO)_{12}$ as the only products. The hydrogen attacks the ruthenium cluster liberating the nitrogen ligand, while a similar reaction occurs with complex **5**. The hydrogenation is complicated by the formation of $H_4Ru_4(CO)_{12}$, a catalyst we used to regioselectively reduce the nitrogen ring in compounds such as quinoline and phenanthridine.[1a] The next reaction studied was that of hydride reagents with **1**, **5**. To our disappointment, neither compound appeared to react with either $LiAlH_4$ or $LiBEt_3H$. These hydride results with complexes **1**, **5** are in contrast to similar reactions of these hydrides with the free ligands. For example, quinoline and phenanthridine react with $LiAlH_4$ to reduce the carbon-nitrogen double bond. This result clearly points out that the dimetalla-azacyclobutenes are not good models for the study of carbon-nitrogen bond cleavage reactions with nucleophilic reagents, since it appears that the ruthenium cluster rather than the complexed nitrogen ligand is the site of reaction. Thus, we will attempt to study the reactions of dimetalla-azacyclopropanes, and in FY 86 we will direct our attention to the synthesis of these compounds.

REFERENCES

1. (a) Fish, R.H., Thormodsen, A.D., and Cremer, G.A. (1982), *J. Amer. Chem. Soc. 104,* p. 5234.
   (b) Fish, R.H., Tan, J.L., and Thormodsen, A.D. (1984), *J. Org. Chem. 49,* p. 4500.
   (c) Fish, R.H. (1983), *Ann. N.Y. Acad. Sci. 415,* p. 292.
   (d) Fish, R.H., Tan, J.L., and Thormodsen, A.D. (1985), *Organometallics 4,* p. 1743.
   (e) Fish, R.H., Thormodsen, and A.D., Heinemann, H. (1985), *J. Mol. Catal. 31,* p. 191.
   (f) Lynch, *et al.* (1982), *J. Mol. Catal. 17,* p. 109.
   (g) Lynch, T.J., Banah, M., Kaesz, H.D., and Porter, C.R. (1984), *J. Org. Chem. 49,* p. 1266.
2. Yin, C.C. and Deeming, A.J. (1975), *J. Chem. Soc. Dalton Trans.,* p. 2091.
3. Eisenstadt, A., Giandomenico, C.M., Frederick, M.F., and Laine, R.M. (1985), *Organometallics 4,* p. 2033.
4. Constable, E.C. (1984), *Polyhedron 3,* p. 1037.
5. Foulds, G.A., Johnson, B.F., and Lewis, J. (1985), *J. Organomet. Chem. 294,* p. 123.
6. Churchill, M.R., Hollander, F.J., and Hutchinson, J.P. (1977), *Inorg. Chem. 16,* p. 2655.
7. Churchill, M.R., DeBoer, B.G., and Rotella, F.J. (1976), *Inorg. Chem. 15,* p. 1843.
8. Bruce, M.I. (1982), in *Comprehensive Organometallic Chemistry,* Chap. 32.5, G. Wilkinson, F.G.A. Stone, E.W. Abel, Eds. Pergamon Press, Oxford.
9. Johnson, B.F.G., *et al.* (1979), *J. Organomet. Chem. 173,* p. 187.
10. Catti, M., Gervasio, G., and Mason, S.A. (1977), *J. Chem. Soc. Dalton Trans.,* p. 2260.
11. Roychowdhury, P. (1973), *Acta Crystallogr., Sect. B. 29B,* p. 1362.
12. Ittel, S.D., and Ibers, J.A. (1976), *Adv. Organomet. Chem. 14,* p. 33.
13. (a) Adams, R.D., Dawoodi, Z., Foust, D.F., and Segmuller, B.E. (1983), *J. Amer. Chem. Soc. 105,* p. 831.
    (b) Adams, R.D. and Dawoodi, Z. (1981), *J. Amer. Chem. Soc. 103,* p. 6510.
    (c) Dawoodi, Z., Mays, M.J., and Raithby, P.R. (1981), *J. Organomet. Chem. 219,* p. 103.
14. Nubel, P.O., Wilson, S.R., and Brown, T.L. (1983), *Organometallics 2,* p. 515.

Hydrodenitrogenation Chemistry: Cleavage of Alkylcarbon-Nitrogen Bonds, Ammonia and Methane Formation in the HDN Reaction of 1,2,3,4-Tetrahydroquinoline with a Nickel Oxide Catalyst Supported on Silica*

R.H. Fish, A.D. Thormodsen, R.S. Moore, D.L. Perry, J. Michaels, and H. Heinemann

As serious attention has been given to the use of shale oil and coal derived liquids as refinery feedstocks, several unique processing problems associated with these materials have been identified. One of the most important is the removal of nitrogen, an undesired component in the final fuels to be made from these synthetic oils. While petroleum contains typically less than 0.3 wt% nitrogen, coal derived liquids can contain up to 0.8 wt%[1] and shale oils can have up to a 2.2 wt% nitrogen content.[2]

The existing process for nitrogen removal, hydrodenitrogenation (HDN), involves the catalytic reduction and cleavage of carbon-nitrogen bonds to remove the nitrogen as ammonia. The processing conditions are quite severe, 300 to 400°C, 1000 psi hydrogen. Typical catalysts are $NiMo/Al_2O_3$ or $CoMo/Al_2O_3$. Under these conditions any aromatic structures are fully reduced before nitrogen removal takes place. This represents an unnecessary and excessive consumption of hydrogen, especially in the case of highly aromatic coal derived liquids.

We have recently demonstrated the ability of transition metal complex catalysts to selectively reduce only the nitrogen containing ring in several polynuclear nitrogen-containing heteroaromatics.[3-7] We have now turned our attention to possible means of cleaving the reduced carbon-nitrogen bonds produced by these transition metal catalysts. By combining a selective reduction with a selective bond cleavage we hope to avoid the wasteful use of hydrogen in the conventional HDN process.

We have investigated the use of heterogeneous catalysts, and especially highly loaded supported nickel catalysts, for C-N bond cleavage in the selectively reduced nitrogen heterocycle, 1,2,3,4-tetrahydroquinoline. While the use of this particular reduced compound as an HDN substrate has not received a great deal of attention prior to this study, the fully saturated compound, decahydroquinoline, has been investigated by Katzer *et al.*,[8] who found that catalysts containing both metal and acidic support sites were apparently necessary to cause HDN. Our use of highly loaded supported catalysts was suggested in part by studies conducted by Maier *et al.*[9] In that study it was found that 40% Pt on SiO_2 was very effective as an HDN catalyst for quinoline under relatively mild conditions (1 atm. H_2, 150–200°C), and that the high metal loading was crucial in this application. In this report, we detail our accomplishments with highly loaded supported catalysts in the HDN reaction with nitrogen heterocyclic substrates.

ACCOMPLISHMENTS DURING FY 1985

Survey of Catalysts

A quick examination was made of the use of a variety of compounds as catalysts for C-N bond cleavage in 1,2,3,4-tetrahydroquinoline, as shown in Table 1. Various bulk metals and metal oxides, as well as a fluid catalytic cracking catalyst, were found to either be entirely inactive or to catalyze the undesired dehydrogenation of tetrahydroquinoline to quinoline.

Several supported nickel catalysts, and one supported rhodium catalyst, all showed the desired C-N bond cleavage activity to varying degrees. Two of these, a 30% Ni/SiO_2 catalyst prepared in our laboratory and a 50% Ni/SiO_2 catalyst supplied as a gift by United Catalyst (C46-7-03), showed the highest activity and were singled out for more detailed studies.

30% Ni Catalyst Results

Table 2 presents the results obtained with a 30% Ni on silica catalyst prepared in our laboratory. The compound, 1,2,3,4-tetrahydroquinoline, was converted at 320°C into a variety of products, the principal ones being quinoline (34.0%), aniline (27.5%), benzene (8.4%), 2-methylaniline (7.2%), and indole (6.5%). The aniline and benzene derivatives are formed via the cleavage of C-N bonds in 1,2,3,4-tetrahydroquinoline and are thus the desired products. Quinoline, formed by dehydrogenation of 1,2,3,4-tetrahydroquinoline, and the side-product indole, are unwanted. At a higher temperature, 360°C, the relative amounts of quinoline and ben-

*This work was supported by the Assistant Secretary for Fossil Energy, Office of Technical Coordination of the U.S. Department of Energy through the Pittsburgh Energy Technology Center under Contract No. DE-AC03-76SF00098.

Table 1. Summary of heterogeneous catalyst results using 1,2,3,4-tetrahydroquinoline as substrate.[a]

Catalyst	Results
Bulk nickel (powder)	Inactive
Bulk manganese (powder)	Inactive
Cr_2O_3 (powder)	Inactive
ZrO_2 (powder)	Inactive
Zeolite (fluid cat. cracking)	Inactive
Bulk copper (granules)	Dehydrogenation[b]
8% Cu, 8% Ni/SiO_2[d]	Dehydrogenation
5% Ni/SiO_2[d]	Dehydrogenation, C-N cleavage[c]
5% Rh/SiO_2[e]	Dehydrogenation, C-N cleavage
30% Ni/SiO_2[d]	C-N cleavage, dehydrogenation
50% Ni/SiO_2[f]	C-N cleavage, dehydrogenation
60% Ni/Al_2O_3[f]	Dehydrogenation, C-N cleavage

[a]Conditions: Approximately 1 cc each catalyst, T = 250°C–350°C, 0.14 cc/hr 1,2,3,4-tetrahydroquinoline, 30 cc/min H_2 at 1 atm. Analysis by capillary gas chromatography.

[b]Formation of quinoline

[c]Formation of alkyl anilines and alkyl benzenes.

[d]Prepared as described in experimental section.

[e]Donated by Dr. A. Bell's research group (UC Berkeley).

[f]Donated by United Catalyst.

zene increased, while the relative amount of aniline derivatives in the product mixture decreased. Importantly, little reduction of the 5,6,7,8 ring of 1,2,3,4-tetrahydroquinoline was observed, indicating the higher selectivity of this system towards bond cleavage as compared to hydrogenation.

The compounds 2-propylaniline and propylbenzene, both plausible intermediates in the HDN of 1,2,3,4-tetrahydroquinoline, were also investigated as substrates. In addition to the expected products of C-N bond cleavage (benzenes) and propyl chain cleavage (anilines), both 1,2,3,4-tetrahydroquinoline and 2-methylindole were formed with 2-propylaniline. Apparently, a catalyzed or free radical mechanism may lead to ring closure of 2-propylaniline to form these two latter products. Since ring opening of 1,2,3,4-tetrahydroquinoline to form 2-propylaniline may be the first step in the HDN of 1,2,3,4-tetrahydroquinoline, the potential reversibility of this ring opening is of great interest.

When propylbenzene was used as a substrate, no condensible products were formed, except for a trace of benzene and toluene. The very high activity of the catalyst towards this material is probably a result of the lack of any basic nitrogen compounds (quinoline or aniline derivatives) in this reaction. These materials are known to be strong catalyst poisons, and in this particular case when they are present they apparently moderate the activity of the catalyst, preventing it from completely reducing and/or cleaving substrates. In the absence of these nitrogen bases, complete hydrogenolysis of the substrate (to methane, see below) or conversion to coke must occur, resulting in no condensible products being observed.

Some of the gas generated during the HDN of 1,2,3,4-tetrahydroquinoline at 320°C was trapped in a water trough (eliminating ammonia) and analyzed by gas chromatography. It was found to be almost entirely methane (99.5%), with traces of ethane, propane, and butane. Much of this methane is presumably formed by the partial or complete hydrogenolysis of only the saturated 1,2,3,4 ring in tetrahydroquinoline. Some may as well result from the entire hydrogenolysis of 1,2,3,4-tetrahydroquinoline, the results of a mass balance with the 50% Ni catalyst (see below) indicate that this total hydrogenolysis may be an important reaction.

50% Ni Catalyst Results

The results for the 50% nickel catalyst, shown in Table 3, are quite similar to those discussed above. The primary difference between the two catalysts is the degree of activity. At temperatures 100°C lower, and with one third as much catalyst, the 50% Ni material exhibited the same overall conversion of 1,2,3,4-tetrahydroquinoline as the 30% catalyst. Additionally, the 50% Ni catalyst was more efficient in catalyzing the C-N bond cleavage reaction, relative to dehydrogenation to form quinoline.

The major products formed from the HDN of 1,2,3,4-tetrahydroquinoline using this 50% Ni catalyst at 250°C were 2-methylaniline (14.3%), quinoline (14.3%), 5,6,7,8-THQ (1.41%), aniline (0.4%), benzene (9.2%), and 2-ethylaniline (8.6%). Relative to the 30% nickel catalyst more aniline and benzene derivatives and less quinoline are produced by this catalyst. Combined with the higher overall activity of this catalyst, this result indicates that the 50% Ni material is more suitable than the 30% Ni material for the HDN of 1,2,3,4-tetrahydroquinoline. This situation is improved further at the slightly higher reaction temperature of 260°C, with the relative amounts of benzenes and anilines increasing, and the amount of quinoline and 5,6,7,8-tetrahydroquinoline decreasing.

Table 2. Results using 30% Ni/SiO_2 catalyst.[a]

Substrate: Temperature: Products (mol%)[b]	1,2,3,4-THQ (320°C)	1,2,3,4-THQ (360°C)	2-Propylaniline (320°C)	Propylbenzene (320°C)
Benzene	8.4%	12.2%	19.3%	trace
Toluene	1.4%	1.8%	2.9%	trace
Ethylbenzene	trace	trace	trace	0.0%
Propylbenzene	trace	trace	5.3%	0.0%
Aniline	27.5%	18.9%	9.3%	0.0%
2-Methylaniline	7.2%	2.7%	5.7%	0.0%
2-Ethylaniline	trace	trace	trace	0.0%
2-Propylaniline	trace	trace	37.0%	0.0%
Quinoline	34.0%	44.5%	0.0%	0.0%
5,6,7,8-THQ	trace	trace	0.0%	0.0%
1,2,3,4-THQ	5.3%	3.5%	5.8%	0.0%
Indole	6.5%	9.1%	trace	0.0%
2-Methylindole	2.1%	0.9%	2.3%	0.0%
Unidentified	7.6%	6.4%	12.4%	0.0%

[a]Conditions: 0.86 g catalyst, 0.14 cc/hr substrate, 30 cc/min H_2 at 1 atm. Products identified by GCMS and verified by comparison with standards (except 2-methylaniline and 2-ethylaniline).

[b]Not included in the product normalization is the amount of gaseous products obtained. For a 340°C 1,2,3,4-tetrahydroquinoline run the hydrocarbon gases produced were analyzed by gas chromatography to give 99.5% CH_4, e.g., 0.1% C_2H_6, 0.4% C_3H_8, e.g., 0.02% C_4H_{10}. Ammonia was also produced.

We observed less cyclization when 2-propylaniline was reacted over the 50% Ni catalyst, as compared to the 30% Ni case. Only traces of 1,2,3,4-tetrahydroquinoline and indoles were produced. The primary products were benzene and propylbenzene, with surprisingly small amounts of toluene and ethylbenzene being formed. Aniline derivatives were also formed in this reaction. As with the 30% Ni catalyst, reaction of propylbenzene over the 50% Ni catalyst provided only trace amounts of benzene and toluene as products. In the absence of the moderating effects of nitrogen bases, the catalyst seems to be extremely active towards total hydrogenolysis.

An analysis of the gas formed during the HDN of tetrahydroquinoline with the 50% Ni catalyst showed that it was almost entirely methane (99.8%). Other gases, if present, were below the detection limit of the gas chromatograph. A mass balance on the liquid products revealed that about 70% of the 1,2,3,4-tetrahydroquinoline was converted to the identified products in the tables, and about 10% of the reactant is converted to unidentified liquids. The 20% that remains cannot be accounted for in the condensible products and presumably is converted to methane (although some may be converted to coke as well). Our apparatus does not trap all of the gases formed, thus a mass balance on the non-condensible products could not be performed.

Additional experiments were done with the 50% nickel on silica catalyst in which quinoline was used as the substrate. The results of these runs, at three different temperatures, are shown in Table 4. In this case the nitrogen-containing ring in quinoline must

Table 3. Results using 50% Ni/SiO_2 catalyst (United Catalyst C46-7-03).[a]

Substrate: Temperature: Products (mol%)[b]	1,2,3,4-THQ (250°C)	1,2,3,4-THQ (260°C)	2-Propylaniline (250°C)	Propylbenzene (250°C)
Benzene	9.2%	15.8%	29.9%	trace
Toluene	1.8%	2.8%	4.3%	trace
Ethylbenzene	trace	trace	trace	0.0%
Propylbenzene	trace	trace	20.8%	0.0%
Aniline	9.4%	16.7%	6.0%	0.0%
2-Methylaniline	14.3%	20.0%	5.4%	0.0%
2-Ethylaniline	8.6%	8.6%	1.4%	0.0%
2-Propylaniline	2.0%	1.6%	21.5%	0.0%
Quinoline	14.3%	9.8%	0.0%	0.0%
5,6,7,8-THQ	14.1%	5.9%	0.0%	0.0%
1,2,3,4-THQ	4.7%	1.6%	trace	0.0%
Indole	2.7%	3.1%	trace	0.0%
2-Methylindole	5.0%	4.5%	trace	0.0%
Unidentified	13.9%	9.6%	10.7%	0.0%

[a]Conditions: 0.26 g catalyst, 0.14 cc/hr substrate, 30 cc/min H_2 at 1 atm. Products identified by GCMS and verified by comparison with standards (except 2-methylaniline and 2-ethylaniline).

[b]Not included in the product normalization is the amount of gaseous products obtained. For the 1,2,3,4-tetrahydroquinoline runs the hydrocarbon gases produced were analyzed by gas chromatography to give at least 99.8% CH_4; other hydrocarbons (if present) were below the detection threshold of the instrument. Ammonia was also produced.

presumably be reduced prior to any cleavage of C-N bonds. At the highest temperature, 280°C, the overall HDN of quinoline was more efficient than that of 1,2,3,4-tetrahydroquinoline, while at 250°C less HDN of quinoline took place. However, for all three of these runs mass balances reveal that a considerable amount of the quinoline is converted to noncondensible products, ranging from approximately 50% at 250°C to 70% at 280°C. This is clearly not a desired reaction, and in this regard the results with 1,2,3,4-tetrahydroquinoline, in which only 20% was "lost" in this way, are superior to those with quinoline.

General Hydrodenitrogenation Scheme

Figure 1 is a schematic representation of the kinds of reactions we propose to account for the products observed in the various reactions described above. The compound, 1,2,3,4-tetrahydroquinoline, may either be ring opened to form 2-propylaniline or dehydrogenated/hydrogenated to form quinoline and 5,6,7,8-tetrahydroquinoline.

The compound, 2-propylaniline, may undergo cyclizations to form indoles, or reform 1,2,3,4-tetrahydroquinoline. Instead, propylaniline can have the nitrogen atom cleaved to form various derivatives of benzene, or have carbon atoms hydrogenolyzed on the propyl group to form other anilines. These anilines may in turn be converted to benzene derivatives.

The path that leads from quinoline to 1,2,3,4-tetrahydroquinoline to propylaniline and finally to

Table 4. Results using 50% Ni/SiO_2 catalyst.[a]

Substrate Temperature Products (mol%)	Quinoline (250°C)	Quinoline (260°C)	Quinoline (280°C)
Benzene	0.6	3.2	21
Toluene	0.7	1.6	5
Ethylbenzene	trace	trace	trace
Propylbenzene	0.1	0.24	trace
Aniline	6	12	20
2-Methylaniline	12	16	15
2-Ethylaniline	8	6.5	2.7
2-Propylaniline	2	1.2	trace
Quinoline	26	26	19
5,6,7,8-THQ	15	7	1.2
1,2,3,4-THQ	9	5	1
Indole	1.5	2	1.6
2-Methylindole	5	5	3
Unidentified	15	14	10.5

[a]Conditions: 0.26 g catalyst, 0.14 cc/hr substrate, 30 cc/min H_2 at 1 atm. Products identified by GCMS and verified by comparison with standards (except 2-methylaniline and 2-ethylaniline).

the benzenes and anilines is the desired course of hydrodenitrogenation. The other paths shown, and the partial reversibility of the above path, are reactions that we wish to avoid. By understanding the nature of these catalysts, we will hopefully be able to control these different types of reactions in a more reasonable fashion.

Characterization of Catalysts

Figure 2 shows a transmission electron micrograph of a used sample of the 30% Ni catalyst. A bimodal distribution of nickel crystallites is apparent here, with many small crystallites in the 200 angstrom size range and a few larger crystals in the 2000 angstrom range. Although not visible in this picture, coke deposits were also found on the surface. A chemical analysis of this same catalyst sample showed a 0.13% carbon content.

A preliminary x-ray photoelectron spectroscopy (XPS) study of this same catalyst has revealed the presence of primarily metallic nickel on the surface, with small amounts of nickel oxide.

An XPS study of the 50% nickel catalyst (Fig. 3) shows a very different spectrum than that found with the 30% nickel catalyst. This spectrum, showing here the nickel $2P_{3/2,1/2}$ lines, indicated that the nickel is present as a tertiary oxide, with nickel ions

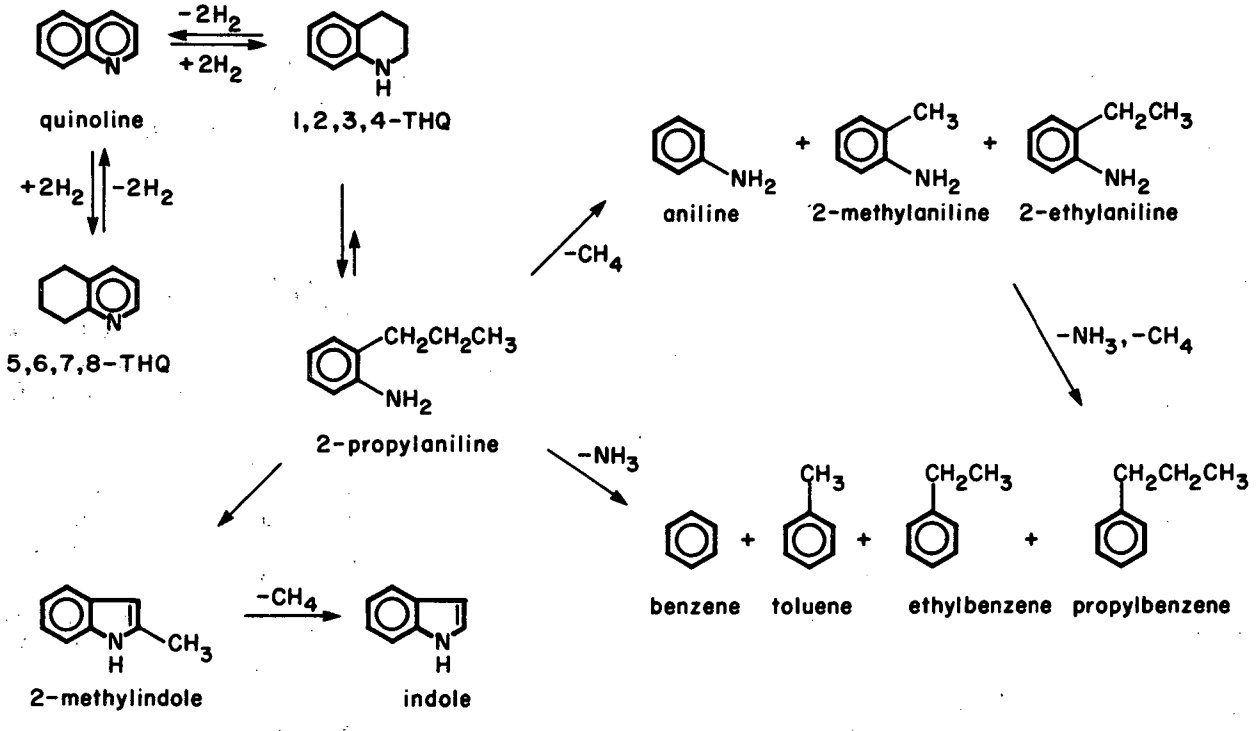

Figure 1. Proposed reaction network for HDN using supported nickel catalyst. (XBL 862-563)

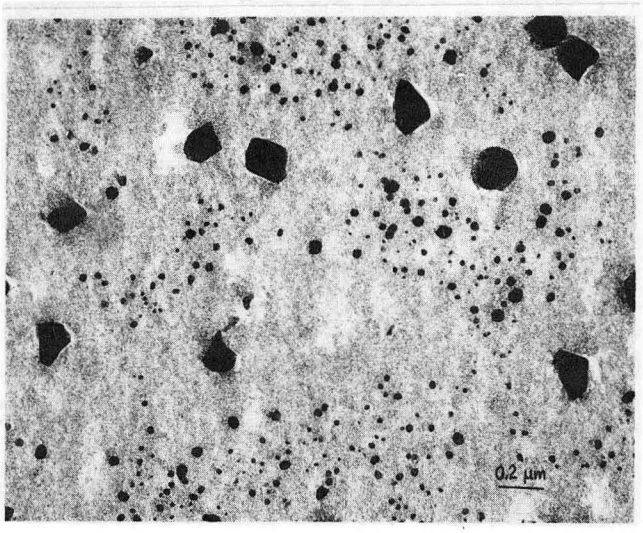

Figure 2. Transmission electron micrograph of 30% Ni/SO_2 catalyst. (XBB 8511-9385)

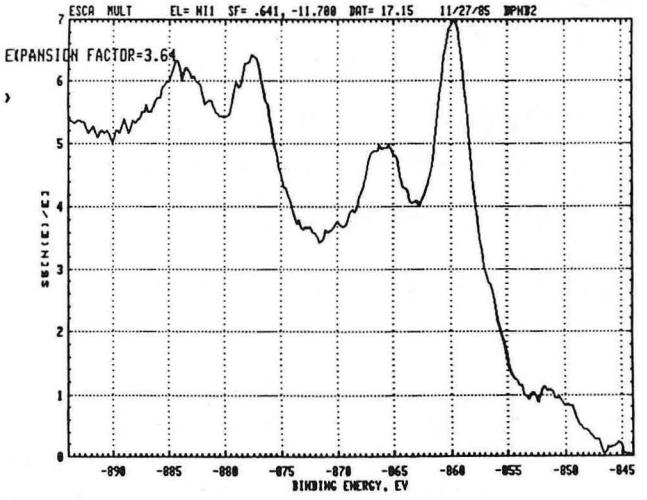

Figure 3. XPS spectrum of Ni $2P_{3/2,\ 1/2}$ lines in used 50% Ni/SiO_2 catalyst. (XBL 862-564)

and support ions in a mixture. Aluminum was also found to be present in this catalyst, allowing for the possibility of nickel aluminate, as well as nickel silicate.

The differences we see between the two nickel catalysts may thus in part be explained by the difference in the state of the nickel on the surface of the catalyst. We are planning further morphological examination of both nickel catalysts in an effort to resolve this issue.

PLANNED ACTIVITIES FOR FY 1986

We plan to use an advanced XYTEL unit to better evaluate the catalysts found to be effective in the studies described above. This device allows for semi-continuous monitoring of the products of reaction by on-line gas chromatography, and should provide accurate kinetic data.

We also plan to probe the structure of the various catalysts using several techniques, including scanning and transmission electron microscopy, x-ray photoelectron spectroscopy, and various surface absorption techniques. By gaining an understanding of the morphological features of the catalysts in relation to their chemical activity, we hope to identify those catalyst features that are essential for the desired C-N bond cleavage activity.

REFERENCES

1. Gorbaty, M.L. and Harney, B.M. (1979), "Refining of Synthetic Crudes," *Advances in Chemistry Series 179,* ACS, Washington, D.C., Chap. 1.
2. Ibid., Chap. 3.
3. Fish, R.H., Thormodsen, A.D., and Cremer, G.A. (1982), *J. Amer. Chem. Soc. 104,* p. 5234.
4. Fish, R.H., Tan, J.L., and Thormodsen, A.D. (1984), *J. Org. Chem. 49,* p. 4500.
5. Fish, R.H. (1983), *Ann. N.Y. Acad. Sci. 415,* p. 292.
6. Fish, R.H., Thormodsen, A.D., and Heinemann, H. (1985), *J. Mol. Catal. 31,* p. 191.
7. Fish, R.H., Tan, J.L., and Thormodsen, A.D. (1985), *Organometallics 4,* p. 1743.
8. Katzer, J.R., Stiles, A.B., and Kwart, H. (1980), *Development of Unique Catalysts for Hydrodenitrogenation of Coal Derived Liquids,* DOE/ET/03297-1.
9. Maier, W.F. and Guttieri, M.J. (1984), *J. Org. Chem. 49,* p. 2875.

Polymer Pendant Ligand Chemistry 2: Reactions of Vanadyl and Nickel Acetylacetonates with Catechol Ligands Bonded to Polystyrene-Divinylbenzene Resins*

R.H. Fish, A. Izquierdo, Gad Friedman, and Robert Price

The use of polymer-supported pendant ligands for metal ion removal is a well-developed field.[1a,b] We have recently reported on the use of polymer-supported catechol ligands for removal of organoarsonic acids and arsenate from solution.[2] We have also discovered a facile regeneration reaction that removes the arsenic compounds, while providing the catechol ligand site for reuse.[2]

In this report, we will describe our results on the reactions of vanadyl and nickel acetylacetonates with the catecholated resins (20% cross-linked) to provide evidence for a ligand exchange, i.e., formation of vanadyl and nickel catechol compounds on the resin with the release of acetylacetone.

ACCOMPLISHMENTS DURING FY 1985

The reaction of the 20% cross-linked catecholated resins with vanadyl acetylacetonate was studied. Table 1 shows the results of this type of ligand exchange reaction with evidence that removal of vanadyl ion is rapid and is enhanced by both a temperature increase and by the addition of a bidentate ligand, 2,2′-bipyridine. The rates of removal can be seen in Fig. 1 and show the rapid uptake that takes place (less than 1 hour), as well as the effect of temperature on the concentration of vanadyl ion removed.

In another experiment, we reacted nickel acetylacetonate with the catecholated resin at 64°C in meOH (1:1 ratio Ni/catechol) and found a 32% removal of nickel from solution.

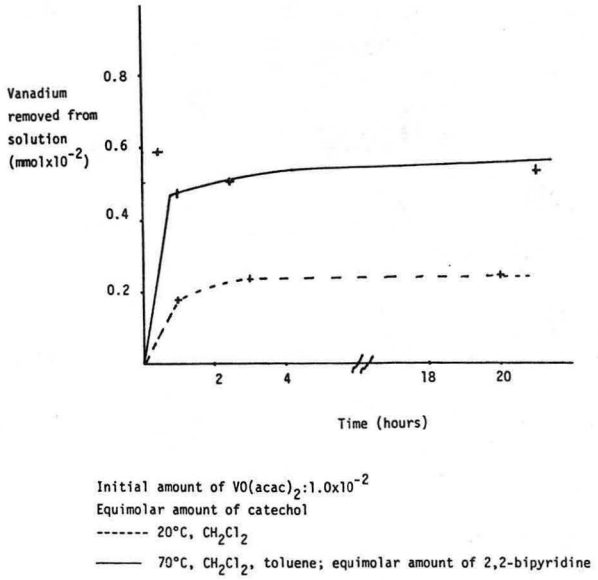

Figure 1. (XBL 862-566)

We also found that Fourier Transform infrared spectroscopy was a powerful tool to ascertain the structure of vanadyl complexes on the beads (Eq. 1).

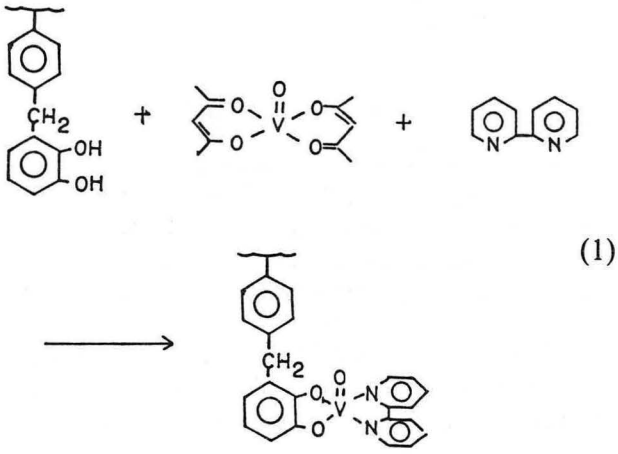

(1)

*This work was supported by the Assistant Secretary for Fossil Energy, Office of Oil, Gas and Shale Technology of the U.S. Department of Energy through the Bartlesville Project Office under Contract No. DE-AC03-76SF00098.

Table 1. Initial amount of $VO(acac)_2$: 1.00×10^{-2} mmol.[a]

Exp No.	Temperature (°C)	Cathecol (mmol $\times 10^2$)	2,2-Bipyridine (mmol $\times 10^{-2}$)	Vanadium removed from solution m(mol $\times 10^{-2}$)
1	20[b]	1.16	—	0.26
2	20[b]	2.30	—	0.51
3	20[b]	0.98	1.04	0.47
4	70[c]	1.00	—	0.38
5	70[c]	0.95	1.04	0.60
6	80[c]	1.04	—	0.45
7	80[c]	2.30	2.26	0.68

[a]Conditions: 5.92% by weight of catechol ligand in the 20% cross-linked polymer.

[b]Solvent: CH_2Cl_2.

[c]Solvent: CH_2Cl_2-toluene.

PLANNED ACTIVITIES FOR FY 1986

We are continuing the polymer-pendant ligand chemistry to more clearly define the rates of removal of vanadyl and nickel compounds from solution and to use Fourier Transform infrared spectroscopy for determination of vanadyl and nickel catecholate structures on the resins.[3]

REFERENCES

1. (a) Frechet, J.M. and Farrall, M.J. (1977), *Chemistry and Properties of Cross-Linked Polymers,* S.S. Labana, Ed., Academic Press, New York. (b) Blasius, E. and Brazio, B. (1967), *Chelating Ion Exchange Resins in Chelates in Analytical Chemistry,* H.A. Flaschlia, and J.A. Barnard, Eds., Marcel Dekker.
2. Fish, R.H. and Tannous, R.S. (1985), *Inorg. Chem. 24,* p. 4456.
3. Fish, R.H., Izquierdo, A., Friedman, G., and Price, R. (to be submitted for publication).

Carbon Oxygen Bond Cleavage Reactions of Model Coal Compounds Using Inorganic Electron Transfer Reagents*

R.H. Fish and J.W. Dupon

Aryl ethers and esters are currently accepted models for the postulated structure of coal. As with coal, rigorous conditions are usually necessary to effect any cleavage of the strong C-O bond.

We have investigated the cleavage of the C-O bonds in aryl ether and ester compounds as models for coal. We have observed efficient and selective cleavage in the presence of M(Ln) compounds where M = alkali metal and Ln = multidentate ligands, such as ethylenediamine and crown ethers. A mechanism involving electron transfer from the oxidation of the metal to a phenyl ring of the ether is proposed.

ACCOMPLISHMENTS DURING FY 1985

Earlier cyclic voltammograms in the literature, on the reductive carbon-oxygen bond cleavage of diaryl ethers, indicate that these compounds can be reduced electrochemically to their radical anion at high negative potential, e.g., −3.05 v *vs* SCE for diphenyl ether.[1] Therefore, in order to accomplish this objective chemically, strong reducing agents were deemed necessary. Mejer *et al.*[2] utilized a five-fold excess of lithium metal and ethylenediamine to cleave benzyl phenyl and diphenyl ethers. The first step of the eventual C-O bond cleavage is believed to be the addition of an electron to a phenyl ring of the ether.

We have studied the reaction of potassium/crown ether complexes with diaryl ethers and esters. A stable solution of electrons is generated at 0°C by the ready oxidation of the metal (Eq. 1).

$$K^{o} + CE \xrightarrow{THF} K^{+} \rightarrow CE + e^{-} \text{ (solvated)}, \quad (1)$$

$$CE \equiv 18 \text{ Crown 6 Ether}.$$

As benzyl phenyl ether was added to the deep blue solution of the potassium/18-crown-6 reagent, the color changed within fifteen minutes to a yellow-orange. The reaction was complete in twenty hours, producing toluene and phenol as the only products in a 1:1 ratio.

Reaction with dibenzyl ether was not as clean. Under the same reaction conditions, bibenzyl and benzaldehyde were produced in addition to toluene and benzyl alcohol. Bibenzyl can result from the coupling of two relatively stable benzyl radicals.

PLANNED ACTIVITIES FOR FY 1986

A survey of the reductive cleavage reactions of various aryl ethers and esters will be utilized to discern relative rates of cleavage. In addition, lithium/12-crown-4 will be used as a reducing agent and compared to the studies with potassium metal. We also intend to synthesize and examine the crown ether complexes of alkali metals with the macrocyclic ethers attached to a polymeric backbone. Immobilization of the crown ether on polyvinyl sytrene would provide enhanced stability and reactivity toward reductive cleavage of the aryl ethers.

REFERENCES

1. Woolsey, N.F. and Bartak, D.E. (1984), *Quantitation of the Reductive Cleavage of Aryl Ethers of SRC and Coals,* Final Report DOE/PC/30227-T3 (DE840 1206).
2. Mejer, S., Ganiecka, K., and Jablonski, L. (1977), *Rosz. Chem. 51,* p. 2477.

*This work was supported by the Electric Power Research Institute through the U.S. Department of Energy under Contract No. DE-AC03-76SF00098.

COAL-RELATED RESEARCH

Processing of Condensate Waters from Coal Gasification*

C.J. King, J.J. Senetar, T.M. Grant, L.J. Poole, and R.E. Thompson

Large volumes of condensate water are formed when reactor effluents from coal gasification are cooled. Water streams from lower-temperature gasification processes contain large concentrations of ammonia, acid gases, and dissolved organics—notably, phenolic compounds. For both economic and environmental reasons, it is necessary to process these waters sufficiently to allow recycling, probably as make-up to a cooling-tower system.

The principal objective of this project is to provide basic understanding enabling development of improved physicochemical processing methods for condensate waters formed during coal-gasification processes. Particular attention is given to solvent-extraction, adsorption, and stripping processes. Other aspects of the project have dealt with chemical characterization of condensate waters, so as to provide a sound basis for research on processing alternatives, and characterization of the mechanism and kinetics of hydantoin compounds, which are formed in the quench-water circuit and tend to concentrate in the blowdowns of cooling towers to which condensate waters would logically be recycled.

Current research focuses upon 1) extraction with both conventional and novel chemically associating solvents which enable effective removal of organic contaminants with promise of low energy consumption, 2) fractionation and removal of organic contaminants by regenerated adsorption and other solid-sorption processes, 3) combining extraction of ammonia with stripping of acid gases in an innovative process which can recover ammonia as an isolated product, and 4) combining Items #1 and/or #2 with Item #3 synergistically.

*This work was supported by the Morgantown Energy Technology Center, Morgantown, WV, through the Assistant Secretary for Fossil Energy, Office of Surface Coal Gasification, Advanced Process Research Program of the U.S. Department of Energy under Contract No. DE-AC03-76SF00098.

ACCOMPLISHMENTS DURING FY 1985

Characterization of Condensate Waters

Analytical results obtained in previous years are described in a recently published paper.[1] The most significant results of the past year have been identification and quantification of thiocyanate and polysulfides, which account for most of the remaining unidentified Chemical Oxygen Demand (COD), organic nitrogen, and organic sulfur in condensate water from Run 101 of the Morgantown Energy Technology Center (METC) gasifier. The full results are shown in Table 1.[2] Our analysis of this water now accounts for 95–96% of the measured COD, 100% of the measured Total Organic Carbon (TOC), 85–100% of the measured organic sulfur, and 94% of the measured organic nitrogen. The uncertainties are associated with polysulfides. For these, only the zero-valent sulfur portion responds to the analysis, and the average number of zero-valent S atoms per mole of divalent sulfur in the polysulfide is unknown.

Analyses of various compositional properties were made for a sample of condensate water supplied from the Great Plains Gasification Associtates demonstration plant. These results were compared with analyses supplied by METC from Argonne National Laboratory and the University of Illinois. Differences were explored and interpreted.

Formation of Hydantoin Compounds

Measurements of the rate of formation of 5,5-dimethyl hydantoin in the presence and absence of various reactants, with various proportions among the reactants, and at various temperatures, revealed 1) that the formation reaction involves, simultaneously, acetone, cyanide, ammonia, and carbon dioxide; 2) that the kinetics are first order in each of these substances; 3) that a "sink" for cyanide exists but is not fully explained; and 4) that there is a strong temperature sensitivity to the reaction. Cyanide is the limiting reagent for the formation of hydantoins in most or all condensate waters. Differences in amounts of hydantoin formation can be interpreted in terms of a) the amount of cyanide formed in the gasifier system, and b) the time, temperature, and mixing conditions within the quench-water circuit.

Table 1. Analysis of METC run-101 condensate water.

	Concentration (mg/L)	COD (%)	TOC (%)
Hydroxybenzenes:		85.7	93.7
Phenol	1,380		
Cresols	1,990		
Xylenols	840		
Dihydroxybenzenes:		2.4	2.8
Catechol	40		
4-methyl catechol	40		
Resorcinol	65		
Hydroquinone	4		
Naphthols	37	0.8	0.9
5,5-dimethyl hydantoin	20	0.2	0.3
Low-MW organic compounds:		1.5	1.6
Acetone	60		
Acetone cyanohydrin	ND[a]		
Acetonitrile	65		
Acetic acid	ND		
Methanol	0		
*Thiocyanate	209 [370][b]	1.9	1.4
*Polysulfide sulfur	[104]	3.0[c]	0.0
Identified COD/TOC (%)		95.8	100.7
Measured COD/TOC (mg/L)		12,250	3,490
Organic nitrogen (mg/L)[d]	120 (94% identified)		
Organic sulfur (mg/L)[d]	404 (100% identified)[c]		

[a]ND: Not determined.
[b]Values in brackets are for a nonacidified sample that had aged.
[c]Assuming polysulfides are in the form SS^{2-}.
[d]Nitrogen and sulfur balances are based on nonacidified samples that had aged.

Extraction of Phenols

Previous work on the use of tri-n-octyl phosphine oxide (TOPO) as an extractant for phenols has now been published.[3]

Distribution coefficients were measured for various condensate-water components extracted into various solvents, including methyl isobutyl ketone (MIBK), benzophenone, tri-n-butyl phosphate (TBP), tributyrin, furan, and 4-methyl cyclohexanone.[2] From an analysis of these results, TBP, a common reagent in the hydrometallurgical and nuclear-processing industries, appears to offer significant potential advantages for removal of organics by solvent extraction. It is a high-boiling solvent, thereby lessening the energy requirement for distillation. Phenol and alkylated phenols can readily be recovered from TBP by distillation. Some means must be provided for removal of higher-boiling phenols from the solvent. Back-extraction into an aqueous base is a possibility for that purpose. Explorations of aqueous ammonia for regeneration of TBP revealed that it should be suitable for those phenols having a forward equilibrium distribution coefficient in the range of 10 to 20. Diluents, such as alcohols, can be used to control the magnitude of the forward distribution coefficient. TBP is also one of the more effective solvents for hydantoins.

Removal of Thiocyanate

Ion-exchange methods for removing thiocyanate have been investigated. Strong-base exchangers effectively remove thiocyanate but are difficult to regenerate. Weak-base exchangers afford a better and effective compromise between capacity and regenerability. Regeneration with aqueous ammonia and other bases has been investigated, and aqueous ammonium carbonate/bicarbonate solution has been identified as a potentially attractive regenerant.

Adsorption of Phenols

Research with adsorbents and polymeric sorbents is directed toward processes which would enable either bulk removal and recovery of organics, or final clean-up following other physicochemical processing methods. Full regenerability with a low energy requirement is a goal. Sorbents considered include conventional activated carbons, chemically treated carbons, and various types of synthetic polymeric resins, in both macroreticular and gel forms. We have initiated studies on the regenerability of phenols from activated carbons, on which there is conflicting information.

Isolation and Recovery of Ammonia

Removal of ammonia by stripping is energy intensive, because of the low pH (about 8.5) resulting from the simultaneous presence of carbon dioxide and hydrogen sulfide in condensate waters. We have been carrying out research on an innovative approach to this problem, wherein ammonia is extracted from condensate water while the acid gases, carbon dioxide and hydrogen sulfide, are simultaneously stripped. This greatly reduces the steam requirement for stripping and serves to isolate the ammonia as a product.

For this purpose, various liquid cation exchangers are being explored. In research so far, we have given the most attention to di-2-ethylhexyl phosphoric acid (D2EHPA) as extractant. Experiments include measurement of equilibrium distribution coefficients, water solubilities of extractants and complexes, phase-settling characteristics, regenerability, and degradation tendencies due to temperature and other chemical constituents. A recent publication describes this work.[4]

Phosphinic-acid extractants have lower acidity and potentially greater thermal stability than the organic phosphoric acids. These properties should make phosphinic acids more effective extractants for ammonia. Cyanex-272 (American Cyanamid Company) is a phosphinic acid extractant developed for the hydrometallurgical industry, where it has excellent properties for cobalt/nickel separation. This material, as supplied, contains substantial amounts of impurities which affect its extraction behavior. A purification method has been developed and utilized for large batches of Cyanex-272. Extraction experiments with Cyanex-272 have confirmed that it possesses near-optimal acidity for regenerable extraction of ammonia. This is evidenced by a sharp rise in the equilibrium distribution coefficient for ammonia at values of pH just below the values (8.0–9.5) typical of condensate waters.

PLANNED ACTIVITIES FOR FY 1986

After an initial literature survey, appropriate experiments will be carried out to reveal the factors determining the degree of reversibility of adsorption of phenol and phenolics on conventional activated carbons. On the basis of the results obtained, surface-treatment methods for carbons will be conceived and pursued. These will have the potential of enhancing the regenerability of phenol-laden carbons, while maintaining satisfactory adsorption capacity.

A literature survey will be made to determine functional groups capable of interacting specifically with phenols, with the interaction being strong enough to give good adsorption capacity, while being weak enough to allow facile regeneration. Polymeric sorbents having these groups will be obtained and/or synthesized and will be tested for their capability of giving regenerable bulk removal of phenolic solutes and/or regenerable final cleanup of condensate waters.

In situ equilibrium distribution coefficients will be measured for extraction of the compounds present in condensate water by means of MIBK and TBP as solvents. These will reveal complexation, micellization, adsorption onto suspended solids, or other complicating factors within the waters.

The properties of the phosphinic acid extractant, Cyanex-272, for extraction of ammonia will continue to be explored. The immediate concern is the thermal stability, as measured by the phosphorous content of an equilibrium aqueous phase, formation of degradation products, and/or loss of extraction ability. Necessary regeneration conditions will be the next item for attention.

Another possibility is to combine the extraction-based method for recovery and isolation of ammonia, on the one hand, with organics removal by means of the same extraction system. This potentially important synergism will be examined through experiments and process calculations.

Computer simulations of ammonia and acid-gas stripping will also be initiated, to give insight into other avenues that may be effective in reducing the energy requirement for removal and isolation of ammonia.

REFERENCES

1. Mohr, D.H. and King, C.J. (1985), "Identification of Polar Organic Compounds in Coal-Gasification Condensate Water by Gas Chromatography–Mass Spectrometry Analysis of High-Performance Liquid Chromatography Fractions," *Environ. Sci. & Technol. 19,* p. 929.
2. Senetar, J.J. and King, C.J. (1986), *Characterization and Treatment of Coal-Gasification Condensate Waters,* LBL-20988.
3. MacGlashan, J.D., Bixby, J.L., and King, C.J. (1985), "Separation of Phenols from Dilute Aqueous Solution by Use of Tri-n-Octyl Phosphine Oxide as Extractant," *Solvent Extraction & Ion Exchange 3,* p. 1.
4. Mackenzie, P.D. and King, C.J. (1985), "Combined Solvent Extraction and Stripping for Removal and Isolation of Ammonia from Sour Waters," *Ind. Eng. Chem. Process & Devel. 24,* p. 1192.

Separations of Polar Organics from Aqueous Solutions by Processes Based upon Reversible Chemical Complexation*

C.J. King, A.S. Kertes, D. Arenson, and J. Tamada

Separations for recovery of various polar organic substances from aqueous solution consume a large amount of energy industrially. Examples include the recovery of ethanol, butanol, acetic acid, glycols, phenols, adipic acid, sugars, and cornstarch products. The need for recovery of such substances will increase still further with the advent of bioprocessing technology, since most of the methods for production of chemicals from biomass generate the product(s) in dilute aqueous solution.

For the most part, these separations are presently accomplished by distillation and evaporation. Reversible chemical complexation provides a low-energy alternative to distillation and evaporation and should be particularly attractive for those solutes which are less volatile than (or comparably volatile to) water. This category includes all the solutes mentioned above. The use of reversible chemical complexation for separation trades upon selective and reversible chemical interaction between functional groups of the solute and the extractant. Many of these are of the Lewis acid–Lewis base (electron acceptor-donor) class.[1]

This project pursues development of chemical and engineering knowledge to enable rational interpretation and modeling of phase-equilibrium and transport mechanisms for such separations. On the basis of this knowledge, further goals are to develop rational criteria for complexation reagents, to develop suitable methods for regeneration and process integration, and to define the most likely applications.

Solutes of particular interest are carboxylic acids, alcohols, and multifunctional compounds containing the -COOH and -OH groups. Carboxylic acids are chosen because of their importance as fermentation products and because it is already known that association with tertiary amines or phosphoryl compounds can provide an effective means of separation. Alcohols, glycols, and related solutes containing -OH groups are chosen because they account for a large fraction of U.S. energy expended for separations and recovery of polar organics from water, and because of their future importance.

The initial phases of the project have dealt with (1) a literature survey of pertinent chemical information for extraction of carboxylic acids and alcohols, (2) measurement and chemical modeling of phase-equilibrium behavior for extraction of carboxylic acids by amine extractants in various diluents, and (3) exploratory measurements designed to identify classes of reagents which may be most attractive for association with alcohols.

*This work was supported by the Assistant Secretary for Conservation and Renewable Energy, Office of Energy Systems Research, Energy Conservation and Utilization Technologies Division of the U.S. Department of Energy under Contract No. DE-AC03-76SF00098.

ACCOMPLISHMENTS DURING FY 1985

Extraction of Carboxylic Acids

A critical survey has been made of the literature covering the chemistry of extraction of carboxylic acids from aqueous solution.[2] This survey covers the acids involved in the pyruvic/tricarboxylic cycle of glucose fermentation, and includes lactic, succinic, tartaric, propionic, citric, pyruvic, fumaric, maleic, malic, and itaconic acids. It includes extraction with hydrocarbon and carbon-oxygen solvents, phosphoryl extractants, and amines.

Experimental measurements have focussed upon the extraction of succinic acid by Alamine 336 (Henkel Corporation—a tertiary amine mixture, with 8 to 10 carbon alkyl groups) in various diluents. Figure 1 shows data for the concentration-based equilibrium distribution coefficient of succinic acid, extracted from water into a solvent mixture of Alamine 336 and methyl isobutyl ketone (MIBK). These equilibrium distribution coefficients are high enough to be of considerable potential industrial interest.

As is evidenced by Fig. 1, the extraction behavior is complex. The pertinent effects appear to include (1) complexation between the amine and the acid, (2) complexation of the first complex with additional acid molecules, facilitating the extraction further, and (3) solvation of these acid-amine complexes by the diluent (MIBK).

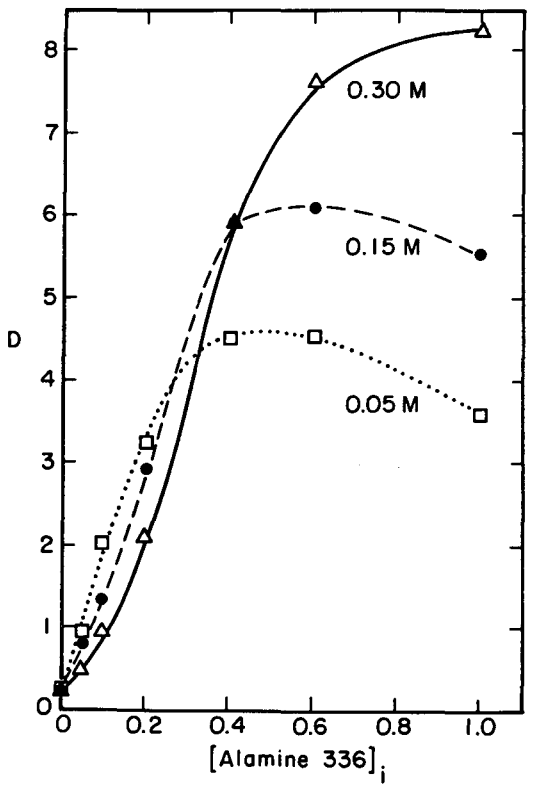

Figure 1. (XBL 862-714)

Similar data obtained with chloroform as diluent show much higher distribution coefficients, probably resulting from stronger solvation of the complexes by the Lewis acid, chloroform.

Experiments carried out for extraction of succinic acid by tri-n-octyl phosphine oxide (TOPO) in MIBK diluent gave much lower values of the equilibrium distribution coefficient, increasing from 0.5 to 1.85 as the molar ratio of TOPO to succinic acid was increased from 1.25 to 5 with a solvent composed of 0.346 molar TOPO in MIBK. TOPO is a strong hydrogen bonding Lewis base. It appears that the ability of the tertiary amines to form an ion pair is an important factor causing them to be more effective extractants than TOPO for succinic acid.

Extraction of Alcohols

A critical and thorough literature survey has been made of the extraction chemistry and solution properties of the lower aliphatic alcohols (methanol, ethanol, propanol, isopropanol, and the four butanols). This study reveals a number of subtle and complex interactions in both aqueous and organic solutions, which can form the basis for generation of improved methods of extraction. Preliminary results of this survey were presented at a DOE conference in October 1985,[3] and the full manuscript is being readied for publication.

From this review and from previous explorations made in our group,[4] the higher alcohols and carboxylic acids have been found to give more attractive combinations of distribution coefficient and selectivity for extraction of ethanol from water than do other common solvents. Extending the resulting concept of strong hydrogen-donor solvents, we have investigated the various isomers of cresol, in various diluents, as extractants for ethanol.

Cresol isomers have been found to give weight-fraction-based equilibrium distribution coefficients around 2.0, which is a very encouraging result. None of the other common solvents gives equilibrium distribution coefficients above 1.0.[4] Noninteracting diluents reduce the equilibrium distribution coefficient in rough proportion to cresol concentration. However, chloroform as a diluent is synergistic, giving distribution coefficients that remain high for solvent mixtures composed of m-cresol and chloroform. Apparently the electron-acceptor characteristic of chloroform serves to solvate the cresol-ethanol complex and/or encourage its formation.

Another strong acid, di-2-ethylhexyl phosphoric acid (D2EHPA) in an alkane diluent, gave rather low equilibrium distribution coefficients for extraction of ethanol. Presumably, the effectiveness of this extractant is hampered by extensive dimerization of the acid in the organic phase. Furthermore, hydrogen-bonding ability is probably a more important form of acidity than is proton ionization for interaction with the alcohol group.

PLANNED ACTIVITIES FOR FY 1986

Extraction of Carboxylic Acids

Chemical modeling is being used for interpretation of the data for extraction of succinic acid by tertiary amine extractants in various diluents. Computer approaches are being implemented for determining the most important complexes and for fitting chemical parameters to experimental data. These methods will be used for our earlier data on extraction of acetic acid by amine-containing solvent mixtures, as well, in order to provide a basis for comparison.

Methods of regeneration of acid-amine extracts will also be explored.

Extraction of Alcohols

Experiments with phenolic extractants will be continued, with different diluents, including chemically active ones. The aims are to determine the most effective phenolic extractants, to establish effective diluents, to assess necessary regeneration conditions, to determine the effect of temperature on the equilibrium, and to interpret experimental results through chemical modeling.

The review of extraction chemistry of alcohols revealed that there are significant effects of isomeric alcohol structures. So as to provide more information on this effect, a series of measurements will be made to determine phase equilibria for extraction of the four isomeric butanols from aqueous solution by means of cresol in an alkane diluent. These results will be interpreted in terms of aqueous and organic phase effects, individually.

Adsorption

Chemical complexation can also be used in separations carried out by adsorption, through the inclusion of specific functional groups on the adsorbent surface, or within a penetrable polymeric sorbent. Preliminary studies will be made of the attractiveness of this approach for recovery of carboxylic acids, alcohols, and glycols from aqueous solution. As an initial step, the efficacy of polymeric resins containing the phenolic -OH group for sorption of alcohols will be examined.

REFERENCES

1. King, C.J. (1986), "Separation Processes Based upon Reversible Chemical Complexation," plenary lecture at Tenth Interamerican Congress of Chemical Engineering, Santiago, Chile, November 1983; *Handbook of Separation Process Technology*, R.W. Rousseau, Ed., Wiley, New York, in press.
2. Kertes, A.S. and King, C.J. (1985), "Extraction Chemistry of Fermentation-Product Carboxylic Acids," presented at 189th Amer. Chem. Soc. Natl. Mtg., Miami, FL, April 1985; *Biotechnol. Bioeng.*, February 1986.
3. King, C.J., Munson, C.L., and Kertes, A.S. (1985), "Extraction of Ethanol from Aqueous Solutions," presented at DOE/ORNL Conference on Separation Science and Technology for Energy Applications, Knoxville, TN, October 1985.
4. Munson, C.L. and King, C.J. (1983), *Ind. Eng. Chem. Process Des. & Devel. 23,* p. 109.

Jet Breakup Enhanced by an Initial Pulse*

D.W. Bousfield and M.M. Denn

The breakup of a liquid jet following an initial finite periodic disturbance of the nozzle exit velocity was analyzed using a nonlinear thin filament theory. Breakup occurs over two distinct time scales, the second of which is characterized by the growth rate calculated from linear stability theory. An approximate analysis of the kinematics during the first time scale enables an analytical prediction of the breakup time.

The surface tension–driven breakup of a filament into droplets was first analyzed by Rayleigh,[1] who calculated the growth rate of an infinitesmal disturbance in the absence of viscosity; the growth of disturbances on Newtonian liquid filaments has subsequently been reviewed by Bogy[2] and McCarthy and Molloy.[3] The growth rate of an infinitesmal disturbance on a viscoelastic liquid filament was computed by Goldin *et al.*[4] and Middleman.[5] Bousfield and coworkers[6,7] have used both one-dimensional asymptotic analysis and a transient finite element method to analyze the growth and ultimate breakup of disturbances that attain finite size on Newtonian and viscoelastic liquid filaments, showing good agreement with experiments; these analyses follow in the tradition established by Rayleigh and subsequent workers, in that the frame of reference is imbedded in the moving filament and temporal growth of an initially small disturbance is studied without regard to possible flow rearrangement associated with the exit from a nozzle.

There is some interest in analyzing filament breakup and droplet formation following the imposition of a large periodic axial velocity at the nozzle; a large velocity pulse using a positive displacement device has been proposed, for example, as a means of controlling droplet size and breakup time in a Kraft recovery furnace for efficient combustion of black liquor.[8] The one-dimensional asymptotic analysis formulated by Bousfield *et al.*[6,7] is well suited for studying this problem, since any initial conditions can be accommodated. In contrast to the usual studies of disturbance growth, we assume here that the filament is of constant radius R_o at time $t = 0$, but is subjected to an initial mean axial velocity

$$(z,o) = v_o \sin(\pi z/L) \quad , \tag{1}$$

where L is the half-wavelength of the induced velocity and v_o is the magnitude of the velocity pulse relative to the mass average exit velocity of the jet. The following parameters appear in the analysis for a Newtonian fluid:

$$\alpha = \frac{R_o}{L} \quad , \tag{2a}$$

$$\beta = \frac{\rho\sigma L^2}{\eta^2 R_o} \quad , \tag{2b}$$

$$U_o = \frac{v_o \eta R_o}{\sigma L} \quad , \tag{2c}$$

where η is the viscosity, ρ is the density, and σ is the surface tension of the Newtonian liquid. $U_o\beta = v_o\rho L/\eta$ is a Reynolds number based on the maximum pulse velocity and disturbance half length. Dilute polymer solutions are further characterized by a polymer relaxation time λ_p and a solution retardation time λ_r, which appear in two additional dimensionless groups:

$$\phi = \frac{\lambda_p \sigma}{\eta R_o} \quad , \tag{2d}$$

$$\Lambda = \frac{\lambda_r}{\lambda_p} \quad , \tag{2e}$$

ACCOMPLISHMENTS DURING FY 1985

Breakup Characteristics

The thin filament analysis is described in detail elsewhere[7] and only results are presented here. The calculations shown on different time scales in Figs. 1 and 2 are typical of all cases studied for Newtonian liquids; the parameters here are $\alpha = 0.16$, $\beta = 1.8$, and $U_o = 1.67$, corresponding to $R_o = 0.5$ mm, $L = 3.14$ mm, and $v_o = 0.47$ m/s, with fluid properties $\eta = 0.67$Pa s, $\rho = 1350$ Kg/m^3, and $\sigma = 0.03$ N/m. There is a very rapid decrease in the minimum radius R_{min}, followed by an approach to a straight line on a semi-logarithmic plot of $(R_o - R_{min})/R_o$. As we shall show subsequently, the

*This work was supported by the U.S. Army, ARRADCOM, under Agreement No. 3311-1412 through the U.S. Department of Energy under Contract No. DE-AC03-76SF00098.

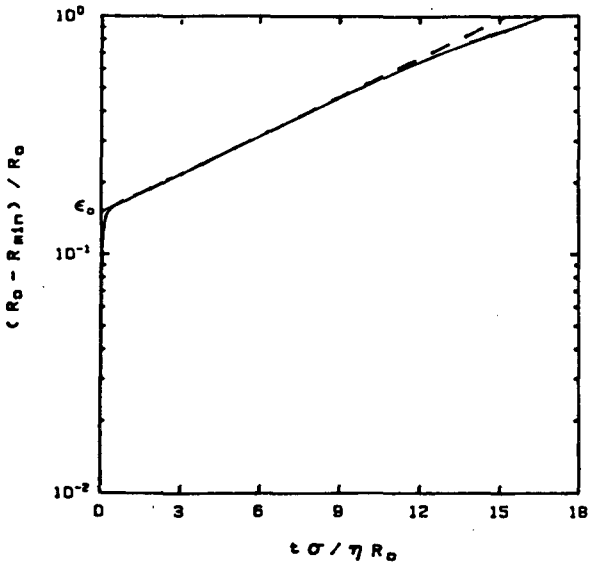

Figure 1. Disturbance growth for α = 1.8, β = 1.8, and U_0 = 1.67. The slope of the dashed line is the growth rate from linear stability theory. (XBL 862-715)

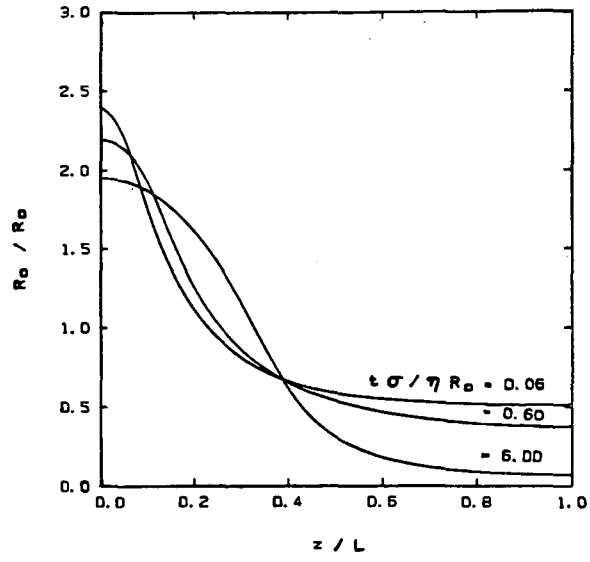

Figure 3. Radius profiles for the calculations of Figs. 1 and 2. (XBL 862-717)

response in this first region is inertially determined and independent of surface tension; the relevant time scale is therefore that appropriate to viscous transport over a length L: $\rho L^2/\eta$. The slope of the dashed straight line is the growth rate given by the linear stability theory for surface tension-driven growth of infinitesmal disturbances, which is close to 0.07 for these values of α and β; the relevant time scale here is $\eta R_0/\sigma$. It is remarkable that the growth rate of this nonlinear process is given so accurately after the initial transient by a linear growth rate. Breakup occurs when $(R_0 - R_{min})/R_0$ reaches unity; deviation from the linear solution is small even approaching breakup. The shape profiles for this case are shown in Fig. 3, where it is obvious that the disturbance relative to the undeformed cylinder ($R = R_0$) is large.

When inertia is an important factor in the sur-

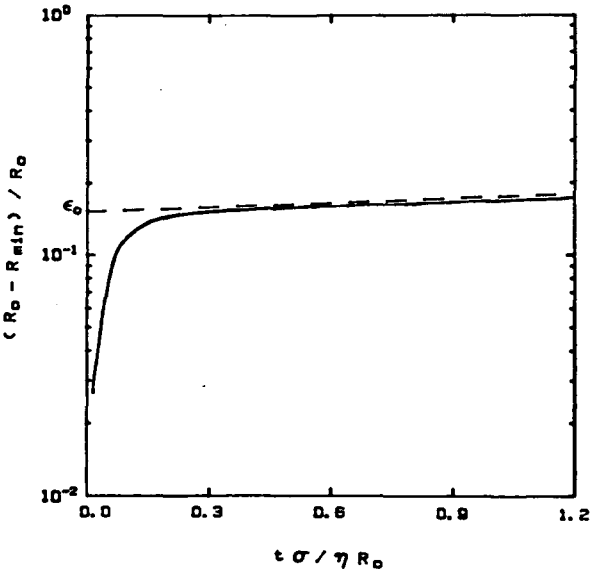

Figure 2. Same as Fig. 1, but over a fifteen-fold longer time scale. Breakup occurs when $(R_0 - R_{min})/R_0$ equals unity. (XBL 862-716)

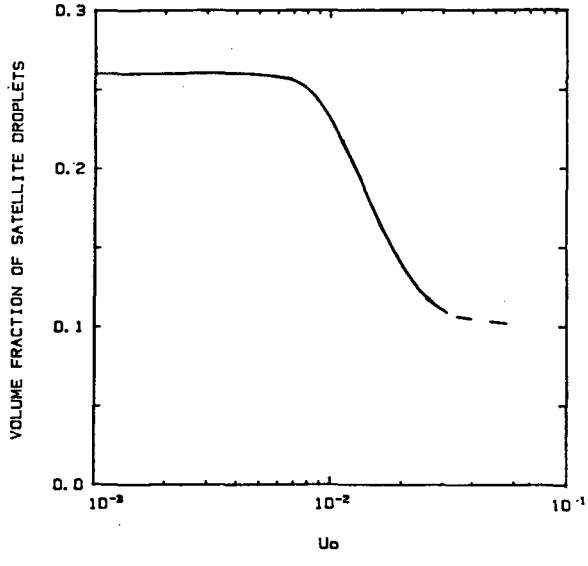

Figure 4. Volume fraction of satellite drop as a function of pulse velocity; α = 0.08, β = 1890. (XBL 862-718)

face tension-driven breakup process (large β), the filament breaks up into primary and satellite droplets. The asymptotic thin filament theory predicts the experimentally observed primary and satellite droplet sizes for small disturbances very well as a function of imposed disturbance wavelength.[7] According to the theory, a large initial velocity ($\beta u_o \sim 10$) supresses the formation of satellite droplets relative to the primary droplet when α is small. A typical calculation is shown in Fig. 4 for $\alpha = 0.08$, $\beta = 1890$; these are parameter values typical of experiments on glycerol-water jets. The satellite droplet size at high values of U_o is not well-characterized because of the difficulty in representing a highly distorted filament with finite differences, but the effect is clear.

The response of a viscoelastic fluid is similar to that of a Newtonian fluid, in that there are responses over two distinct time scales. A typical response is shown in Fig. 5, where the parameters are the same as those in Figs. 1 through 3, except that $\phi = 0.18$ and $\Lambda = 0$ (a "Maxwell fluid"). The response over the time scale $\rho L^2/\eta$ now includes a damped oscillation; as discussed below, this is the typical inertial response of an underdamped viscoelastic material. Following the initial short-time response, the response over the time scale of order $\eta R_o/\sigma$ follows the linear theory for a viscoelastic liquid.[4,5] The linear theory approximates the disturbance growth until breakup for parameter values studied in this work, but it is known[7] that for sufficiently large values of ϕ (depending on Λ) the breakup is governed at long times by viscoelastic nonlinearities and that the breakup time can be of a different order of magnitude from that computed by linear theory.

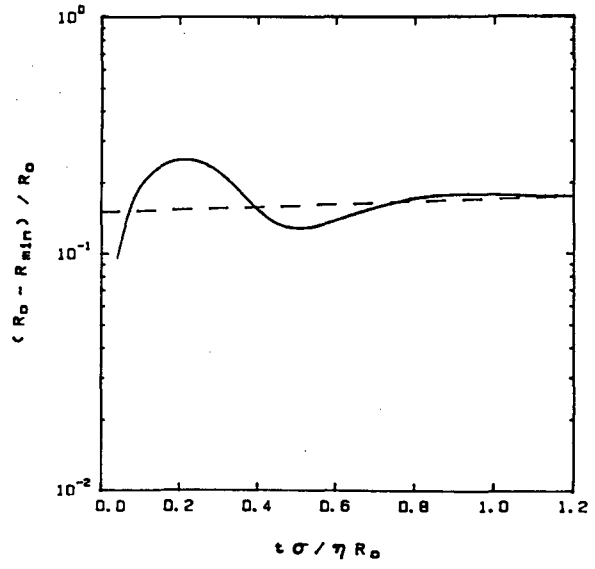

Figure 5. Disturbance growth for a viscoelastic liquid for the conditions in Fig. 1, but with $\phi = 0.18$ and $\Lambda = 0$. (XBL 862-719)

Analytical Estimates

The computed results suggest an approximation procedure that can enable analytical solutions for the breakup time. Following the initial transient, the disturbance growth is closely approximated by linear theory until breakup. The linear growth rate is known analytically. If it were possible to estimate the intercept (denoted ϵ_o in Figs. 1 and 2), then the time (or time-of-flight) to breakup could be estimated analytically in terms of geometry, fluid properties, and the maximum velocity v_o and half wavelength L of the positive displacement device.

A rough estimate of ϵ_o, which is surprisingly accurate for Newtonian liquids, can be obtained in the following way. The velocity perturbation imposed at time $t = 0$ will initially die out because of viscous dissipation; the interaction of inertial and viscous stresses occurs on a time scale $\rho L^2/\eta$, which is usually much less than the time scale $\eta R_o/\sigma$ for surface tension–driven flows. Linear stability theory would predict the axial velocity decay to occur as

$$v(z,t) = - v_o \sin(\pi z/L) \exp(-3\pi^2 \eta t/\rho L^2) \quad . \quad (3)$$

The area-averaged continuity equation expressed in terms of the radius R(z,t) is

$$\frac{\partial R}{\partial t} = - \frac{R}{2} \frac{\partial v}{\partial z} - v \frac{\partial R}{\partial z} \quad . \quad (4)$$

Equation (4) can be solved exactly if we take Eq. (3) as the expression for the velocity. The solution so obtained remains finite only at $z = L$ (the minimum) or $z = 0$ (the maximum), but not both, and it is inconsistent with the assumed uniform initial radius. It nevertheless appears to give a reasonable description of the short-time response in the neighborhood of the minimum, $z = L$. The solution that is finite at $z = L$ is

$$R(z,t) = \frac{\text{constant}}{(1 - \cos \pi z/L)^{1/2}} \exp\left[- \frac{\beta U_o}{6\pi} + \frac{\beta U_o}{6\pi} \exp(-3\eta\pi^2 t/\rho L^2) \right] \quad . \quad (5)$$

This function approaches a limit for $t \gg \rho L^2/3\pi^2\eta$; we thus obtain

$$\epsilon_o = 1 - \frac{R(z,\infty)}{R(z,0)} = 1 - \exp(-\beta U_o/6\pi) \quad . \quad (6)$$

Equation (6) is plotted in Fig. 6, together with the values of ϵ_o obtained by extrapolating the semi-logarithmic region of the growth curve to t = 0 for $\alpha = 0.16$, $\beta = 1.8$ (the conditions shown in Figs. 1–3 for $U_o = 1.67$). Agreement is quite good up to a predicted initial perturbation of 0.4, and probably adequate at still higher pulsing velocities. Since the linear theory of surface tension-driven instabilities predicts the breakup time quite well for given initial perturbation ϵ_o, a completely analytical estimate of the breakup time or time-of-flight is thus available.

The equivalent result for a dilute polymer solution is obtained by replacing the coefficient of time, $-3\pi^2\eta/\rho L^2$, in Eqs. (3) and (5) with $-\gamma$, where γ is the root of

$$\frac{\gamma(1 + \lambda_p\gamma)}{1 + \Lambda\lambda_p\gamma} = -\frac{3\pi^2\eta}{\rho L^2} \quad . \quad (7)$$

This quadratic equation will have complex roots whenever the discriminant

$$\text{dis} = \frac{12\eta\pi^2\lambda_p}{\rho L^2} - \left[1 + \frac{3\eta\pi^2\Lambda\lambda_p}{\rho L^2}\right]^2 \quad (8)$$

is positive, with a period of oscillation given by

$$T = 4\pi\lambda_p/(\text{dis})^{1/2} \quad . \quad (9)$$

This short-time behavior is seen in the complete thin filament calculations in Fig. 5. The damped oscillatory response to an initial deformation is characteristic of the inertial response of viscoelastic liquids; see the squeeze flow analysis of Lee et al.[9] for example.

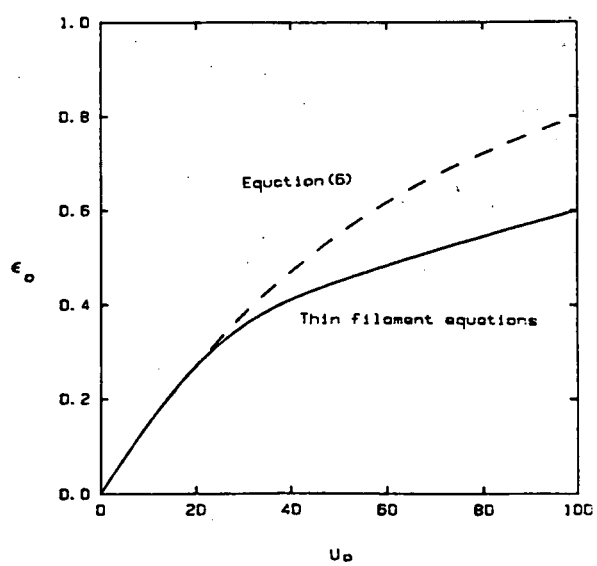

Figure 6. ϵ_o as a function of U_o. The broken line is the analytical estimate from Eq. (6). (XBL 862-720)

Conclusion

The observation that the disturbance following a finite pulse grows over two distinct time scales, and that the second of these is characterized by the linear growth rate for a surface tension-driven disturbance, enables an analytical estimate of the breakup time or time-of-flight. Together with Eq. (6), we therefore have a closed form algebraic design equation for the breakup length of jets in which the finite initial disturbance is imposed by an oscillating positive displacement device.

PLANNED ACTIVITIES FOR FY 1986

Work in FY 1986 will focus on the use of transient finite element methods for analyzing the growth and deformation of inviscid inclusions in polymeric liquids in which the far field is extensional.

ACKNOWLEDGEMENT

This problem was first brought to our attention by I.H. Stockel. We have had helpful conversations with G. Marrucci.

NOTATIONS

L	half wavelength of disturbance
R	filament radius
R_o	initial filament radius
t	time
T	period of oscillation
U_o	dimensionless peak velocity
v	averaged axial velocity
v_o	initial axial peak velocity
z	axial coordinate
α	dimensionless geometric parameter
β	dimensionless fluid properties
γ	linear analysis growth factor
ϵ	dimensionless disturbance magnitude
ϵ_o	effective initial disturbance
η	fluid viscosity
Λ	ratio of relaxation and retardation times
λ_p	polymer relaxation time
λ_r	retardation time
ρ	fluid density
σ	surface tension
ϕ	dimensionless relaxation time

REFERENCES

1. Rayleigh, Lord (1879), "On the Capillary Phenomena of Jets," *Proc. Royal Soc. Lond. A29,* p. 71.
2. Bogy, D.B. (1979), "Drop Formation in a Circular Liquid Jet," *Ann. Rev. Fluid Mech. 11,* p. 207.
3. McCarthy, M.J. and Molloy, N.A. (1974), "Review of Stability of Liquid Jets and the Influence of Nozzle Design," *Chem. Eng. J. 7,* p. 1.
4. Goldin, M., Yerushalmi, J., Pfeffer, R., and Shinnar, R. (1969), "Breakup of a Laminar Capillary Jet of a Viscoelastic Fluid," *J. Fluid Mech. 38,* p. 689.
5. Middleman, S. (1965), "Stability of a Viscoelastic Jet," *Chem. Engng. Sci. 20,* p. 1037.
6. Bousfield, D.W., Marrucci, G., and Denn, M.M. (1984), "Dynamics of Liquid Filament Breakup," *Proc. IX Intl. Congress on Rheology 2,* p. 239.
7. Bousfield, D.W., Keunings, R., Marrucci, G., and Denn, M.M. (1986), "Nonlinear Analysis of the Surface Tension-Driven Breakup of Viscoelastic Filaments," *J. Non-Newtonian Fluid Mech. 21,* p. 79.
8. Stockel, I.H. (1985), "Research on Droplet Formation for application to Kraft Black Liquors," DOE technical report DOE/CE/40626-T1.
9. Lee, S.J., *et al.* (1984), "Compressive Flow Between Parallel Disks: II. Oscillatory Behavior of Viscoelastic Materials Under a Constant Load," *J. Non-Newtonian Fluid Mech. 14,* p. 301.

Removal of H_2S from Coal-Derived Synthesis Gas*

R. Hix, S. Lynn, D. Neumann, S. Sciamanna, and C. Stevens

When coal is gasified, most of the organic sulfur is converted to hydrogen sulfide and must be removed before the gas can be utilized either as a fuel or as synthesis gas. Similarly, most sources of natural gas contain H_2S, as do many refinery gases. The problem of removing the hydrogen sulfide varies with the nature of the gas that has been produced and with the purpose to which the gas is to be put. In some cases one wishes to remove only hydrogen sulfide, in others one wishes to remove carbon dioxide as well, and in still others there are hydrocarbons that can profitably be recovered as separate products. The UC Berkeley Sulfur Recovery Process (UCBSRP) is a new approach to this problem being developed at the Lawrence Berkeley Laboratory that consists of

- absorbing the hydrogen sulfide in a polar organic solvent;
- converting the dissolved hydrogen sulfide to sulfur by reacting it with an equivalent amount of sulfur dioxide dissolved in the same solvent;
- recovering co-absorbed gases from the solvent by stripping;
- recovering elemental sulfur from the solvent by crystallization; and
- generating the sulfur dioxide for the process by burning hydrogen sulfide or sulfur, recovering heat from the combustion gas in a waste-heat boiler, and recovering SO_2 by scrubbing the gas with cooled solvent from the crystallization step.

The overall objectives of this project are to obtain the physical and chemical data needed to design process configurations that utilize the steps enumerated above, and to evaluate these process configurations to determine their economic potential. The work to meet these objectives has been subdivided into the following tasks:

- To determine the solubilities of H_2S, SO_2, CO_2, CH_4 and other hydrocarbon gases, water, and sulfur in the organic solvent as functions of pressure, temperature, and solvent composition;
- To determine the effects of temperature and solvent composition on reaction kinetics;
- To investigate the suitability of steel and other materials of construction for this system;
- To determine the parameters controlling

*This work was supported by the Assistant Secretary for Fossil Energy, Office of Coal Utilization, Division of Surface Coal Gasification, of the U.S. Department of Energy under Contract No. DE-AC03-76SF00098.

the crystal size distribution of sulfur so that crystals of 100 microns or greater will be formed in the process;

- To determine the parameters controlling reactive absorption of hydrogen sulfide by solutions containing sulfur dioxide;
- To set up a computer model of this process to aid in its evaluation and evolution; and
- To compare the anticipated costs of this process with those of conventional technology.

ACCOMPLISHMENTS DURING FY 1985

The gases of interest in the UCBSRP are SO_2, H_2S, CO_2, propane, and butane. The solvents of interest are characterized by low vapor pressure, miscibility with water, and good solvating power for these gases. The following polyglycol ethers are currently under investigation:

- Diglyme: Diethylene glycol dimethyl ether,
- Triglyme: Triethylene glycol dimethyl ether,
- Tetraglyme: Tetraethylene glycol dimethyl ether,
- Dowanol DM: Diethylene glycol methyl ether,
- Dowanol TBH: Triethylene glycol butyl ether.

Also of interest is the effect of water on the solubilities of gases in these solvents.

The solubility of SO_2 in these solvents was determined first, and a paper based on this work was published recently.[1] The results obtained for H_2S, CO_2, and propane to date are given in Table 1. As seen from the uncertainties on the coefficients, the experimental technique is quite reproducible. For comparison purposes Table 2 shows Henry's Law values for these three gases at 25°C expressed on a weight fraction basis. The lower glymes have a slightly higher capacity for dissolved gases than do the higher glymes. The diethers are generally better than the monoethers as solvents for these gases. The effect of temperature on solubility is such that at 100°C Dowanol DM (a monoether) is slightly better than tetraglyme (a diether). Also, the selectivity for H_2S relative to CO_2 is greater at 25°C than at 100°C for all of the solvents. Propane solubility is somewhat higher than carbon dioxide solubility in these solvents. In Dowanol TBH, the tert-butyl ether of diethylene glycol, the solubility of propane is almost double that of CO_2 because of the increased aliphatic character of this solvent.

Table 1. Constants for Henry's law correlation for H_2S and CO_2 in organic solvents. $H = \exp [A/T + B]$.[a]

	H_2S	
Solvent	A	B
Diglyme	−2095.9 ± 1.8%	13.483 ± 0.8%
Triglyme	−2147.2 ± 3.4%	13.443 ± 1.5%
Tetraglyme	−2257.1 ± 0.4%	13.616 ± 0.2%
Dowanol DM	−1943.2 ± 1.0%	13.255 ± 0.4%
Dowanol TBH	−1817.2 ± 1.7%	12.500 ± 0.7%
	CO_2	
Solvent	A	B
Diglyme	−1378.0 ± 1.7%	12.829 ± 0.6%
Triglyme	−1370.7 ± 0.2%	12.729 ± 0.1%
Tetraglyme	−1363.7 ± 4.0%	12.581 ± 1.0%
Dowanol DM	−1250.8 ± 2.5%	12.971 ± 0.6%
	Propane	
Solvent	A	B
Triglyme	−1325.2 ± 1.14%	12.130 ± 0.44%
Tetraglyme	−1238.6 ± 2.01%	11.824 ± 0.43%
Dowanol DM	−1135.1 ± 0.02%	12.465 ± 0.48%
Dowanol TBH	−1414.3 ± 0.19%	12.342 ± 0.20%

[a] H = kPa/mole fraction, T = Kelvin.

Table 2. Henry's law values at 25°C for gases in organic solvents (MPa/Wt. fraction).

Solvent	H_2S	CO_2
Diglyme	2.50	11.18
Triglyme	2.69	13.77
Tetraglyme	2.75	15.16
Dowanol DM	2.97	17.67
Dowanol TBH	4.10	19.48

A detailed study of the catalysis of the reaction between H_2S and SO_2 by N,N-dimethyl aniline (DMA) in polyglycol ethers was reported at the ACS meeting in Philadelphia in August, 1984, and will be published shortly.[2] The reaction is first-order with respect to both reactants. The reaction-rate constant exceeds 10 liters/mole-s at ambient temperature when the DMA content is 10 wt%, so that reaction is substantially complete in less than 10 seconds. A study now in progress shows that the same rate constant is found at the 1-wt% level for many heterocyclic nitrogen compounds.

A computer program that simulates the complete process is nearing completion. The program subroutines for each of the unit operations work well; the remaining programming effort will determine the most effective method for linking the subroutines for a complete simulation. The program is currently being used to test alternative process configurations. It utilizes all of the physical and chemical data that have been obtained to date and will be expanded to use new results as they are obtained.

A comparative study is being made of one application of the UCBSRP. The gas to be treated is the recycle stream from a high-pressure (2000 psia) hydrodesulfurization plant (Fig. 1). It is primarily hydrogen but also contains light hydrocarbons as well as H_2S. The flowsheet for this application is shown in Fig. 2. Co-absorbed gases are compressed and sweetened for delivery to the refinery's fuel gas system. The stack gas from the process is to contain about 10 ppm SO_2. The scale of operation is 100 long tons of sulfur per day. The flowsheet for conventional technology to accomplish the same treatment is shown in Fig. 3. A diethanol amine absorber-stripper operation feeds H_2S to a Claus plant that is followed by a SCOT tail-gas clean-up unit.

Comparison of the two flowsheets shows that there are significantly fewer unit operations in the UCBSRP. The capital costs for the two processes were estimated from the purchased costs of the major items of equipment. The capital for the UCBSRP is about 60% that for the conventional technology. The energy equivalent of the electricity and low-pressure steam for the UCBSRP will be less than the energy in the high-pressure steam produced, whereas the conventional process is a substantial net energy consumer.

The process configuration for the UCBSRP will vary with process conditions. Different flowsheets would be used in the treatment of gas streams at pressures of 100 to 600 psia and at near-atmospheric pressure. Examples of these are being developed with the aid of the computer model.

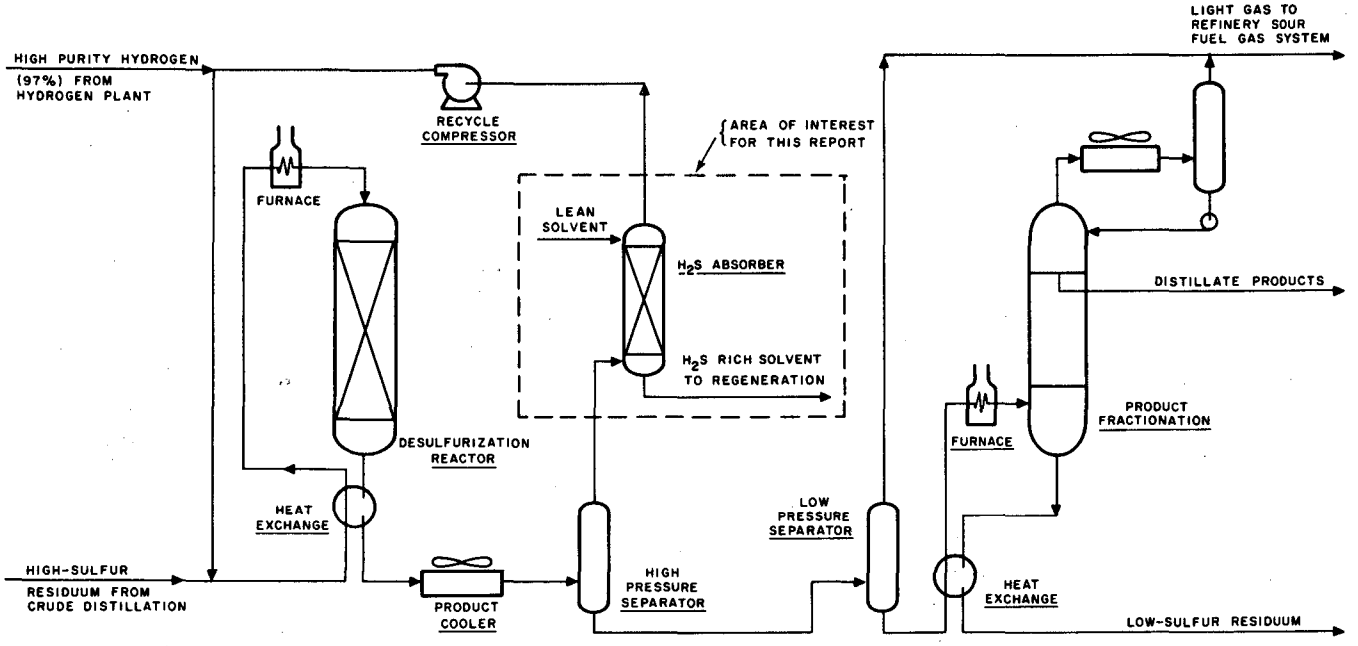

Figure 1. Simplified process flow diagram, residuum desulfurization process. (XBL 861-340)

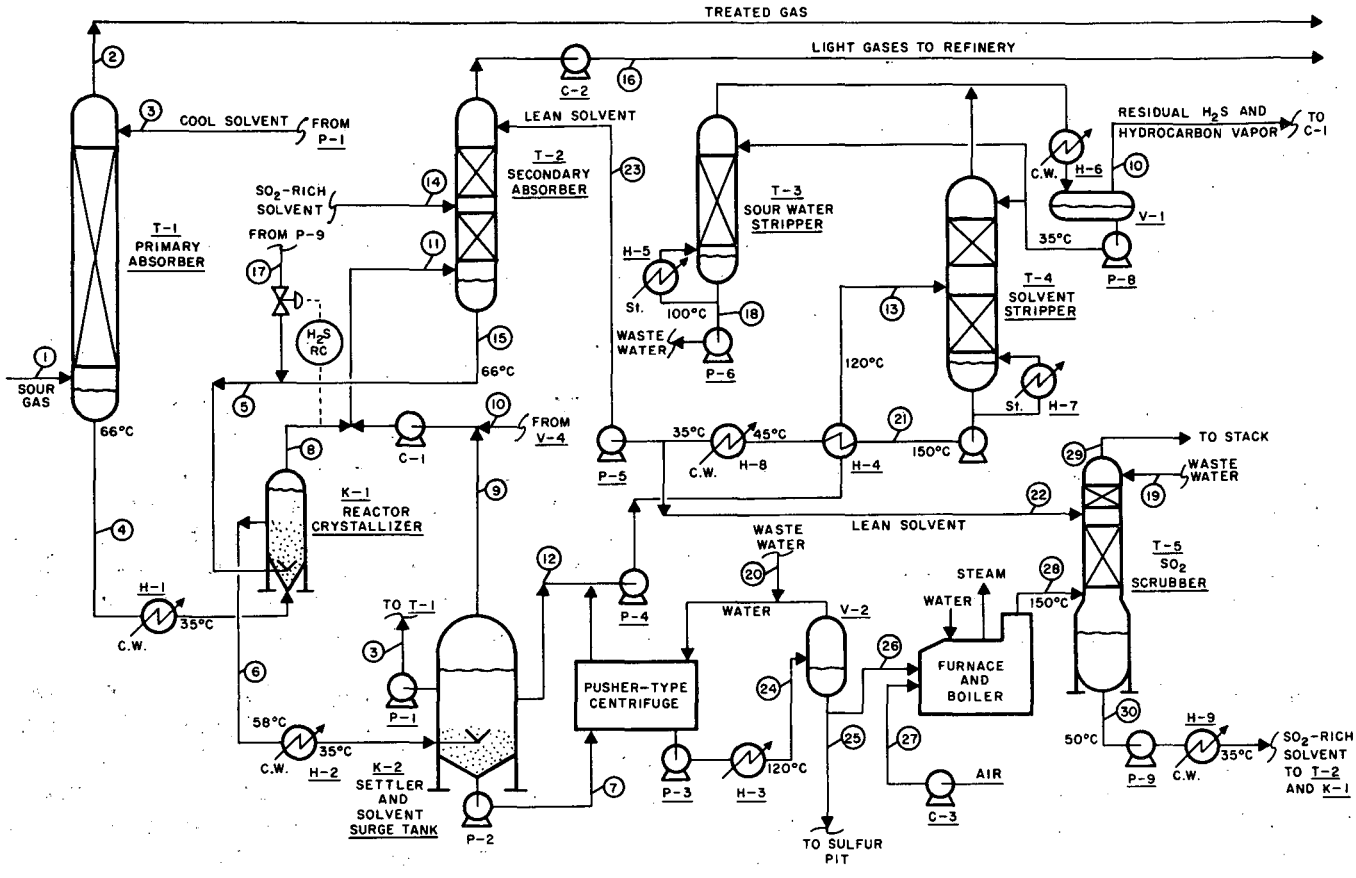

Figure 2. Process flow diagram, UCB sulfur recovery process. (XBL 861-341)

PLANNED ACTIVITIES FOR FY 1986

The determination of gas solubilities is nearly completed. The final solute gas will be butane. Determining the effect of water on the solubilities of H_2S, SO_2, and propane in one monoether and one diether will complete the study.

The study of reaction kinetics at ambient temperature will be completed in the first half of the current fiscal year. New equipment and a different experimental procedure are needed to study the reaction at elevated temperatures and in very dilute solutions. Work on this project is just starting.

Short-term corrosion studies have found no perceptible attack on any of the metals tested. Long-term studies at elevated temperatures are now being prepared.

The equipment for studying the factors controlling crystal size distribution has been assembled, and experimentation will start in January, 1986.

The theory for modeling absorption with chemical reaction when both reactants are volatile is being developed. It will be used in the interpretation of the experiments that will also start in January.

Computer modeling and cost analysis of the UCBSRP will continue during the fiscal year.

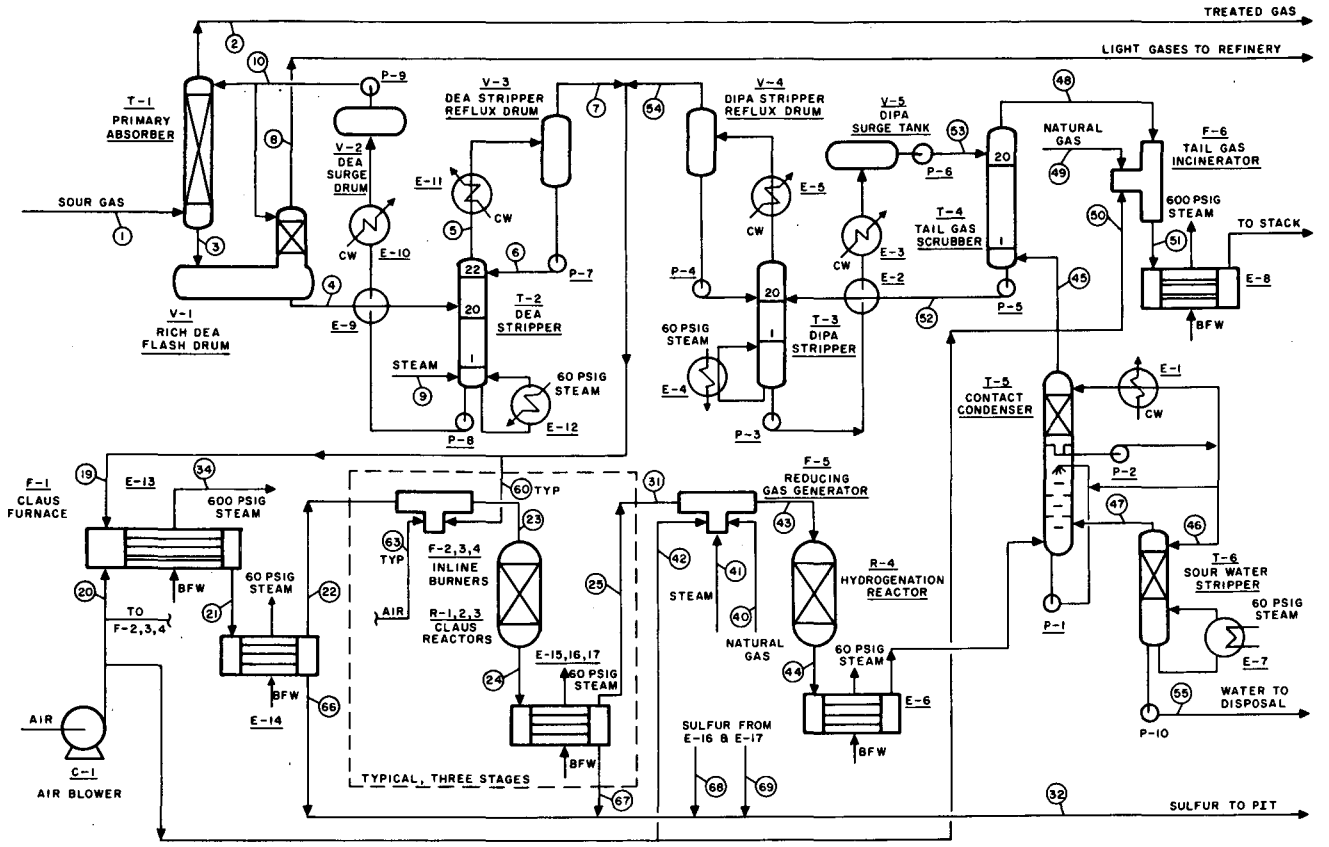

Figure 3. Process flow diagram, conventional processing. (XBL 861-342)

REFERENCES

1. Demyanovich, R.J. and Lynn, S. (1985), "Use of a Polar Organic Solvent to Control Emissions from a Sulfuric Acid Plant," in *Processing and Utilization of High Sulfur Coals*, Y.A. Attia, Ed., Elsevier Science Publishers, Amsterdam.
2. Neumann, D.W. and Lynn, S. (1986), "The Kinetics of the Reaction of Hydrogen Sulfide and Sulfur Dioxide in Organic Solvents," *I&EC Process Design and Development 25* (in press).

Production of Sugars from Cellulose: The Kinetics of Endoglucanase in Cellulose Hydrolysis*

(This article has been reprinted from the FY 1984 Annual Report.)

B. Elzufon, D. Wiley, H. Blanch, C. Wilke, and A. Sciamanna

The research of the Biochemical Process Group has focused on the hydrolysis of lignocellulosic materials to sugars and their subsequent fermentation by yeast to ethanol and other fuel-grade chemicals. Various studies have examined the kinetics of enzymatic hydrolysis of cellulose and hemicellulose fractions for optimal sugar production, the physical and chemical nature of the raw materials, the optimal production and recovery of enzymes, and the use of new organisms for converting polymeric pentosans and hexosans to sugars.

Cellulase is composed of three individual enzymes that function synergistically to break down cellulose. An overall kinetic model of cellulase behavior is being developed based on models of the behavior of the individual enzymes. In this article, an effort to develop a kinetic model of endoglucanase, one of the three cellulase enzymes, is reported.

ACCOMPLISHMENTS DURING FY 1984

A modified viscometric technique was developed to assay endoglucanase activity and was used to determine its kinetic parameters. Endoglucanase was found to be more active in its pure form than as part of the cellulase system. This may be due to the accumulation of cellobiose, a product of cellobiohydrolase, which inhibits endoglucanase. The influence on endoglucanase activity of cellobiose and glucose, known inhibitors of cellulase, was also studied. Cellobiose was found to inhibit endoglucanase via partial mixed-type inhibition. Glucose, however, was found to be a nonessential activator of endoglucanase.

An analytical technique was developed to measure enzyme activity that takes advantage of the polymeric characteristics of cellulose. Once developed, this technique was used to study endoglucanase behavior. A kinetic model was then developed based on experimentally determined kinetic parameters. An additional model based on these inhibition and activation mechanisms was developed and was successful in predicting endoglucanase behavior.

A typical single polymeric carbohydrate component from biomass contains molecules of many different chain lengths. A molecular weight measure will therefore yield only an average value. There are three methods of averaging the molecular weight of different polymer chains in a mixture: (1) a molecule-number average molecular weight, M_n; (2) a weight average molecular weight, M_w; and (3) a viscosity average molecular weight, M_v.

M_n is determined by counting the number of molecules in a sample of a given weight and determining the average weight on the basis of the number of molecules at each weight. Molecular weights can be measured by determining the number of molecules in a sample of known weight by chemically reacting the end groups with some compound so that they can be distinguished from the other monomer units. An example is the colorimetric reaction.[1] This method of molecular weight determination is also the basis for the reducing sugar assay. M_n is usually the most probable molecular weight and lies near the peak of a molecular weight distribution curve, as shown in Fig. 1.

M_w determines average molecular weight by the weight percent of each molecule present. The ratio of M_w to M_n is a measure of the range of the molecular weight distribution and is called the polydispersity; for carboxymethyl cellulose (CMC), polydispersity is assumed to be two.[2]

M_v is determined by relating molecular weight to solution viscosity and is the simplest experimental method for measuring the molecular weight of a polymer. It lies between M_n and M_w and is usually closer to M_w, as shown in Fig. 1. Since M_v is close to M_w it is approximately equal to M_w; therefore, $M_v \approx M_w \approx 2M_n$. Thus the viscosity method for assaying endoglucanase activity is also the basis for measuring the molecular weight of a polymer.

*This work was supported by the Office of Energy Research, Office of Basic Energy Sciences, Chemical Sciences Division of the U.S. Department of Energy under Contract No. DE-AC03-76SF00098 and by the Solar Energy Research Institute under Contract No. DX-4-04059-1.

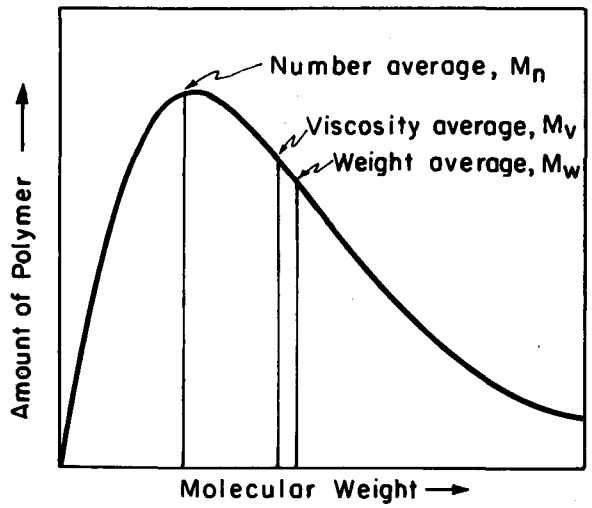

Figure 1. Molecular weight distribution of a typical polymer.[3] (XBL 839-6385)

M_v is related to the intrinsic viscosity of a polymer by the Mark-Houwink equation:

$$[\eta] = H(M_v)^x \quad , \tag{1}$$

where H and x are constants and $[\eta]$ is the intrinsic viscosity.[3] Intrinsic viscosity is a physical property of the polymer and is defined as a measure of the polymer's ability to increase the viscosity of a solvent in the absence of polymer-polymer interaction or at infinite dilution.[2] The relationship between viscosity and concentration that is most suited to CMC is the Baker relation:

$$\frac{\eta}{\eta_s} = \left(1 + \frac{[\eta]}{C_s}\right)^8, \tag{2}$$

where η_s is the solvent viscosity and η is the solution viscosity.[2] The Baker relationship is only valid for polymer solutions of low concentration.

This method of molecular weight determination is applied to the viscometric assay by measuring the viscosity change in a dilute solution with time once the enzyme has been added. Viscosity is related to M_n by the relation:

$$\eta \underset{(a)}{\longrightarrow} [\eta] \underset{(b)}{\longrightarrow} M_v \underset{(c)}{\longrightarrow} M_n \quad ,$$

where (*a*) is Eq. (2), (*b*) is Eq. (1), and (*c*) is the polydispersity.

CMC was used as a substrate for all the kinetic experiments; it is a cellulose ether produced by reacting alkali cellulose with sodium monochloracetate. Its structure is close to that of cellulose except that, on some of the monomer units, a carboxymethyl group ($-OCH_2COO^-$) is substituted for the hydroxyl group attached to the sixth carbon. While structurally similar to cellulose, CMC is water soluble. Therefore, it can be used to examine the kinetic behavior of endoglucanase or cellulase on long polymer chains.

The CMC used was medium viscosity; obtained from Sigma Chemical (No. C-4888), it had a reported viscosity average molecular weight of 250,000 daltons, an average degree of polymerization of 1100, and a degree or substitution of 0.7. The molecular weight of this lot of CMC ranged from 130,000 to 250,000 daltons as determined viscometrically. The CMC was dissolved in 0.05 *M* sodium acetate buffered to a pH of 5.0. The polydispersity was assumed to be two, and the Mark-Houwink constants from Eq. (1) were $H = 2.17 \times 10^{-5}$ and $x = 0.83$ (Ref. 2).

At low concentrations, CMC solutions are Newtonian fluids, but, at higher concentrations, they exhibit power-law behavior. For the kinetic experiments done in this study, the solution concentrations ranged from 10 to 30 g/L. The rheological behavior of CMC in this range is summarized in Table 1. In the concentration range used, CMC behaved as a power-law fluid. For the inhibition experiments, glucose and cellobiose were also added to the solutions, which did not affect the rheological behavior of the solution.

The mutant strain of *Trichoderma reesei*, Rutgers-C30, produced the cellulase enzyme used in this study. Endoglucanase and cellobiohydrolase are extracellular enzymes, while β-glucosidase is primarily cell-bound.[4] The fermentation broth was ultrafiltered with 0.005 *M* ammonium carbonate and concentrated to 238 grams of soluble protein per liter.[5] The raw cellulase had specific endoglucanase

Table 1. Rheology of concentrated, medium-viscosity CMC.

M_v (dalton)	CMC (g/L)	K[a] (P/sec)	n[a]	η_{app}[b] (cp)
280,000	10	0.816	0.87	37.4
250,000	30	41.7	0.65	512
	20	5.54	0.78	148
	10	0.424	0.89	21.9
130,000	30	5.47	0.80	165
	20	1.18	0.86	51.0

[a] $\tau = K(D)^n$, where τ is shear stress and D is shear rate.

[b] $\eta_{app} = K(D)^{n-1}$ for $D = 400\ sec^{-1}$.

activity of 6.0 units per mg of soluble protein and a specific β-glucosidase activity of 2.6 units per mg. A unit of activity is the micromoles of bonds broken or micromoles of reducing sugars produced per minute when an appropriate substrate is enzymatically reacted.

The cellulase was fractionated using ion exchange chromatography;[5] and seven separate peaks were collected. The results of the typical ion exchange are shown in Table 2. Fractions II and V showed significant endoglucanase activity. Fraction II was a low molecular weight protein that also had β-glucosidase activity. Fraction V was a high molecular weight protein with a very low β-glucosidase activity, approximately 96% pure endoglucanase, used in this study. Gel electrophoresis showed it to have two components. The major component had a molecular weight of approximately 66,000, and the minor component had a molecular weight of approximately 29,000. Each enzyme component obtained in the ion exchange was purified further by gel permeation chromatography (GPC). Fraction V-A was shown to be pure protein via gel electrophoresis, and it had a specific endoglucanase activity of 25.4 U/mg. The other peak, V-B, was also high in endoglucanase activity with a specific activity of 10.2 U/mg.

In order to correlate viscosity with intrinsic viscosity, and thus with molecular weight, it was necessary to obtain samples covering a range of molecular weights typical of those found over the assay reaction period. This was done by adding varying amounts of cellulase to a polymer solution and allowing the reaction to take place at 40°C for 5 minutes. The reaction was quenched by increasing the pH of the solution to 10, temporarily deactivating the enzyme. The cellulase was then denatured by heating the solution to 90°C for about 5 minutes, and the solution was returned to its original pH of 5.

Samples of different molecular weights were prepared this way, and the apparent viscosity of each sample was determined at the high substrate concentrations. Each sample was then diluted and its intrinsic viscosity measured. Correlation curves were developed in this manner for 10, 20, and 30 g/L CMC solutions. The relationships developed were used to correlate viscosity, η, to intrinsic viscosity, $[\eta]$, and were of the form,

$$[\eta] = a + b\eta \quad . \tag{3}$$

The values of a and b that were determined are listed in Table 3. These correlations are considered valid for CMC solutions of number average molecular weights ranging from 50,000 to 130,000.

A Couette viscometer was used to measure the rheology of the concentrated solutions, and a capillary viscometer was used to measure the viscosity of the dilute solutions. The assay, when performed in a Couette viscometer, was at a constant shear rate for the entire reaction period. The original viscosity of the CMC solution was measured, cellulase or endoglucanase was added to the solution, and the solution was returned to the viscometer. Viscosity change was measured with respect to time by measuring the change in torque with respect to time at a constant shear rate. A typical degradation curve is shown in Fig. 2. The reaction progress was recorded in this manner for approximately 5 minutes or until the viscosity change became very small. All assays were

Table 2. Cellulase enzyme description.

Cellulase fraction	Wt.% of total soluble protein	β-Glucosidase activity (U/mg)		Endoglucanase activity (U/mg)	
		ion exch.	gel perm.	ion exch.	gel perm.
Total cellulase	100.0	2.6		6.0	
I-A	10.1	27	146.0	0.32	1.0
I-B			7.3		0.4
II	31.0	4.2	0.2	16.0	27.2
III	17.3	0.03	0.05	1.3	3.7
IV	8.0	0.03	0.03	0.74	0.78
V-A	8.3	0.04	0.04	24.8	25.4
V-B	0.3		0.03		10.2
VI	11.4	0.05	0.09	1.6	5.0
VII	13.9	0.01	0.0	0.53	0.29

Source: Ref. 5.

Table 3. Parameters for viscosity–intrinsic viscosity correlation for medium viscosity carboxymethylcellulose.

CMC (g/L)	a[a]	b[a]
10	0.251	1.40×10^{-2}
20	0.254	2.51×10^{-3}
30	0.257	6.04×10^{-4}

[a]Parameters fitting Eq. (3).

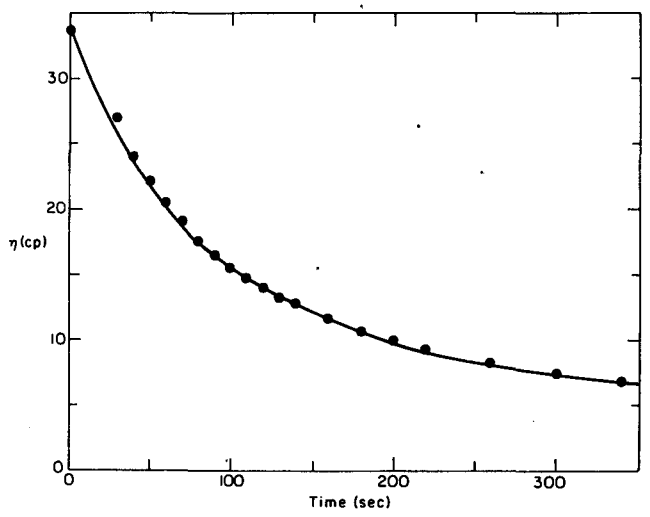

Figure 2. Effect of enzymatic degradation on solution viscosity. (XBL 839-6388)

performed at 40°C, which is near the optimum temperature of 45°C for cellulase activity and is consistent with kinetic experiments carried out by others.[2] Activity was determined from the slope of the linear portion of a plot of $1/M_n$ versus time according to Eq. (1). A typical plot is shown in Fig. 3. Activity was measured as a function of substrate concentration for different enzyme concentrations, and inhibition parameters were then determined for cellulase and endoglucanase. At a constant enzyme concentration, activity was measured at different cellobiose concentrations; these experiments were repeated using glucose. In order to determine the type of inhibition present, experiments were performed in which both glucose and cellobiose were added to the reaction mixture.

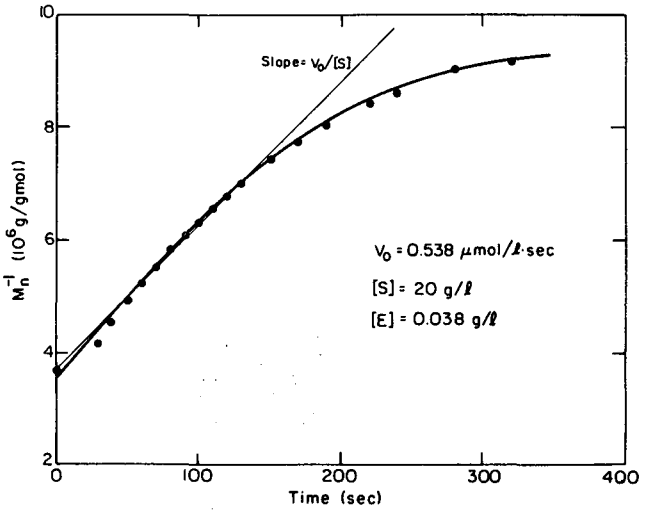

Figure 3. Activity determination for endoglucanase. (XBL 839-6389)

The kinetic parameters describing the behavior of endoglucanase were determined from experimental data. First, the effect of enzyme concentration on reaction velocity, v_o, was examined. Second, the role of glucose in endoglucanase regulation along with the effect of cellobiose on endoglucanase activity was considered. Third, the behavior of purified endoglucanase was compared to the behavior of endoglucanase in the presence of the other cellulolytic enzymes. Using initial rate models for activation and inhibition, kinetic parameters were fit to the data and incorporated into an overall model of endoglucanase behavior.

An assumption of Michaelis-Menten kinetics[6] is that the reaction velocity is directly proportional to the concentration of the enzyme substrate complex,

$$v_o = k_p[ES] \quad . \tag{4}$$

It then follows that the maximum reaction velocity is proportional to the total enzyme concentration,

$$V_{\max} = k_p[E_t] \quad , \tag{5}$$

where k_p is the rate constant for the product-forming step. Lineweaver-Burk plots were prepared for various enzyme concentrations, and $V_{\max}$ was determined at each concentration for both cellulase and endoglucanase. In the range of enzyme concentrations tested, $V_{\max}$ was a linear function of E_t as can be seen in Figs. 4 and 5.

The advantages of the Couette viscometric technique are that it can measure initial rates and allows the use of higher enzyme and substrate concentrations. On the basis of the consistency of the results of the kinetic studies, it is an effective method for studying initial rate kinetics. However, it is limited for the study of reaction progress versus time because the molecular weight distribution and how it changes with time is not known. If the initial value of the polydispersity can be determined exactly, then the assay can measure absolute activities rather than relative values.

While the $V_{\max}$ values may be slightly inaccurate, the values of the Michaelis constant and the inhibition and activation parameters will not be affected by a change in the value used for k. A serious limitation of the assay is that the dependence of the molecular weight distribution on time must be determined concurrently, such as with GPC.

Endoglucanase activity was evaluated assuming that Michaelis-Menten kinetics could be applied

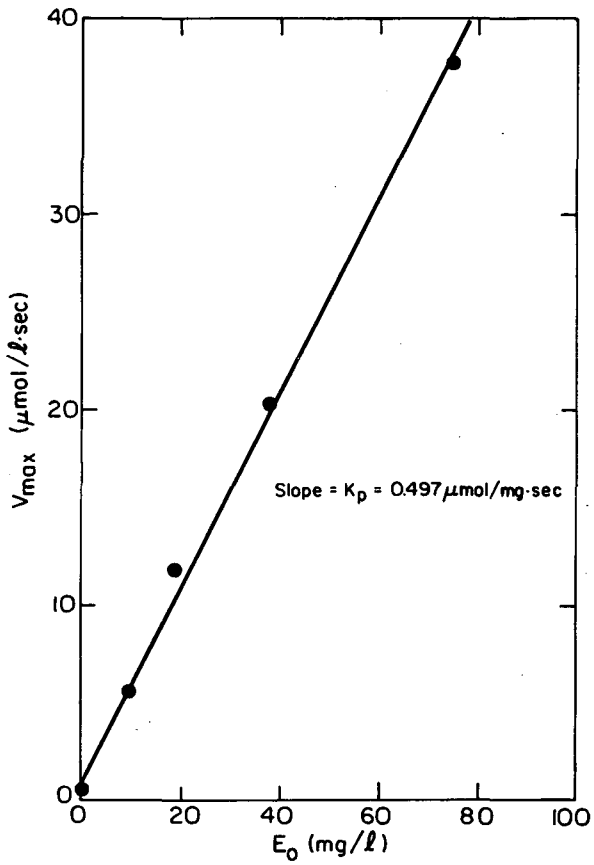

Figure 4. Determination of k_p for cellulase. (XBL 839-6390)

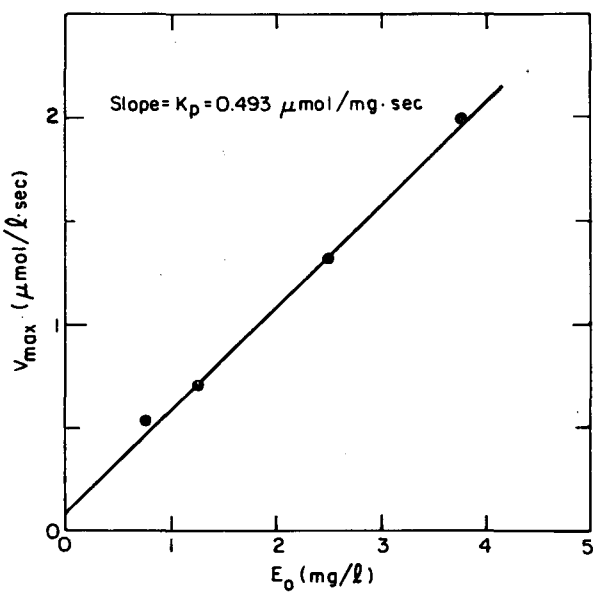

Figure 5. Determination of k_p for endoglucanase. (XBL 839-6391)

under the given experimental conditions. The assumptions on which the Michaelis-Menten model are based appear to be reasonable for the experimental conditions in this study. One of these assumptions is that V_{max} is directly proportional to the total enzyme concentration. As can be seen in Figs. 4 and 5, a linear enzyme dilution curve was obtained. Glucose and cellobiose have been identified as inhibitors of the cellulase system. Their effect on endoglucanase was studied. Cellobiose was found to inhibit endoglucanase via a partial mixed-type inhibition mechanism. Glucose, on the other hand, was found to be a nonessential activator of endoglucanase. The overall model of endoglucanase behavior can be represented schematically by Fig. 6. This is a model of a nonessential activator in competition with a partial mixed inhibitor. The values of the kinetic parameters for this model are summarized in Table 4.

PLANNED ACTIVITIES FOR FY 1985

The results reported here will be incorporated into an overall model for the cellulase system of enzymes derived from the *T. reesei* mutant strain Rut-C30.

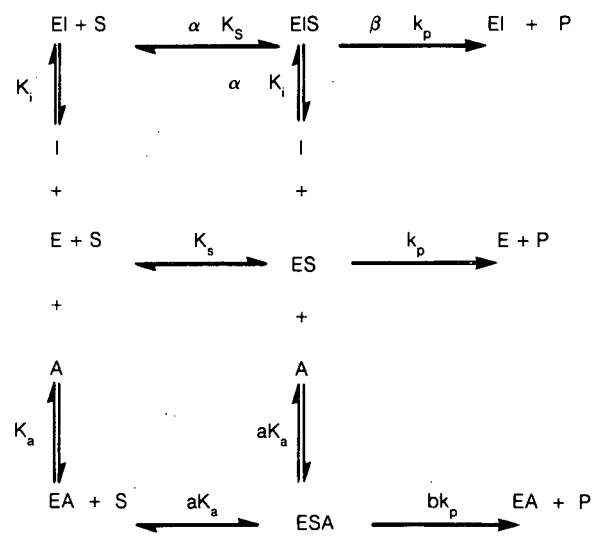

Figure 6. Schematic model of endoglucanase behavior: A nonessential activator in competition with a partial mixed-type inhibitor. (XBL 8311-4474)

Table 4. Kinetic parameters for endoglucanase activity.

	Cellulase	Endoglucanase
K_m	0.030	0.028
K_i	0.012	0.004
α	1.26	1.70
β	0.572	0.606
K_a	2.00	0.250
a	0.468	0.470
b	2.21	1.15

REFERENCES

1. Orichowskyj, S.T. (1982), "Recovery of Cellulase Enzymes by Countercurrent Adsorption," M.S. Thesis, University of California, Berkeley.
2. Almin, K.E., and Eriksson, K.E. (1967), "Enzymic Degradation of Polymers (I), Viscometric Determination of Enzymic Activity," *Biochim. Biophys. Acta. 139*, p. 248.
3. Billingham, N.C. (1977), in *Molar Mass Measurement in Polymer Science,* Wiley and Sons, New York.
4. Ghose, T.K. (1977), in *Advances in Biochemical Engineering,* Vol. 6, p. 39, T.K. Ghose, A. Fiechter, and N. Blakebrough, Eds., Springer-Verlag, Berlin.
5. Wiley, D. (1985), *Mechanism and Kinetics of Cellulose Hydrolysis,* Ph.D. Thesis, University of California, Berkeley.
6. Segel, I.H. (1975), in *Enzyme Kinetics,* Chapters 3–5, Wiley and Sons, New York.

Production of Sugars from Cellulose: Cellulase Production by *T. Reesei* in Continuous Culture in Lactose Medium*

(This article has been reprinted from the FY 1984 Annual Report.)

F. Castillo, H. Blanch, and C. Wilke

In the process of cellulose utilization, perhaps the most obvious area for major improvement is the production of cellulase enzyme for hydrolysis of wood and agricultural residues that can then be fermented into ethanol fuel. Nearly 50% of the cost of producing glucose from cellulosic material is attributed to enzyme production alone. Improvements in this step would therefore have dramatic impact and are important if economical hydrolysis processes are to be realized.

The first major thrust in this area has been the development of improved mutant strains of the filamentous fungus *Trichoderma reesei*, free from catabolite repression and capable of constitutive cellulase production. One such hyperproducing mutant, developed at Rutgers University (Rut-C30) and isolated,[1] presents an interesting potential for the development of processes aimed at the commercial production of cellulases.

Lactose is utilized by this microorganism; when it grows on this disaccharide, the enzymes of the cellulase complex are induced. This fact suggests that milk or cheese whey may be used as a medium to grow Rut-C30 and produce the enzymes. This procedure may also be an efficient method of whey treatment, reducing its high biological oxygen demand (BOD).[2,3] Additional advantages of whey utilization are its solubility and ease of handling as a fermentation medium compared to insoluble cellulose and its rich composition in nutrients[4,5] that may require only a few economical supplementations.

ACCOMPLISHMENTS DURING FY 1984

The objectives of this work are twofold: (1) to obtain information on the regulatory controls operating on the synthesis of the cellulases and (2) to study the effects of environmental variables on the production of the enzymes.

Rut-C30 strain was used throughout the experiments. The fermentation medium consisted of a double concentration of salt solution modified from that of Ryu *et al.*[6] to insure lactose limitation. It contained per liter: 25 g lactose, 4 g $(NH_4)_2(SO_4)$, 2 g KH_2PO_4, 0.3 g $MgSO_4 \cdot 7\ H_2O$, 0.15 g $CaCl_2 \cdot 2H_2O$, and 0.2 mL surfactant (Tween 80). For foam control, General Electric silicon AF-60 at 0.05 to 0.1

*This work was supported by the Assistant Secretary for Conservation and Renewable Energy of the U.S. Department of Energy under Contract No. DE-AC03-76SF00098 and by the Solar Energy Research Institute under Contract No. DR-0-9058-1.

v/v% was used. For continuous culture, a Chemap 20 L fermentor was used, with a 5 L reactor vessel (2.5 to 2.8 L working volume). Regulation of pH was carried out by automatic addition of 2 *N* ammonium hydroxide.

After samples were withdrawn aseptically from the reactor vessel, they were divided into two fractions: one was frozen whole while the second was filtered through 0.45 micrometer polycarbonate membranes, with the filtrate frozen until it was assayed. Assays for enzyme activities included determinations of filter paper activity, endoglucanase (CMCase), and cellobiohydrolase (cotton activity) by methods described previously[7]; cellobiase (β-glucosidase) and lactase (β-galactosidase) were assayed with p-nitrophenyl glucopyranoside (p-NPG) and o-nitrophenyl galactopyranoside as substrates, respectively, at 5 m*M* final concentrations. Activities of both enzymes as functions of temperature and pH indicated that, for cellobiase activity determined with p-NPG, the optimum pH was 4.6 and the optimum temperatures were 73°–75°C. For lactase activity, they were 4.6 and 62°–65°C, respectively.

The organism is a complete prototroph and grew well in this simple medium. Dry weight, intra- and extracellular protein, and total biomass (dry weight and extracellular protein) as functions of dilution rate are shown in Figs. 1 and 2. As can be seen, reduction of antifoam concentration from 0.1 to 0.05% produced slight increases in the cellular protein. In this medium, the maximum yield obtained was 0.486 g total biomass/per gram lactose utilized, and the maintenance coefficient was calculated at 6

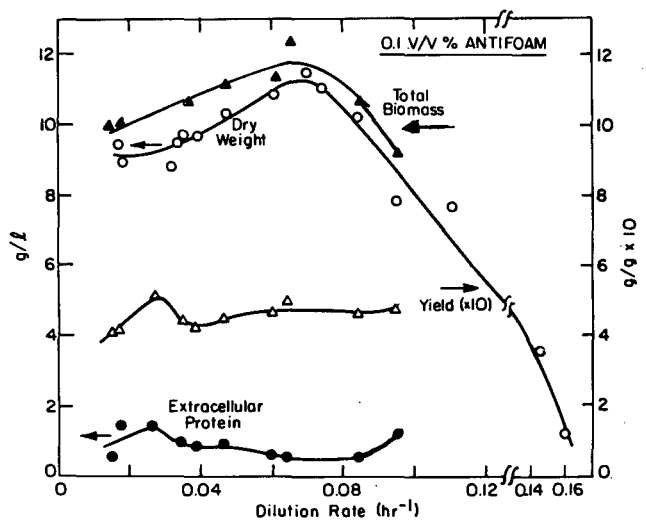

Figure 1. Various parameters of Rut-C30 growth in submerged culture vs. substrate (lactose) dilution rate in the presence of 0.1 v/v% antifoam. (XBL 8311-6604)

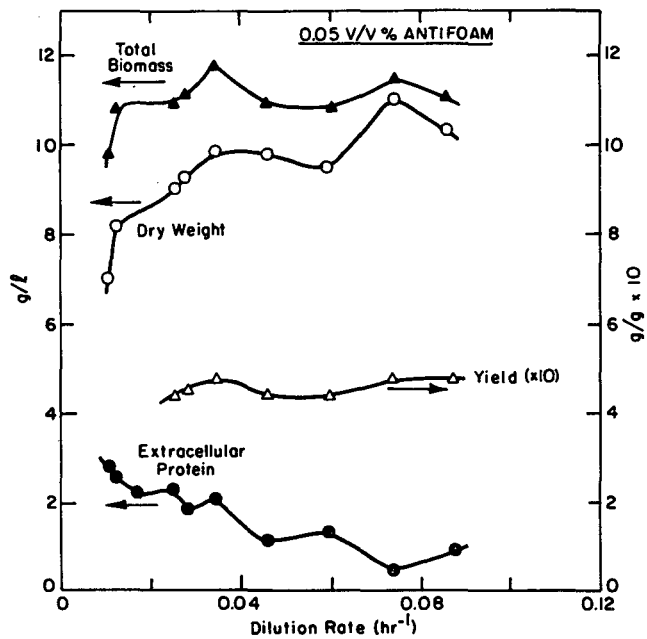

Figure 2. Various parameters of Rut-C30 growth in submerged culture vs. lactose dilution rate in the presence of 0.05 v/v% antifoam. (XBL 8311-6605)

mg lactose per gram of total biomass per hour. Maximum specific growth rate was 0.12 per hour, and the saturation constant for lactose was estimated at 0.763 g/L (0.77 m*M*).

The profiles of enzyme production and specific activities as functions of dilution rate when the medium contained 0.1% antifoam are shown in Figs. 3 and 4. In subsequent experiments, antifoam was not added and the foam was easily kept under control by reducing the aeration rate. The profiles obtained for production of the enzyme (Fig. 3) indicate the presence of dual regulatory mechanisms for the synthesis of the enzymes, their induction, and catabolite repression.[8]

The organism was found to produce a lactase, and the activity of this enzyme was assayed only in the filtrates. Although the enzyme was present outside of the cell, no significant levels of glucose were detected in the medium even at high dilution rates. This lactase may be excreted by the organism along with the other enzymes, or its presence in the medium may result from cell lysis or fragmentation caused by the high-speed agitation, or both.

To study the effects of temperature and pH on the production of the enzymes, the dilution rate was fixed. One parameter was varied at a time, and the

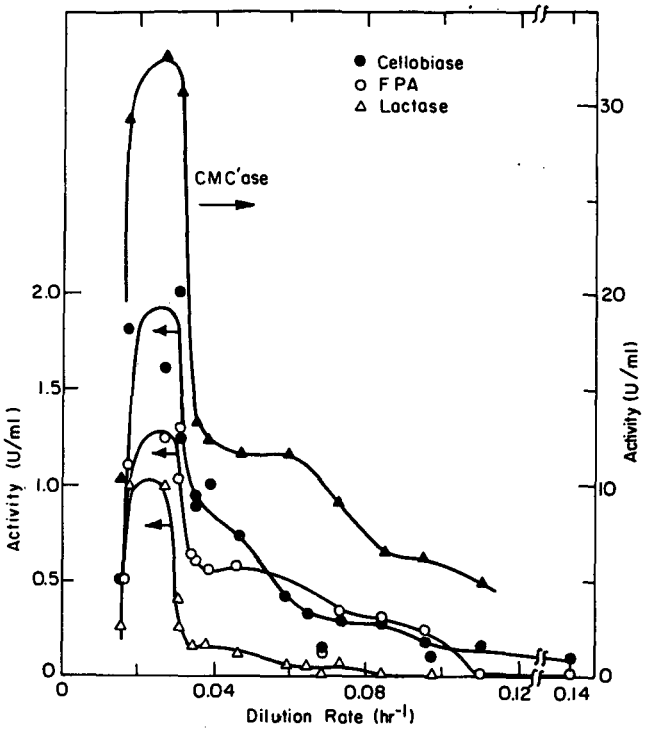

Figure 3. Growth profiles of enzyme components vs. dilution rate in the presence of 0.1 v/v% antifoam. (XBL 8311-6606)

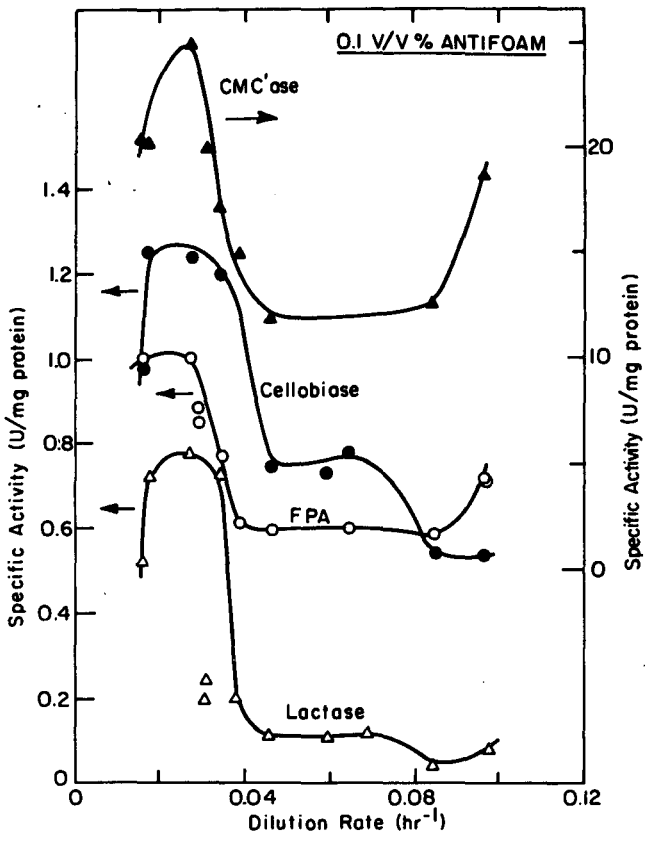

Figure 4. Specific growth profiles of enzyme components vs. dilution rate in the presence of 0.1 v/v% antifoam. (XBL 8311-6607)

new steady states were allowed to stabilize after each variation. Figures 5, 6, 7, and 8 show the steady-state values for biomass, protein, and enzymes as functions of temperature and pH.

For the next set of experiments, 26°C and pH 5 were selected and maintained. To study the effects of nutrient addition, pulses (equivalent to 1% of working volume) were added to the reactor vessel and the responses studied with respect to time. Addition of a yeast nitrogen base (YNB) pulse at 50 times the standard concentration produced increases in all of the enzymes (Fig. 9). When pulses of glucose or lactose were applied, transient decreases in the levels of all five enzymes were observed, such as would occur in catabolite repression. When the different groups of nutrients from YNB were tested separately, none induced the observed increase in enzyme productivity as when whole YNB was used.

Addition of the surfactant Tween 80 did increase the levels of the enzymes. Other nutrients and compounds used in the past, such as urea, proteose peptone, or corn-steep liquor, did not enhance enzyme levels. When the medium was shifted to 2 times the standard concentration, the original transient decrease in all enzymes was followed by an increase to new high levels.

PLANNED ACTIVITIES FOR FY 1985

Capital and energy costs concentrate in the enzyme production step of the biomass hydrolysis process. When steam-exploded wood is used as the cellulose source, in the overall process, about 12% of the total input is used in enzyme production. Process economic evaluation indicates that the use of delignified or soluble carbon sources such as lactose in whey is favorable in fed-batch or continuous cultivation, respectively. The optimum conditions for the initial batch period using this substrate will be determined. The effect of feeding regimes and aeration conditions on enzyme production will be studied. Experiments in which application of pulses with combinations of different groups of nutrients and use of a more concentrated medium are contemplated.

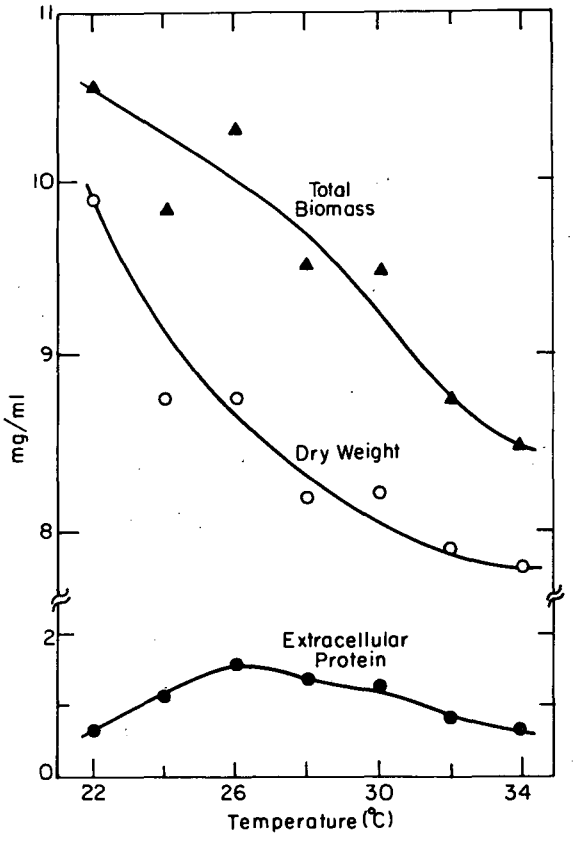

Figure 5. Steady-state growth of Rut-C30 vs. temperature. (XBL 8311-6608)

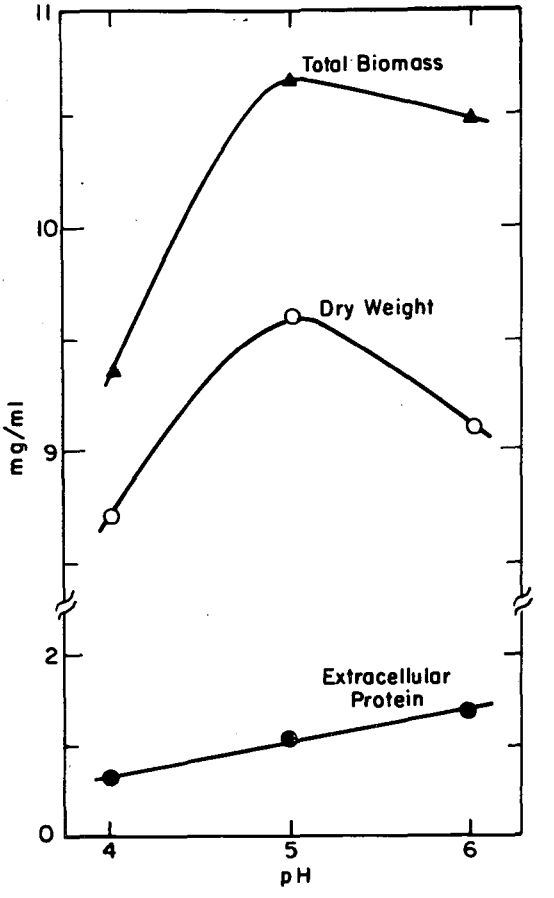

Figure 7. Steady-state growth of Rut-C30 vs. pH. (XBL 8311-6610)

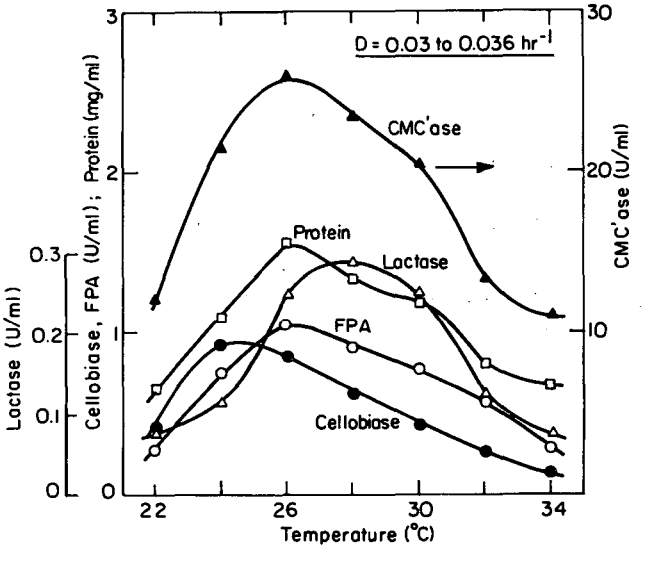

Figure 6. Growth profiles of enzyme components vs. temperature at dilution rates of 0.03 to 0.036 hr^{-1}. (XBL 8311-6609)

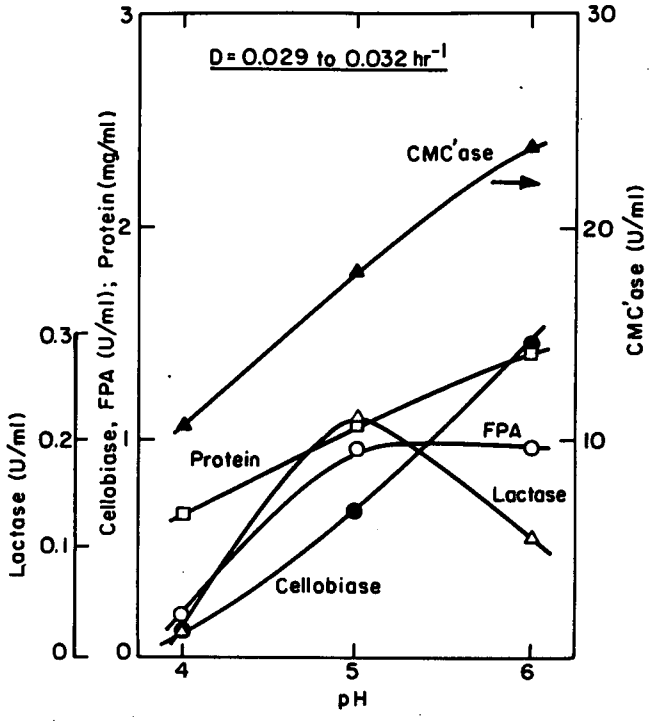

Figure 8. Growth profiles of enzyme components vs. pH at dilution rates of 0.029 to 0.032 hr^{-1}. (XBL 8311-6611)

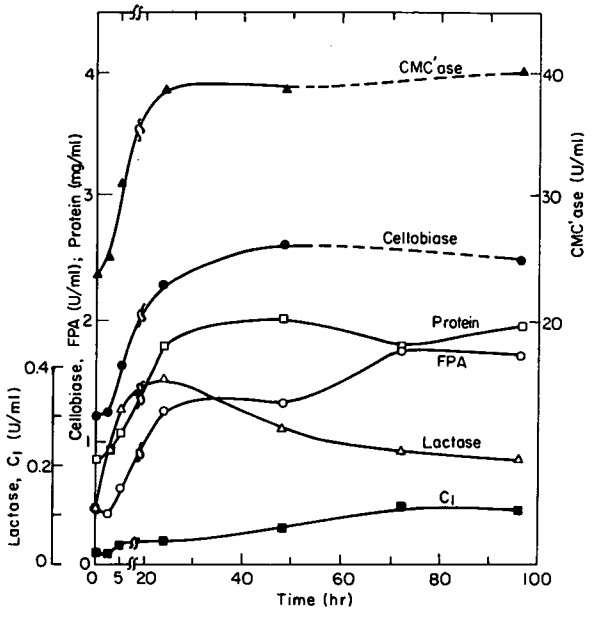

Figure 9. Growth of enzyme components over time with added yeast nitrogen base, 30 mL, 50× standard concentration. (XBL 8311-6612)

REFERENCES

1. Montenecourt, B.S. and Eveleigh, D.E. (1977), "Preparation of Mutants of *T. reesei* with Enhanced Cellulase Production," *Appl. Environ. Microbial. 34*, p. 777.
2. Kosikowski, F.V. (1977), *Cheese and Fermented Milk Foods,* Edward Brothers, Inc., Ann Arbor, Michigan.
3. Wix, P. and Woodbine, M. (1958), "The Disposal and Utilization of Whey; a Review," *Dairy Sci. Abstracts 20*, p. 537, Part 1; p. 621, Part 2.
4. Mairopoulou, I.P. and Kosikowski, F.V. (1972), "Composition, Solubility and Stability of Whey Powders; Free Amino Acids and Soluble Peptides of Whey Powders," *J. Dairy Sci. 56*, p. 1128, Part 1; p. 1135, Part 2.
5. Glass, L. and Hedrick, T.I. (1977), "Nutritional Composition and Major Factors Including Amino Acids in Sweet and Acid Type Dry Wheys; Vitamins, Mineral and Calorie Contents of Dry Wheys," *J. Dairy Sci. 60*, p. 185, Part 1; p. 190, Part 2.
6. Ryu, D., Andreotti, R., Mandels, M., Gallo, B., and Reese, E.T. (1979), "Studies on Quantitative Physiology of *Trichoderma reesei* with Two-Stage Continuous Culture for Cellulase Production," *Biotechnol. Bioeng. 21*, p. 1887.
7. Wilke, C.R. and Blanch, H.W. (1981), *Bioconversion of Cellulose,* LBL-14219.
8. Toda, K. (1981), "Induction and Repression of Enzymes in Microbial Culture," *J. Chem. Tech. Biotechnol. 31*, p. 775.

ELECTROCHEMICAL ENERGY STORAGE RESEARCH

Technology Base Research Project for Electrochemical Energy Storage*

E.J. Cairns, K. Kinoshita, and F.R. McLarnon

The Lawrence Berkeley Laboratory (LBL) is lead center for management of the Technology Base Research (TBR) Project, which is supported by the Electrochemical Branch of DOE's Office of Energy Storage and Distribution. The purpose of this project is to provide the research base to support DOE efforts to develop electrochemical energy conversion systems for electric vehicle and stationary energy storage applications. The specific goal is to identify the most promising electrochemical technologies and transfer them to industry and/or another DOE program for further development and scale-up.

The TBR project is divided into three major elements: Exploratory Research, Applied Science Research, and Air Systems Research. The generic research topics included in each of these elements are listed in Table 1.

The general research areas addressed by the TBR Project include identification of new electrochemical couples for advanced batteries, determination of technical feasibility of the new couples, improvements in battery components and materials, establishment of engineering principles applicable to electrochemical energy storage and conversion, and the investigation of fuel cell and metal/air systems for transportation applications. Major emphasis of the project is given to applied research that will lead to superior performance and lower life-cycle costs.

The LBL scientists who participate in the program are E.J. Cairns, K. Kinoshita, and F.R. McLarnon of the Applied Science Division, and L.C. DeJonghe, J.W. Evans, R.H. Muller, J.S. Newman, P.N. Ross, and C.W. Tobias of the Materials and Molecular Research Division.

Table 1. Topics covered by the Technology Base Research Project for Electrochemical Energy Storage.

I. EXPLORATORY RESEARCH
- New Rechargeable Electrochemical Cells
- Thermally Regenerative Cells

II. APPLIED SCIENCE RESEARCH

A. Engineering-Science Research
- Electrode Morphological Studies, Chemical/Structural Analysis
- Transport Phenomena, Electrocatalysis, Electrode Kinetics,and Cell Thermodynamics
- Modeling of Electrochemical Cells and Battery Systems
- Advanced Physicochemical Methods for Electrochemical Research

B. Materials Research
- Ceramic, Molten-Salt, Glass, and Polymeric Electrolytes
- Corrosion Problems in Electrochemical Storage Devices
- Novel Electrode Structures
- New Component Fabrication Techniques
- Battery Separators

III. AIR SYSTEMS RESEARCH
- Air Electrodes
- Metal/Air Cells
- Fuel Cells
- New Electrolytes
- New Electrocatalysts

ACCOMPLISHMENTS DURING FY 1985

LBL conducted a vigorous in-house research program and monitored 30 subcontracts during FY 1985. A description of the research projects conducted by the subcontractors can be found in the recent annual report, *Technology Base Research Project for Electrochemical Energy Storage* (LBL-19545), and the in-house work, "Electrochemical Energy Storage," is summarized in the next article and in the *Materials and Molecular Research Division 1985 Annual Report* (LBL-20230). Highlights of the subcontracted work follow.

*This work was supported by the Assistant Secretary for Conservation and Renewable Energy, Office of Energy Storage and Distribution of the U.S. Department of Energy under Contract No. DE-AC03-76SF00098.

Exploratory Research

- Duracell has continued their investigation of a novel rechargeable $Li/LiAlCl_4-SO_2/C$ cell that offers attractive specific energy (524 Wh/kg theoretical), stability of the lithium electrode, and the ability to withstand limited overcharge. All of these are attractive characteristics for a secondary lithium cell. Duracell has now achieved 60–90 cycles (100% depth-of-discharge) to 2.6 V cutoff in small cells (0.5 Ah). A gradual loss in capacity of about 1% per cycle is observed, which is attributed to the poor mechanical structure of the positive electrode, and electrolyte starvation on deep discharge.
- Experimental measurements at the University of Pennsylvania demonstrated that divalent cations (Mg^{2+} and Pb^{2+}) can be ionic conductors in poly(ethylene oxide); this result is contrary to early predictions. This study could lead to new classes of secondary batteries using polymeric electrolytes.
- Dow Chemical completed their investigation of a new high-temperature Na/S cell that uses a glassy electrolyte. They recently found that the corrosion of glasses D406 ($Na_2O-2\ B_2O_3-0.2\ SiO_2-0.16$ NaCl) and T806 ($Na_2O-1.1\ B_2O_3-1.3\ SiO_2$) by sulfur at 400°C is virtually stopped by the addition of 0.5 wt% of a hydrocarbon polymer (poly(4-methyl-1-pentene)) to sulfur.

Applied Science Research

- Argonne National Laboratory (ANL) has achieved over 375 cycles (3500 hour) at 397°C with a small prismatic cell (25 Ah) with a dense upper-plateau FeS_2 electrode, a Li-Al negative electrode, and LiCl-LiBr-KBr electrolyte (m.p. 310°C). Cell data indicate a 50% increase in specific energy and specific power (versus a standard two-plateau cell), and utilization is about 85% with virtually no loss in capacity after more than 375 cycles. If comparable performance is achieved with realistic cell hardware, this cell chemistry could lead to a very high-performance battery (>200 W/kg, >180 Wh/kg).
- Experimental studies at Rockwell International, Inc. indicate that ZrO_2-toughened β''-alumina should contain between 10–15 vol% ZrO_2 to obtain the optimum strength and ionic conductivity. Ceramatec, Inc., is now investigating techniques to process this new material into practical electrolyte tubes.
- ANL has identified a glass composition (42 mol% Na_2O–8 mol% Al_2O_3–5 mol% ZrO_2–45 mol% SiO_2) that has chemical stability (at 400°C in Na, Na_2S_3, Na_2S_4, and S) on a par with other candidate solid electrolytes, β''-alumina and DOW glass, for use in high-temperature Na/S cells.
- A family of glasses with composition analogous to NASIGLAS ($Na_{1+x}Zr_{2-x}/3Si_3P_{3-x}O_{12-2x}/3$) has been synthesized by the Massachusetts Institute of Technology. The conductivity at 350°C for several of the sodium-based glasses is as high as 10^{-4} $ohm^{-1}cm^{-1}$.
- Brookhaven National Laboratory (BNL) has continued their investigation of the kinetics of Zn deposition in Zn/halogen cell environments. Measurements at BNL show that the presence of Ca on a Zn surface does not inhibit layer growth, but it does accelerate the kinetics for Zn deposition in acid electrolytes. On the other hand Cd on Zn surfaces appears to inhibit layer growth and accelerate nucleation.
- Lawrence Livermore National Laboratory (LLNL) has extended their measurements of mutual diffusion coefficients for aqueous, high-purity $ZnCl_2$ systems at 25.00 ± 0.005°C. Measurements have been completed for 2.4999 M $ZnCl_2$–1.25 M KCl and 2.5001 M $ZnCl_2$–4.0002 M KCl.
- Raman spectroscopy studies at ANL of Zn^{2+} in concentrated KOH show conclusively that there is only one dominant Zn^{2+} coordination environment; Zn^{2+} ions are probably present in an octahedral or tetrahedral complex with Zn^{2+} to hydroxyl linkages.

Air Systems Research

- Energy Research Corporation has demonstrated that perovskite-catalyzed bifunctional air electrodes can operate for >800 cycles at 10/20 mA/cm^2 (charge/discharge), with stable overpotentials of 600/−280 mV with respect to a Hg/HgO reference electrode. This performance is comparable

to prior Westinghouse technology, yet the catalyst composition is simpler, and corrosion of the perovskites does not appear to be a problem.

- Pinnacle Research Institute was selected for research on metal/air batteries on the basis of proposals received in response to a Request for Proposals (RFP) by LBL. Their program will involve research and development of particulate zinc electrodes for Zn/air batteries, with emphasis on optimizing the charge and discharge characteristics of these electrodes.
- ELTECH Systems, Inc., has continued their role as prime contractor for research and development of the Al/air battery. A 5-cell Al/air stack was assembled at ELTECH Systems Corp. and testing is under way. Performance using 99.999% aluminum anodes agrees with the values calculated from the performance of individual components.
- ELTECH Systems, Inc., is now testing aluminum alloys containing 0.1% In and 0.05% Ga that show a low corrosion rate (11 mA/cm^2 at open circuit and 7 mA/cm^2 at 600 mA/cm^2) and reasonable potentials (1.76 V open-circuit potential and 1.35 V at 600 mA/cm^2) in 4 N NaOH at 60°C.
- Los Alamos National Laboratory (LANL) has continued their role as Technology Center for fuel cell R & D. Studies at LANL on steam-reforming of methanol, which is the preferred portable fuel for fuel cells, suggest that rapid oxygen exchange occurs on the catalyst (Cu-ZnO) surface. Experimental evidence indicates that methanol adds to an oxide vacancy and reacts with lattice oxygen atoms to generate CO_2.
- United Technologies Corp. has found that the performance of iron TMPP supported on Black Pearls 2000 in a phosphoric acid fuel cell increases with the heat-treatment temperature of the catalyst. The O_2-reduction performance reaches a maximum with a catalyst that is heat-treated at 950°C.
- Experiments at the University of Virginia suggest that for Pt-Cr alloys, the composition range of greatest interest for fuel-cell applications is within the ordered solid-solution structure between 17 and 35 a/o Cr.

PROGRAM CHANGES IN 1985

Funding support for the following projects was initiated in 1985:

- Spectroscopic Studies of the Passive Film on Alkali and Alkaline Earth Metals in Non-Aqueous Solvents. A Surface Science Approach—Case Western Reserve University;
- Battery Separator Research—Sandia National Laboratory;
- Technology Base Research on Zinc/Air Battery Systems—Pinnacle Research Institute.

Funding support for the following projects ended in 1985:

- Research on Materials Relating to the Sodium Heat Engine—Ford Motor Company;
- Improve the Lifetime of the Hollow Fiber Sodium/Sulfur Cell—Dow Chemical Company;
- Reaction Profiles in Porous Electrodes—Lockheed Missiles & Space Company;
- Semiconductor Electrochemistry Approach to the Study of Oxide Films—SRI International;
- Research on Separators for Alkaline Zinc Batteries—Pinnacle Research Institute;
- Zinc/Nickel Oxide Battery Membrane Separator Studies—Brigham Young University;
- Development of Bifunctional Oxygen Electrodes for Alkaline Metal-Oxygen Rechargeable Cells—Energy Research Corporation.

PLANNED ACTIVITIES FOR FY 1986

New initiatives include the following:

- Selections will be made from proposals on research and development of novel concepts for rechargeable lithium cells submitted in response to a Request for Proposals (RFP) issued by the TBR Project.
- Applied research will be conducted on the characterization of components for secondary batteries.

Battery Electrode Studies*†

E.J. Cairns, F.R. McLarnon, T.C. Adler, M.J. Isaacson, R. Jain, P.M. Lessner, K.G. Miller, S.A. Naftel, M.L. Smith, K.A. Striebel, and J. Winnick‡

The purpose of this research is to study the behavior of electrodes used in secondary batteries and to investigate practical means for improving their performance and lifetime. Systems of current interest include ambient-temperature rechargeable cells with zinc electrodes [Zn/air, Zn/NiOOH, Zn/AgO, Zn/Cl_2, Zn/Br_2, and $Zn/Fe(CN)_6^{-3}$]; rechargeable high-temperature cells (Li/S, $Li\text{-}Al/FeS_2$, $Li\text{-}Si/FeS_2$, and Na/S); fuel cells; and liquid-junction photovoltaic cells. The approach used in this investigation is to study life- and performance-limiting phenomena under realistic cell operating conditions.

ACCOMPLISHMENTS DURING FY 1985

Measurement of Concentrations in Porous Zinc Electrodes Using Micro-electrodes

(M.J. Isaacson, F.R. McLarnon, and E.J. Cairns)

The purpose of this work is to develop reference micro-electrodes as useful analytical tools, and use them to measure species concentration changes in secondary porous zinc electrodes. Cadmium, zinc, and α-palladium reference micro-electrodes are currently being investigated. The use of cadmium electrodes was discontinued due to poor stability. Stable and reproducible Zn electrode potentials were measured at various hydroxide and zincate concentrations; the results shown in Fig. 1 agree with and supplement the work of Dirkse,[1] and Hampson, Herdman, and Taylor.[2] Some α-Pd potential measurements in zincate-containing alkaline electrolytes are shown in Fig. 2.

Electrochemical cells are currently being fabricated for the porous electrode experiments. The cell provides for as many as eleven Zn and α-Pd electrodes. A multiplexer controlled by a microcomputer monitors the micro-electrodes while the cell is being charged and discharged. Future work will emphasize the implementation and interpretation of the porous electrode experiments.

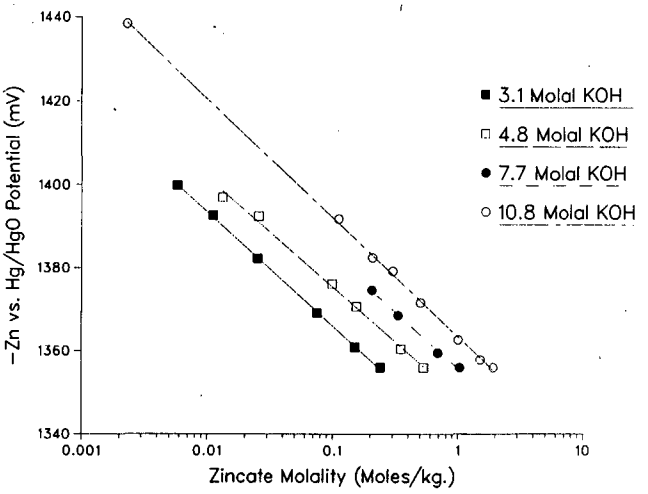

Figure 1. Variation of zinc electrode rest potential with $K_2Zn(OH)_4$ molality at constant hydroxyl-ion molality. Potentials are measured versus an Hg/HgO reference electrode in the same solution, and the temperature is 25°C. (XBL 861-242)

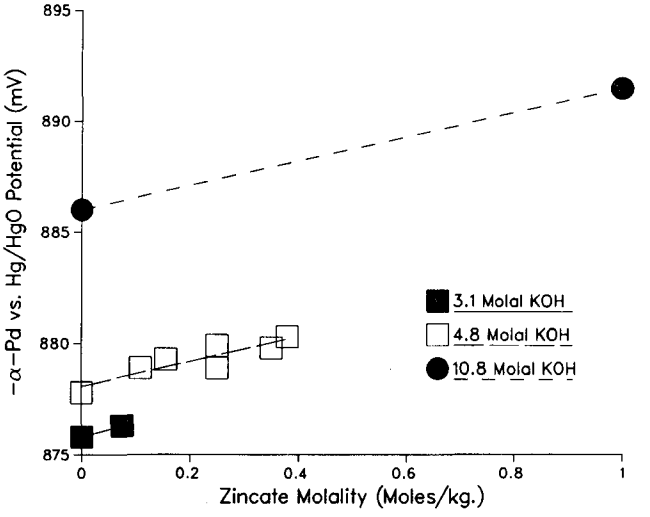

Figure 2. Variation of α-Pd electrode rest potential with $K_2Zn(OH)_4$ molality at constant hydroxyl-ion molality. Palladization is approximately 55 coulombs/cm^2, potentials are measured versus an Hg/HgO reference electrode in the same solution, and the temperature is 25°C. (XBL 861-243)

*This work was supported by the Assistant Secretary for Conservation and Renewable Energy, Office of Energy Storage and Distribution of the U.S. Department of Energy under Contract No. DE-AC03-76SF00098.

†This project is part of a larger effort, "Electrochemical Energy Storage," described in the Materials and Molecular Research Division 1985 Annual Report.

‡Department of Chemical Engineering, Georgia Institute of Technology, Atlanta, GA.

The Effect of Calcium Hydroxide on Secondary Zinc Electrodes

(R. Jain, F.R. McLarnon, and E.J. Cairns)

The aim of this research is to investigate the addition of calcium hydroxide to the zinc electrode as a practical means of reducing zinc species solubility in strong alkaline electrolytes. The reduced zinc solubility is expected to slow the rate of active material redistribution in the zinc electrode, thereby increasing its cycle life.

Identical pairs of zinc electrodes, containing 0%, 10%, 25%, and 40% $Ca(OH)_2$ by weight, were fabricated. Fabrication, cell assembly, and cycling procedures were similar to those used by J.T. Nichols, *et al.*[3] and M.H. Katz *et al.*[4] All negative electrodes had the same dry weight, so as more $Ca(OH)_2$ was added, less excess zinc was used. Two sintered nickel oxide positive electrodes were used in a cell, and the $Ca(OH)_2$-free zinc electrodes had 3.0 times the capacity of the NiOOH electrodes. The electrolyte was ZnO–saturated 31 wt% KOH-1 wt% LiOH. The 1.3-Ah cells were charged at a 5-hour rate and discharged at a 2.5-hour rate, limited by either the cell voltage or the zinc electrode potential.

The $Ca(OH)_2$-free electrode showed significant zinc redistribution after cycling. Many areas of the electrode were bare of zinc or showed very little material. The general direction of material movement was away from the center of the electrode, but some dense island regions of zinc remained in the central area. The material near to the electrode edges was also dense.

The 10%-$Ca(OH)_2$ electrodes also showed considerable zinc redistribution. Again, the general direction of material movement was away from the center of the electrode. However, unlike the $Ca(OH)_2$-free electrode, there were no bare areas and there remained a uniform "background" amount of zinc material over the electrode. KEVEX x-ray analysis showed that this material was a calcium-zinc compound. These electrodes also had dense island growths in the center and dense growths at the edges, and analysis showed these regions to be predominantly Zn. The overpotential of the negative electrode in the 10%-$Ca(OH)_2$ cell was slightly greater than that in the $Ca(OH)_2$-free cell.

The 25%-$Ca(OH)_2$ cells appeared to behave the best of the cells tested. Again, there was general zinc material movement toward the edges of the negative electrodes. However, for these electrodes there were fewer dense island regions and less thickening at the electrode edges. Also, there was significantly more background zinc material. Cells x-rayed at cycles 100 and 150 showed very few differences, implying that the background zinc material is fairly stable. The zinc-electrode overpotential in the 25%-$Ca(OH)_2$ cell was higher than that of the 10%-$Ca(OH)_2$ cell. Also, the current density during charge had to be decreased by 25% for the cell to function properly.

The 40%-$Ca(OH)_2$ cells operated for only a few cycles. They displayed high overpotentials, and their operation would have required charge currents which would have been too low to be practical.

Scanning Electron Micrographs were taken of various regions of the electrodes; KEVEX x-ray analysis, x-ray fluorescence analysis, atomic adsorption analysis, and powder x-ray diffraction studies were also performed, and zinc material balances were obtained.

The Effect of Pulse-Charging Regimes on the Cycle-Life Performance of Zinc/Nickel Oxide Cells

(T.C. Adler, F.R. McLarnon, and E.J. Cairns)

Previous studies of the effect of pulse charging on the cycle-life performance of Zn/NiOOH cells employed sheet current collectors[4] or were cycled at a low depth of discharge.[5] The purpose of this study is to evaluate promising pulse-charging regimes using mesh current collectors and a demanding (100% depth of discharge) cycling regimen.

Several pulse-charging modes were evaluated in which the frequency, peak current density (pcd), and on-time/off-time ratios were varied. A cell pulse-charged at a pcd of 15.7 mA/cm^2, 30 ms on/90 ms off, retained over two-thirds of its zinc-covered area when cycling was stopped at cycle 125. Comparison of SEM photographs of the discharged zinc electrodes for cells charged with constant current showed the pulse-charged zinc electrode to have a more densely textured surface than the constant-current charged electrode. This effect may be attributed to the larger number of nucleation sites generated during pulse-charging.

Mathematical Modeling of the Zinc Electrode

(K.G. Miller, F.R. McLarnon, and E.J. Cairns)

Factors limiting the cycle life of the zinc electrode are redistribution of active material over the face of the electrode[6,7] and passivation.[8] A one-dimensional, time-dependent model is being developed to predict the cause and extent of Zn

redistribution and passivation as the electrode is cycled. This model will take into account changes in current density, overpotential, and species concentration. The equations for the model are complete, and the appropriate computer program is being written.

Transient potential and current step experiments have been carried out to determine exchange current densities for the zinc electrode in electrolytes of various KOH and zincate concentrations. The 99.999% pure Zn disc electrodes were fabricated from 1-mm diameter wires polished with successive abrasives to a final polish with 0.3μ Al_2O_3. Zinc counter and reference electrodes were used, and the electrolyte solutions were deaerated. Preliminary results for experiments of 200 ms duration show exchange current densities in the 0.1–0.25 mA/cm^2 range. Subsequent experiments will employ 98% Zn–2% Pb electrodes, as well as pure Zn deposited onto a Pb substrate, in order to simulate the conditions expected in a working cell.

Mathematical Modeling of the Sodium/Sulfur Cell

(S.A. Naftel, F.R. McLarnon, and E.J. Cairns)

A set of equations has been developed to describe the behavior of the sulfur electrode in sodium/sulfur cells. The mathematical description takes into account the effects of diffusion, convection, and migration on the behavior of the electrode, unlike that of previous work.[9,10] An attempt will be made to measure ionic potentials throughout the cathode, in order to confirm the results of modeling. An additional experiment to measure the capillary pressure of sulfur and Na_2S_x in graphite felt has been designed in order to obtain data necessary for predicting convective and wicking effects.

Glass Electrolytes for Lithium/Sulfur Cells

(M.L. Smith, J. Winnick, F.R. McLarnon, and E.J. Cairns)

Novel Li/S cells, which employ a fast-lithium-ion conducting lithium chloroborate glass as the solid electrolyte, have been built and operated at 400°C. The composition of glass used for this study,[11] 7.3 mol% $(LiCl)_2$, 25.7 mol% Li_2O, and 67.0 mol% B_2O_3, had an ionic conductivity of 2.9×10^{-3} $(\Omega^{-1}\cdot cm^{-1})$ at 400°C, which was somewhat lower than those of other lithium chloroborate glasses,[12] which have shown ionic conductivities as high as 2×10^{-2} $(\Omega^{-1}\cdot cm^{-1})$.

The current-voltage characteristics of these cells were examined; they were found to be capable of supporting pseudo-steady-state current densities up to 15 mA/cm^2 for 15–20 hours. A limiting current was found to exist at approximately 23 mA/cm^2. These cells could be charged and discharged with approximately equal polarization in either direction. However, the accumulation of a crystalline reaction layer on the surface of the electrolyte during discharge caused the cells to fail before the completion of a full charge-discharge cycle.

These cells were also used to measure the the solubility of lithium (as a polysulfide) in sulfur. The solubility limit was found to occur at $0.04\ ^{+0.03}_{-0.01}$ mol% Li at 400°C. This is in agreement with the value reported by Sharma.[13]

Oxygen Reduction on Platinum in Fuel Cell Electrolytes

(K.A. Striebel, F.R. McLarnon, and E.J. Cairns)

Preliminary rotating ring–disk electrode (RRDE) studies of oxygen reduction in dilute Cs_2CO_3 and KOH showed that solutions with higher carbonate anion concentrations supported higher oxygen reduction currents.[14,15] These experiments have been supplemented by a series of RRDE experiments in mixed electrolytes (KOH, KCO_3 and KF) with the aim to identify the independent effects of ionic strength, pH, and carbonate anion concentration. At a constant ionic strength of 0.7M, both OH^- and $CO_3^=$ appear to have a positive effect on the kinetic current at 0.9 V vs Reference Hydrogen Electrode (RHE), with the highest kinetic currents observed when both of these ions are present. Peroxide is generated as an unwanted side product and is detected with the ring during a RRDE experiment. Carbonate ion appears to suppress peroxide formation while OH^- appears to increase peroxide formation.

Oxygen reduction experiments in K_2CO_3 and KOH have been completed at concentrations up to 1.0M. When results are adjusted for differences in oxygen solubility, kinetic currents (at 0.9 V vs RHE) are 2 to 2.5 times higher in K_2CO_3 than in KOH at the same concentration. However, lower oxygen solubilities in carbonate electrolytes may lead to higher mass transfer overpotentials in a fuel cell.

Two new all-PTFE cells have been designed and built to carry out measurements at elevated temperatures in more concentrated alkaline electrolytes, on both smooth platinum and supported-platinum gas-diffusion electrodes.

Engineering Analysis of Photoelectrochemical Cells

(P.M. Lessner, J. Winnick, F.R. McLarnon, and E.J. Cairns)

We are studying the electrochemistry of the aqueous polysulfide redox couple because of its potential application in energy conversion and storage devices such as photoelectrochemical cells and redox batteries.[16–18] Our efforts have concentrated on the fundamental measurement of kinetic and transport parameters by a transient potential step method, steady-state measurements on rotating disk electrodes, modifications of solution chemistry through addition of organic cosolvents, and construction and testing of porous electrodes.

The transient potential step method was used to obtain data on exchange current density and active species concentration.[19–21] The applicability of this technique in the low (linear) overpotential region has been well analyzed.[22,23] Cobalt was chosen as the electrocatalyst for most of the studies, but platinum and MoS_2 were also used. Experiments were performed over the temperature range of 25–80°C. The cell used for these experiments was constructed of a 1/2-inch nylon tube cross, wrapped in heating tape and insulation for operation at elevated temperature. Data were recorded on a digital storage oscilloscope over a time interval of several milliseconds. An attempt was made to fit (using nonlinear least squares)[24] each data set to an analytical expression for a current-time transient for a multistep redox reaction under kinetic-diffusion control.[23] At temperatures below about 48°C the fit was good, but as temperature increased the fit became poor. A fit to the short-time data at higher temperatures underestimated the experimental currents at longer times.

The overall reaction in the aqueous polysulfide electrolyte can be written:

$$1/3S_4^{2-} + 4/3H_2O + 2e^- \rightleftarrows 4/3HS^- + 4/3OH^- \quad (1)$$

The points in Fig. 3 show a plot of the active species concentration versus temperature which was determined from the fitting procedure mentioned above. The bulk concentrations of the species in Reaction 1 are orders of magnitude higher than the concentration of the active species determined from the potential step measurements. The radical anion S_2^- (supersulfide) is in equilibrium with tetrasulfide:

$$S_4^{2-} \rightleftarrows 2S_2^- \quad (2)$$

Its concentration was evaluated from published

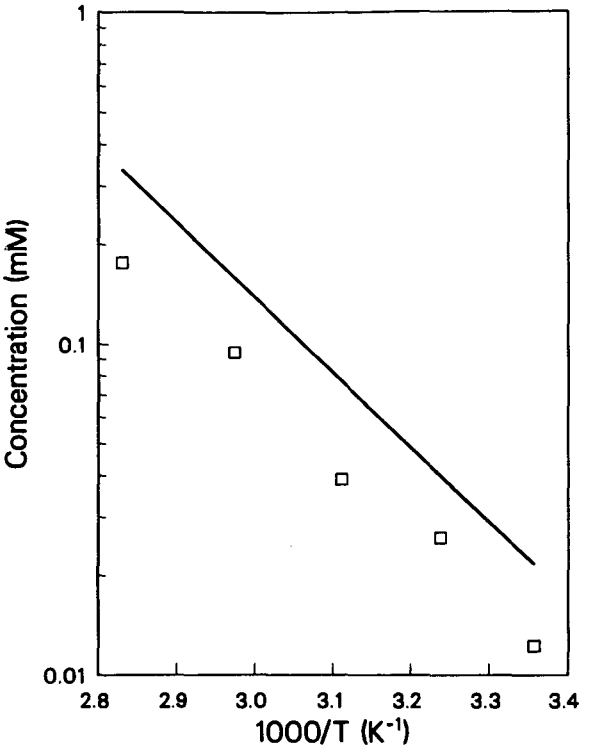

Figure 3. Active species concentration in 1M Na_2S_4 at pH = 12: □ calculated from diffusion parameter; ____ calculated from Ref. 25. (XCG 861-7035)

equilibrium data,[25] and the line in Fig. 3 shows the concentration of supersulfide as a function of temperature. There is good agreement between the calculated concentration of supersulfide and the experimentally obtained concentrations, which suggests that supersulfide is the electrochemically active species.

The deviations between the fit to the analytical form of the current-time transient and the experimental data can now be understood. At lower temperatures, and for the time scales considered here, very little conversion of tetrasulfide to supersulfide takes place (low rate of reaction and thin boundary layers), so it is the supersulfide initially present that determines the response. As the temperature increases, the forward rate of Reaction 2 becomes a significant factor, but at low overpotentials it is not the sole rate-determining step. One of the assumptions made in deriving the analytical form of the current time transient[23] is that there is only one rate-determining step; this assumption is violated here, which explains the deviation between experiment and theory.

The correct form of the material balances and boundary conditions for an electrode reaction with two steps that occur at comparable rates, at least one

of which is homogeneous, were formulated.[26] The nonlinear partial differential equations were solved numerically using a VAX 8600 computer, and comparison of experimental data and model predictions is shown in Fig. 4. The agreement is excellent, and the derived dimerization rate constant agrees with that determined for other radical anion reactions.[27] The exchange current densities are the order of 1 mA/cm^2 and are significantly higher than those previously reported.[28]

Steady-state data are needed to evaluate performance of candidate electrocatalysts. Before constructing a porous redox electrode we need to estimate the ratio of true to projected area needed and the appropriate hydrodynamic conditions for operation. The rotating disk electrode was chosen for these evaluations because it can be polished to a reproducible surface and can be operated under well-known hydrodynamic conditions. It was found that at 77°C a current of about 3 mA/cm^2 could be sustained on smooth cobalt electrode at 50 mV polarization and a rotation rate of 1000 rpm. Our preliminary design goals[19] should then require a ratio of true to projected area of about 4, under these hydrodynamic and temperature conditions.

In aprotic, organic solvents containing C=O, S=O and P=O structural units, the equilibrium of Reaction 2 is shifted to the right,[29,30] and the resulting increase in supersulfide concentration would be expected to improve electrode reaction rates. A previous study using N,N-dimethylformamide (DMF) showed that as it was added to an aqueous polysulfide solution, supersulfide was produced at the expense of tetrasulfide.[31] Current-voltage curves for a water-DMF and pure aqueous polysulfide solutions were recorded at cobalt and platinum electrodes. Figure 5 shows a comparison of the responses. Addition of DMF increases the current density by over 100% at the same temperature and total overpotential.[32,33]

Porous flow-through electrodes fabricated from screens could achieve the ratio of true to projected area and hydrodynamic boundary layer thicknesses with only small parasitic power losses. A cell and flow system for evaluating screen electrode performance has been constructed. We plan to test screens fabricated from several metals and metal sulfides as well as aqueous solutions containing organic cosolvents.

PLANNED ACTIVITIES FOR FY 1986

Continuing research efforts on secondary alkaline zinc electrodes will focus on the application of *in-situ*

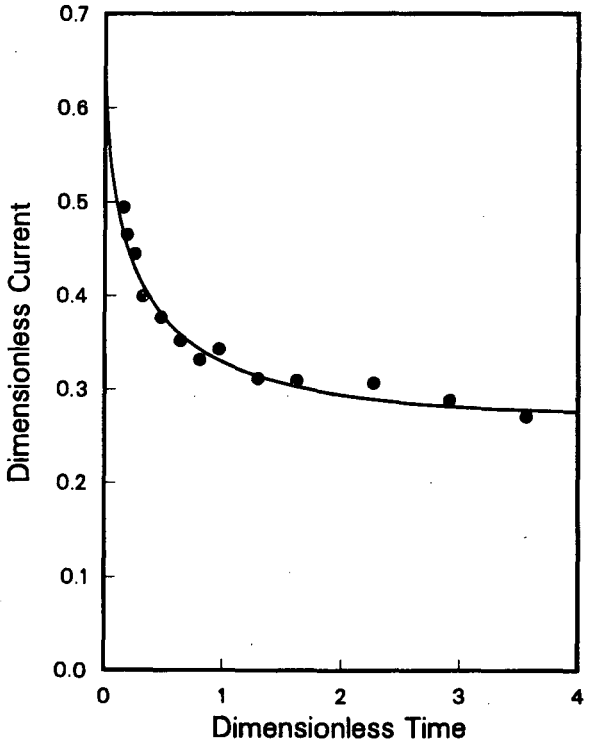

Figure 4. −20.1 mV step at 80.4 °C: • experimental data; ___ calculated response with k_f = 0.15 sec^{-1}. (XCG 861-7036)

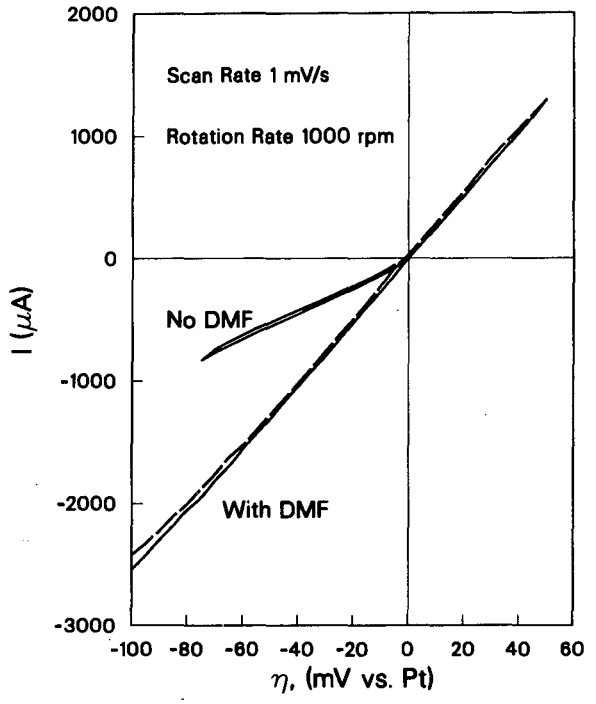

Figure 5. Addition of DMF to a 1M Na_2S_4 aqueous solution; response at a 0.2 cm^2 Co electrode, 77°C. (XCG 861-7037)

microelectrode potential measurements to determine electrolyte species concentrations in operating zinc electrodes; the development of a comprehensive mathematical model and complementary testing of Zn/NiOOH cells to verify the model; the performance of cycle-life experiments to complement mathematical analysis of zinc-electrode current collection; the evaluation of optimized pulsed-current charging regimes with electrolyte and electrode formulations that exhibit reduced zinc-species solubility; and the microscopic study of model zinc electrodes.

High-temperature alkali metal/sulfur cell studies will include measurement of capillary pressures in sulfur electrodes; mathematical modeling of the sulfur electrode and complementary operation of Na/S cells; and a thermodynamic stability analysis of solid electrolytes for use in Li/S cells.

Research on advanced electrolytes for fuel cells will include the fabrication of porous gas diffusion electrodes to test the performance of alkaline-carbonate electrolytes. Advanced electrocatalysts will be evaluated in sulfur/polysulfide redox electrolytes.

REFERENCES

1. Dirkse, T.P. (1954), "The Nature of the Zinc-Containing Ion in Strongly Alkaline Solutions," *J. Electrochem. Soc. 101*, p. 328.
2. Hampson, N.A., Herdman, G.A., and Taylor, R. (1970), "Some Kinetic and Thermodynamic Studies of the System Zn/Zn(II), OH^{2-}," *J. Electroanal. Chem. 25*, p. 9.
3. Nichols, J.T., McLarnon, F.R., and Cairns, E.J. (1985), "Zinc Electrode Cycle-Life Performance in Alkaline Electrolytes Having Reduced Zinc Species Solubility," *Chem. Eng. Commun. 37*, p. 355.
4. Katz, M.H., McLarnon, F.R., and Cairns, E.J. (1982), "Computer Control of Electrochemical Experiments with Application to Zinc/Nickel Oxide Cells," LBL-15546.
5. Wagner, O.C. and Almerini, A. (1984), *Proc. 31st Power Sources Symp.*, The Electrochemical Society, Pennington, NJ, p. 255.
6. McBreen, J. (1972), "Zinc Electrode Shape Change in Secondary Cells," *J. Electrochem. Soc. 119*, p. 1620.
7. Choi, K.W., Bennion, D.N., and Newman, J. (1976), "Engineering Analysis of Shape Change in Zinc Secondary Electrodes. I. Theoretical," *J. Electrochem. Soc. 123*, p. 1616; "Engineering Analysis of Shape Change in Zinc Secondary Cells. II. Experimental," *ibid.*, p. 1628.
8. Sunu, W.C. and Bennion, D.N. (1980), "Transient and Failure Analysis of the Porous Zinc Electrode. I. Theoretical," *J. Electrochem. Soc. 127*, p. 2007; "Transient and Failure Analyses of the Porous Zinc Electrode. II. Experimental," *ibid.*, p. 2017.
9. Jacquelin, J. and Pompon, J.P. (1979), "A Mathematical Model of the Behaviour of the Molten Sodium Polysulfide Electrode," in *Power Sources*, Vol. 7, p. 713, J. Thompson, Ed., Academic Press, London.
10. Breiter, M.W. and Dunn, B. (1979), "Potential Distribution Model for Rechargeable Sulphur-Electrodes in Sodium-Sulfur Cells," *J. Appl. Electrochem. 9*, p. 291.
11. Smith, M.L., McLarnon, F.R., and Cairns, E.J. (1985), "Investigation of a Vitreous Electrolyte for Use in Lithium/Sulfur Cells," LBL-20737.
12. Button, D.P., Tandon, R.P., Tuller, H.L., and Uhlmann, D.R. (1981), "Fast Lithium-Ion Conduction in Chloroborate Glasses. II. Diborates and Metaborates," *J. Solid State Ionics 5*, p. 655.
13. Sharma, R.A. (1972), "Equilibrium Phases in the Lithium-Sulfur System," *J. Electrochem. Soc. 119*, p. 1439.
14. Striebel, K.A., McLarnon, F.R., and Cairns, E.J. (1985), "The Effect of Carbonate Ions on the Reduction of Oxygen at Platinum Electrodes in Dilute Alkaline Electrolytes," 167th Meeting of the Electrochemical Society, Toronto, Canada, Paper No. 410.
15. Applied Science Division (1985), Annual Report for FY 1984, LBL-18750, pp. 1-40 to 1-44.
16. Ellis, A.B., Kaiser, S.W., Bolts, J.M., and Wrighton, M.S. (1977), "Study of n-type Semiconducting Cadmium Chalcogenide-Based Photoelectrochemical Cells Employing Polychalcogenide Electrolytes," *J. Am. Chem. Soc. 99*, p. 2839.
17. Russak, M.A. and Creter, C. (1984), "Vacuum Evaporated $CdSe_{1-x}Te_x$ Thin Films for Electrochemical Photovoltaic Cells," *J. Electrochem. Soc. 131*, p. 556.
18. Licht S., *et al.* (1985), "High Efficiency n-Cd(Se,Te)/$S^{=}$ Photoelectrochemical Cell Result- ing From Solution Chemistry Control," *Appl. Phys. Lett. 46*, p. 608.
19. Lessner, P., Winnick, J., McLarnon, F.R., and Cairns, E.J. (1985), "Porous Counterelectrodes For Aqueous Polysulfide Photoelectrochemical Cells," 167th Meeting of the Electrochemical

Society, Toronto, Canada, Paper #666.
20. Lessner, P., Winnick, J., McLarnon, F.R., and Cairns, E.J. (1985), "Electrode Kinetics in Aqueous Polysulfide Electrolytes: Transient Experiments," LBL-20603, submitted to The Electrochemical Society for the Boston, MA, Meeting, May 1986.
21. Lessner, P., Winnick, J., McLarnon, F.R., and Cairns, E.J. (1986), "Kinetics of Aqueous Polysulfide Solutions: Part II. Electrochemical Measurement of the Rates of Coupled Electrochemical and Chemical Reactions by the Potential Step Method," LBL-20990, submitted to *J. Electrochem. Soc.*
22. Nagy, Z. (1980), "On The Theory of the Potential and Voltage Step Relaxation Techniques for the Investigation of Fast Electrode Reactions," *Electrochim. Acta 25*, p. 575.
23. Nagy, Z. (1982), "Error Analysis of the Potential and Voltage Step Relaxation Technique for the Measurement of Kinetics of Electrode Reactions," *J. Electrochem. Soc. 129*, p. 1943.
24. More, J.J., Garbow, B.S., and Hillstrom, K.E. (1980), Argonne National Laboratory Report ANL-80-74.
25. Giggenbach, W. (1971), "The Blue Solutions of Sulfur in Water at Elevated Temperatures," *Inorg. Chem. 10*, p. 1306.
26. Lessner, P., Winnick, J., McLarnon, F.R., and Cairns, E.J. (1986), "Kinetics of Aqueous Polysulfide Solutions: Part I. Theory of Coupled Electrochemical and Chemical Reactions, Response to a Potential Step," LBL-20989, submitted to *J. Electrochem. Soc.*
27. O'Reilly, J.E. and Elving, P.J. (1971), "Electrochemical Reductions of Pyrimidine in Acetonitrile. Behavior of the Anion Free Radical," *J. Am. Chem. Soc. 93*, p. 1871.
28. Allen, P.L. and Hickling, A. (1957), "Electrochemistry of Sulfur: Part 1. Overpotential in the Discharge of the Sulfide Ion," *Trans. Faraday Soc. 53*, p. 1626.
29. Rauh, R.D., Shuker, F.S., Marston, J.M., and Brummer, S.B. (1977), "Formation of Lithium Polysulfides in Aprotic Media," *J. Inorg. Nucl. Chem. 39*, p. 1761.
30. Abraham, K.M., Rauh, R.D., and Brummer, S.B. (1978), "A Low Temperature Na-S Battery Incorporating a Soluble S Cathode," *Electrochim. Acta. 23*, p. 501.
31. Giggenbach, W. (1968), "On the Nature of the Blue Solutions of Sulfur," *J. Inorg. Nucl. Chem. 30*, p. 3189.
32. Lessner, P., Winnick, J., McLarnon, F.R., and Cairns, E.J. (1985), "Addition of DMF to Aqueous Polysulfide Electrolytes: Response at Co and Pt RDE," LBL-20604, submitted to The Electrochemical Society for Boston Meeting, May 1986.
33. Pfeiffer, C.R. (1985), "Improved Aqueous Polysulfide Redox System Utilizing an Organic Cosolvent—Philip M. Lessner, Frank R. McLarnon, Elton J. Cairns and Jack Winnick," DOE Case No. IB-620.

ADVANCED THERMAL ENERGY STORAGE RESEARCH

Solid-State Radiative Heat Pump*

P. Berdahl, K. Ghaffari, G. Ng, and L. Shaffer

The purpose of this research is to establish the research basis for the development of a new class of heat pump. This new heat pump would be a solid-state device that accepts input energy in the form of electricity and pumps infrared (heat) radiation across a thermally insulating gap. An important potential application is the cooling of buildings, in conjunction with thermal storage.

Semiconductor materials with direct narrow bandgaps in the range of 0.03–0.25 eV emit equilibrium thermal radiation which is in large part due to electron-hole recombination. An excess or deficit of infrared radiation, compared to the thermal equilibrium value, can be produced when the concentrations of electrons and holes are varied from their thermal equilibrium values by electrical means. Two techniques for varying the concentrations of electrons and holes are of special interest here: (1) electrical bias of a p-n junction to produce carrier injection or, for reverse bias, carrier extraction; (2) the magneto-concentration effect in which orthogonal electric and magnetic fields are used to enhance (or deplete) the concentrations of electrons and holes near the semiconductor's surface. The p-n junction technique seems particularly promising for the development of technologically mature devices, while the magneto-concentration effect offers the opportunity for the study of key recombination phenomena in a simpler experimental system.

ACCOMPLISHMENTS DURING FY 1985

The primary line of research was the construction of the Galvano-Magnetic Luminescence (GML) spectrometer, its first application to determine the GML spectrum of indium antimonide, and the theoretical interpretation of this data to give new measurements of the room temperature carrier lifetime of InSb. Also, experimental work was started toward the explicit demonstration of a continuous cooling effect.

The GML phenomenon is the departure from the equilibrium luminescence emitted by an object in the presence of mutually orthogonal electric and magnetic fields, both parallel to the emitting surface. The new instrument for GML measurements consists of an oscillator and power amplifier to produce an alternating electric field in the sample, a laboratory electromagnet for producing a static magnetic field, and a sensitive synchronous detection scheme to measure the quantity and spectrum of infrared radiation which varies in synchronism with the alternating electric field. The optical portion of the detection system consists of several mirrors, a grating monochromator, and a liquid nitrogen cooled $Hg_{1-x}Cd_xTe$ photoconductive infrared detector. The optical system is calibrated by replacing the sample by a heated blackbody source, modulated with a mechanical chopper. The GML spectrum of intrinsic (pure) InSb obtained with the new spectrometer is shown in Fig.1.[1] The solid dots are the experimental measurements; the theoretical curve will be discussed shortly. The integral of the spectrum is 3.5 W m^{-2} for the noted experimental conditions. This

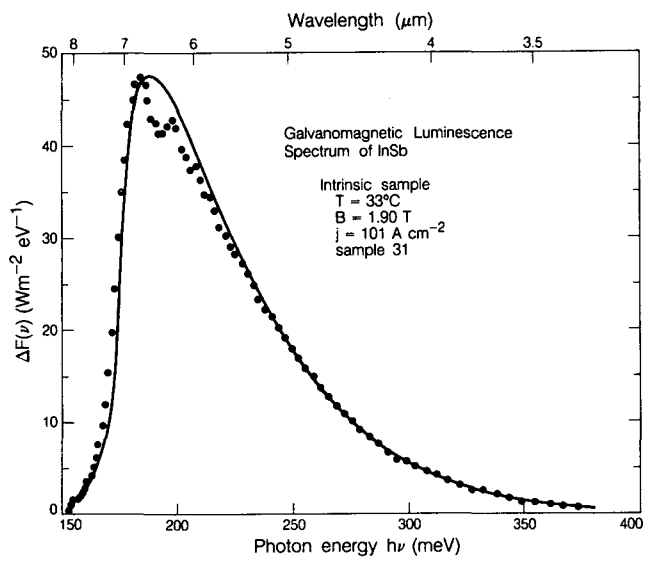

Figure 1. Measured and computed spectra of galvanomagnetic luminescence from intrinsic InSb. The sample thickness is 0.36 mm. The structure in the data near the peak is an artifact due to water vapor in the optical path. (XBL 854-9949)

*This work was supported by the Assistant Secretary for Conservation and Renewable Energy, Office of Energy Storage and Distribution of the U.S. Department of Energy under Contract No. DE-AC03-76SF00098.

radiant heat flow is pumped into and out of the sample alternately, at the 2 kHz frequency of the exciting field.

Prior observations of the GML phenomenon with InSb have been made in Russia[2,3] and Japan.[4] However our measurements have resolved the line shape under conditions of low excitation (carrier concentrations not greatly different from equilibrium values) and are calibrated in absolute units. These facts make it particularly interesting to compare the data with a theoretical calculation. This calculation[1] proceeds by solving the transport equations for electrons and holes in crossed electric and magnetic fields to determine the rate at which these carriers approach the free surface. The carriers accumulate at the surface and recombine radiatively (producing photons) or non-radiatively. Each emitted photon then has a certain probability to avoid reabsorption and reflection at the crystal surface and to emerge from the crystal. For the opposite polarity of the electric field, carriers are withdrawn from the crystal surface, producing a deficit of infrared emission (compared to thermal equilibrium conditions), a phenomenon sometimes termed negative luminescence. The theoretical result for the modulated radiant energy flux per unit photon energy is

$$\Delta F(\nu) = \qquad (1)$$

$$\frac{8N}{(N+1)^2}\,\tau\left(\frac{\pi b(\nu)}{L+\alpha^{-1}(\nu)}\right)\left(\frac{\mu_e\mu_h B}{\mu_e+\mu_h}\right)\left(\frac{j}{qn_o}\right),$$

where N is the index of refraction, τ is the excess carrier lifetime, $b(\nu)$ is the Planck blackbody spectrum per unit solid angle per unit photon energy, $\alpha(\nu)$ is the equilibrium optical absorption coefficient, L is the effective ambipolar diffusion length (a quantity known in terms of the other parameters),[1] μ_e and μ_h are the electron and hole mobilities, B is the magnetic field (z-direction), q is the electron charge, n_o is the intrinsic carrier concentration, and j is the current density (x-direction). The photon energy is $h\nu$, where h is Planck's constant. The crystal surface is in the y = 0 plane, and the emission occurs across this plane in the negative y-direction. Since all the parameters in Eq.(1) are known except the carrier lifetime τ, this lifetime can be determined by fitting the expression (1) to the data. This fit is shown as the continuous curve in Fig. 1. The resulting value of τ is 12 ns. Thus GML measurements provide a new technique for the determination of carrier lifetimes in semiconductors.

The GML measurements show directly how well a GML solid-state radiative heat pump works. However, the deduction of carrier lifetimes from the GML measurements makes it possible to evaluate materials also as parts of other types of solid-state radiative heat pumps, such as the large-area junction types which will require no magnetic field. For any radiant heat pump the quantum efficiency η_q, which is the probability that an excess electron-hole pair will produce a photon, is the key materials parameter. It is given by the relation $\eta_q = \tau/\tau_r$, where τ_r is the radiative lifetime, a quantity which can easily be computed from optical absorption data. For intrinsic InSb the radiative lifetime (at 33°C) is 580 ns; and, thus, the quantum efficiency is 2%. The eventual development of high efficiency heat pumps, with, say, 50% of the Carnot coefficient of performance, will require a correspondingly high efficiency for radiative recombination. GML spectroscopy accompanied by quantitative spectral analysis is a new tool for understanding how η_q varies with parameters such as temperature and doping and to identify materials which may have suitably high values of η_q.

GML measurements were also performed on p-type InSb. This material has cadmium (about 50 ppm) present as a dopant. The luminescence is qualitatively different from that of pure InSb. There is less luminescence at room temperature, but the intensity of the luminescence increases rapidly with increasing current (and, presumably, with increasing temperature). This behavior is not yet understood. Other features of the measurements, also different from pure InSb, are that the intensity is a nonlinear function of magnetic field, and that the spectrum of emission extends into the "forbidden" energy gap. This feature is of particular interest because of the relatively small number of materials with small energy gaps.

Another activity was experimental work designed to explicitly show a continuous (nonalternating) cooling effect in a vacuum, using a thin crystal in orthogonal electric and magnetic fields. A schematic diagram of the experimental device is shown in Fig. 2. Sample fabrication is proving to be challenging. One requires single crystals with an area of 1 cm^2 which are preferably only a few microns thick.

PLANNED ACTIVITIES FOR FY 1986

Successful completion of the continuous cooling experiment is a key goal. It is intended to produce a small (about 1 mW) cooling effect, to be detected by a thermocouple. This cooling effect may be masked by parasitic heating effects, in which case its existence will be demonstrated by showing that

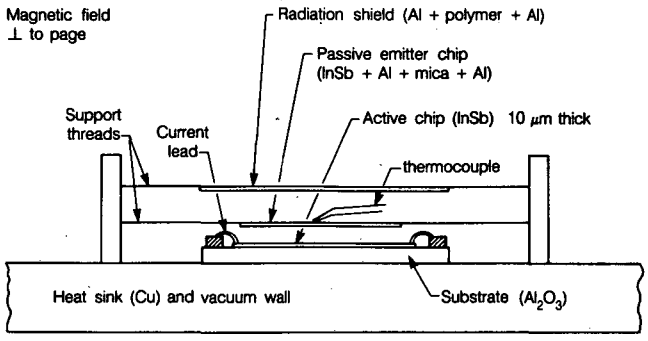

Figure 2. Diagram of the apparatus for the continuous cooling effect experiment. (XBL 859-10788)

reversal of a magnetic field, while maintaining constant electric power input, causes the thermocouple's temperature to decrease. Observation of this cooling effect will confirm the theoretical expectation that galvanomagnetic luminescent devices can function as cooling devices, and increase confidence that future p-n junction solid-state radiative heat pumps will also be capable of producing cooling.

The GML measurements will be continued on InSb, and extended to cover a larger range of temperature and doping concentrations. The preparation of thinner samples will enhance signal-to-noise levels because higher current densities can be employed. These measurements will culminate in a comprehensive paper on the galvanomagnetic luminescence of indium antimonide. Also, GML measurements will be initiated with one of the narrow-bandgap lead salts, probably $Pb_{1-x}Sn_xTe$. Due to qualitatively distinct band structure, the parasitic Auger recombination mechanism which shortens the carrier lifetimes in InSb may be less important. Finally, theoretical calculations in support of the experimental work will continue.

REFERENCES

1. Berdahl, P., and Shaffer, L. (1985), *Appl. Phys. Lett. 47,* p. 1330.
2. Ivanov-Omskii, V.I., Kolomiets, B.T., and Smirnov, V.A. (1965), *Sov. Phys. Dokl. 10,* p. 345.
3. Bolgov, S.S., Malyutenko, V.K., and Pipa, V.I. (1979), *Sov. Tech. Phys. Lett. 5,* p. 610.
4. Morimoto, T. and Chiba, M. (1981), *Phys. Lett. A85,* p. 395.

Thermochemical Energy Conversion and Storage by Direct Solar Heating*

A.J. Hunt, J. Ayer, and R. Otto

The objective of this research is to investigate the use of concentrated solar energy to drive the endothermic portion of a thermochemical energy storage cycle. A thermochemical cycle provides a means to store energy collected by a solar thermal power plant on clear days and to produce electricity during the night or on cloudy days. The cycle consists of two steps: (1) an endothermic step in which energy is supplied to dissociate the gas and (2) an exothermic step in which the products of decomposition are combined over a catalyst to release heat energy at high temperatures. The heat can be used to operate a turbine or for industrial processes.

In particular, we are investigating the decomposition reaction of gases adsorbed on the surface of small particles that act both as the solar absorber and catalyst. This is an application of the direct-flux small-particle solar reactor known as the STARR (Solar Thermally Activated Radiant Reactor), described in the Solar Energy Program chapter of the Annual Report. The STARR uses a suspension of small particles (diameter less than 1 μm) as the solar absorber, heat exchanger, and in this case, catalyst for the reaction. The advantages of using small particles for this application are: (1) they are excellent absorbers of sunlight, (2) only a small mass of particles is required, (3) the small particle size provides a large surface area per gram of material, which greatly enhances catalysis of a gas phase reaction, (4) small particles can rapidly heat the surrounding gas to a high temperature, (5) the overall system efficiency is high because direct absorption eliminates the need for conventional heat exchangers. and (6) if the particles act as photocatalytic sites the reaction can take place at temperatures below that required for equilibrium dissociation.

*This work was supported by the Assistant Secretary for Conservation and Renewable Energy, Office of Systems Research, Energy Storage Division of the U.S. Department of Energy under Contract No. DE-AC03-76SF00098.

ACCOMPLISHMENTS DURING FY 1985

The decomposition reaction of SO_3 was chosen to investigate the feasibility of the STARR concept for thermochemical energy storage for several reasons: SO_3 has a very large endothermic enthalpy of dissociation, both SO_3 and SO_2 (the product of the dissociation reaction) can be stored as liquids near ambient temperatures; the thermodynamic process of dissociation is well known;[1] and there are extensive evaluations of thermochemical storage cycles using this reaction.[2,3]

Hematite (Fe_2O_3) particles were chosen for the absorber and catalyst for the experimental research for several reasons. First, it is an established catalyst for SO_3 dissociation. Second, small particles of hematite are excellent solar absorbers. In addition to heating the gas and acting as a dissociation site, hematite also has the proper characteristics to initiate photocatalytic dissociation of SO_3.

Theory

Figure 1 illustrates the equilibrium fraction of SO_3 dissociated versus temperature at a total constant pressure of 1 atmosphere. Starting from pure SO_3, the percent of SO_3 dissociated cannot exceed the thermodynamic limit at that temperature and therefore must lie on or below the curve in the shaded region. The experimental results obtained by Rocket Research Co. using Fe_2O_3 are plotted in Fig. 1, and it can be seen that they fall below the equilibrium concentrations.[1] In the STARR concept, small particles of hematite are entrained in the SO_3 gas and injected into a reactor with a transparent window. The particles absorb sunlight and act as the sites for the catalytic decomposition. Because the particles are (1) hotter than the gas, and (2) the molecular transport to and from their surface is not hindered by a substrate, they should be more effective than conventional catalysts.

In addition to improved performance due to the nature of the heat and mass transfer processes in STARR, photo processes may also play a role. It is possible to photodissociate SO_3 at ambient temperatures using near UV light. In this case, the degree of dissociation may be maintained *above* the equilibrium value if the photon flux is sufficient to overcome the thermal reaction rates tending toward equilibrium (see Fig. 1). The SO_3 molecule absorbs a UV photon directly to initiate this process. Solar photons contain sufficient energy to dissociate SO_3 since the enthalpy of dissociation is 23 kcal/mole, or 1.0 eV/molecule, an energy well below the peak of the solar spectrum. However, SO_3 is not absorbing at most solar wavelengths. Photodissociation can occur if there is a way to transfer the energy from solar photons to the SO_3 molecule. If it can be accomplished, a degree of dissociation exceeding that of the equilibrium value at a given temperature can be

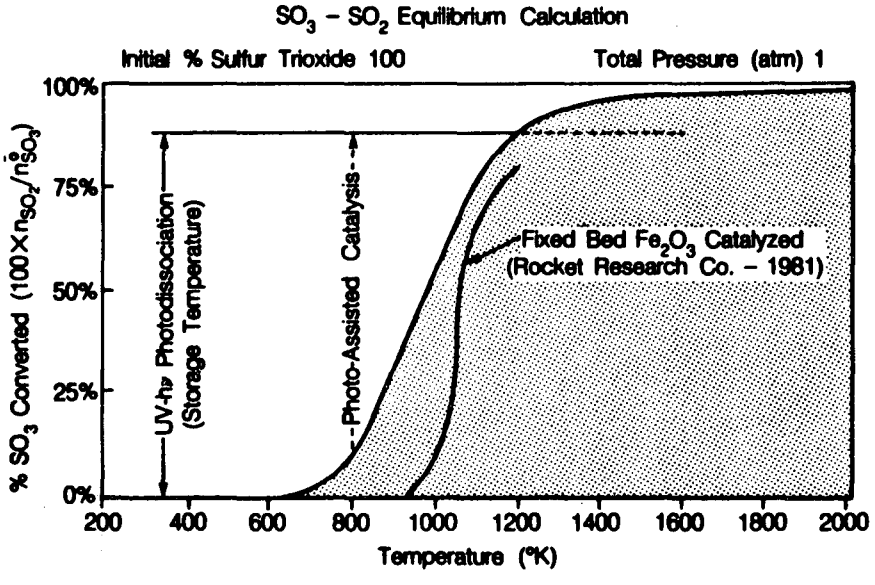

Figure 1. Equilibrium dissociation yields and photothermal pathways for SO_3 dissociation. (XBL 853-1888A)

achieved. Thus, a SO_2/SO_3 storage system directly utilizing solar photons can operate at a lower temperature and higher efficiency than one based on thermodynamic equilibrium.

Several mechanisms for photodissociation are possible because of the presence of the absorbing particles. Reduced sites may be produced on the surface of the Fe_2O_3 particles by photodissociation of the hematite as is illustrated in Fig. 2. Upon contact with SO_3, these sites regain the lost oxygen atom, thereby releasing SO_2. This mechanism is consistent with that proposed by Rocket Research.[1] Another coupling mechanism is the production of electron-hole pairs by photoabsorption in a semiconducting particle and their subsequent transport to the particle surface. The photoproduced charges reach the surface and react with adsorbed SO_3 molecules in a combined oxidation-reduction reaction to initiate dissociation. Hematite particles are good candidates for this process because they have semiconductor properties and a bandgap (2.2 eV) well within the solar spectrum.

Experimental System

An experimental system was designed and built to study the dissociation of SO_3 as a function of temperature and radiant flux density. The apparatus has

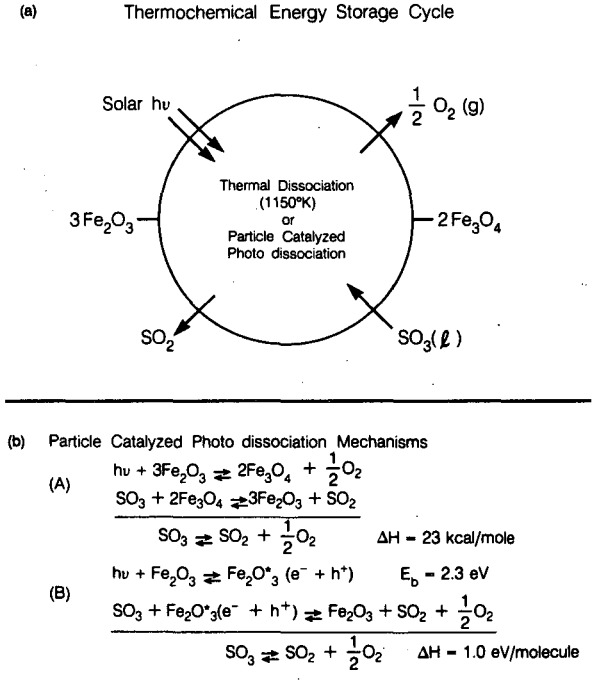

Figure 2. A conceptualization of a storage cycle for a solar thermally activated radiant receiver using small particles as heat exchanger and catalyst. (XBL 865-11120)

two principal components, the SO_3 transfer system and the radiant reactor. These components are described below.

Because SO_3 is an extremely reactive and toxic compound, great care was taken to build a transfer apparatus that is both safe and easy to use in a laboratory environment. Small containers of SO_3 (100 grams) were received in the form of sealed pyrex vials which, once opened, cannot be resealed. However, because only a small amount of SO_3 is required for each run, a method to transfer small quantities of SO_3 was developed. After opening, the glass SO_3 vial is placed in a resealable stainless steel container equipped with vacuum valve. The valve is attached to the transfer system and is hand controlled to allow small quantities of SO_3 vapor to be transferred into the reactor. The container is airtight to avoid contact of SO_3 with water vapor, since this will result in the rapid exothermic production of corrosive sulfuric acid. The design of the transfer system has several unique features. The apparatus was built completely from stainless steel, teflon, quartz, and pyrex because SO_3 does not react with these materials. The system is evacuated so that only pure SO_3 is transferred into the reacting chamber. Because SO_3 condenses at 41°C, the entire transfer system is maintained above this temperature to keep the SO_3 from condensing in the transfer lines. A schematic diagram of the apparatus is given in Fig. 3.

The function of the reactor is to provide an environment to study the dissociation of SO_3 under either isothermal conditions or when subjected to a combination of thermal heating and simulated concentrated solar flux. The reactor (Fig. 4) must be transparent to allow radiant energy to enter and interact with the gas and particles. It must hold a vacuum while connected to the transfer apparatus, and seal completely when removed from it. For the initial experiments the particles are not entrained in the gas but are distributed on a quartz disk suspended in the reaction zone. The particles are widely spaced to simulate a particle-gas suspension. The gas in the reaction zone can be sampled while the reaction is occurring by the use of an argon purge system.

The reaction temperature must be measured to determine the degree of dissociation of the SO_3. Accurate measurement of the temperature in the reaction zone is difficult for several reasons. Because of the corrosive environment, thermocouple wire may be corroded. Measuring temperatures in a radiant environment is difficult because a thermocouple will absorb incident radiation and heat, thus giving

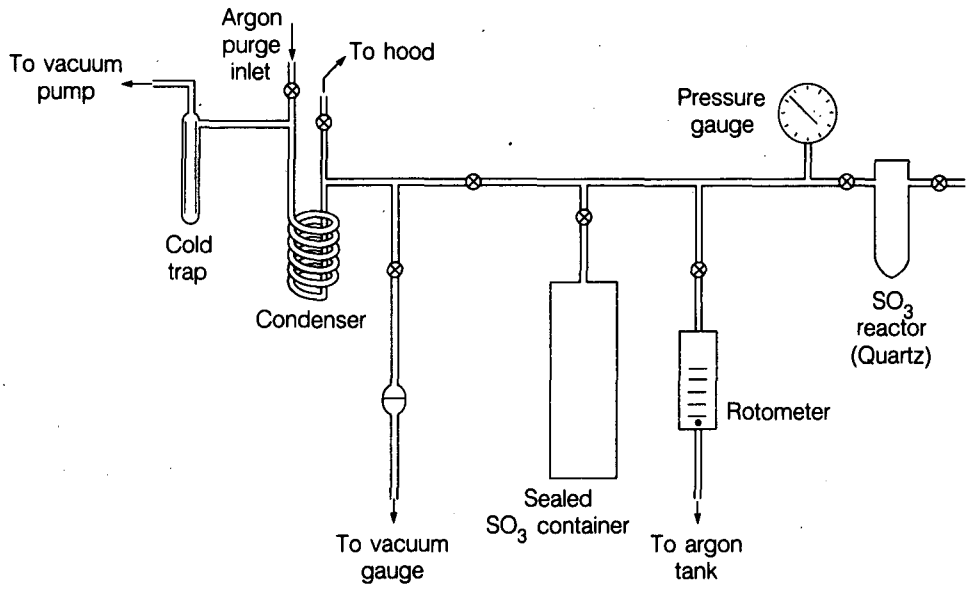

Figure 3. The SO_3 transfer system. (XBL 861-9707)

inaccurate results. Optical pyrometers will not give reliable measurements because of the intense radiant flux in the reactor zone. Given these limitations, it was decided that the temperature in the reactor would be measured with an insulated thermocouple separated from the reactor zone by a thin quartz plate. It is not subjected to the most intense radiant flux because it is beyond the focus and partly shielded by the particles on the quartz disk (see Fig. 4). The radiant source for this experiment is a 2.2 kW xenon arc lamp that provides a peak light intensity of 2600 kW/m^2 at the focus. The lamp has a spectrum similar to the solar spectrum and is filtered to remove the UV.

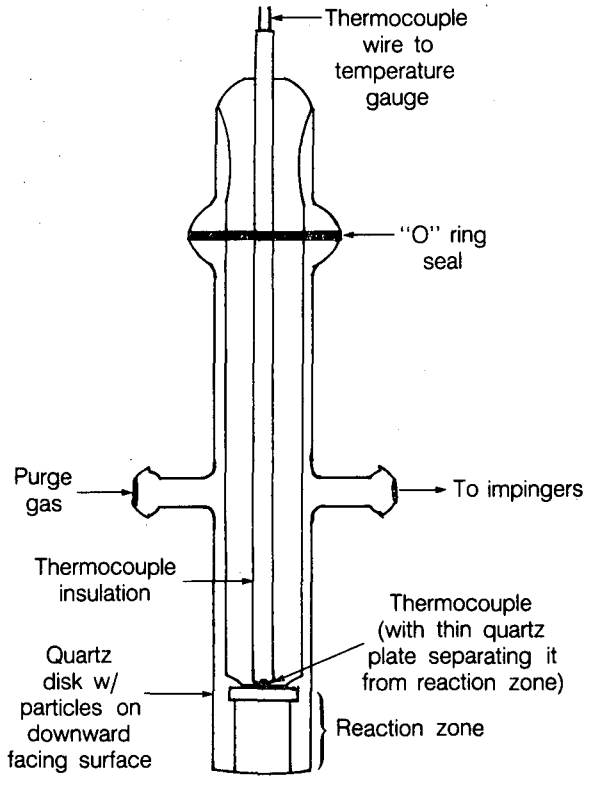

Figure 4. Conceptualization of a small particle radiant reactor. (XBL 861-9708)

PLANNED ACTIVITIES FOR FY 1986

During FY 1986, the SO_3 dissociation experiments will be carried out. There are two phases to each experiment. The first phase is the dark reaction. In this step, the reactor is held at temperature until equilibrium is attained, and a small amount of gas is sampled. In the second phase, known as the light-on phase, the lamp is turned maintained at the same temperature as before, and the gas is again sampled. The SO_2/SO_3 gas stream passes through an aqueous bubbler solution containing formaldehyde to quench the dissociation reaction and preserve the bisulfite ion. Relative amounts of SO_2 and SO_3 in the solution will be measured using ion chromatography, and the light reaction and dark reaction will be compared. If photoassisted catalysis occurs, the SO_2/SO_3 ratio will be greater in the light reaction than in the dark reaction at the same temperature.

REFERENCES

1. Schmidt, E.W., *et al.* (1980), *Development of a Long-Life High-Temperature Catalyst for the SO_2/SO_3 Energy Storage System,* Rocket Research Co. Report RRC-80-R-697.
2. Chubb, T.A. (1974), "Analysis of Gas Dissociation Solar Thermal Power System," *Solar Energy 17,* p. 129.
3. Dayan, J., Lynn, S., and Foss, A. (1979), "Evaluation of Sulfur Oxide Chemical Heat Storage Process for a Steam Solar Electric Plant," LBL-7864.

Constant-Volume Three-Phase Thermal Storage Module*

V.P. Carey

The overall objectives of this research are to demonstrate the feasibility of a new three-phase storage module concept and to experimentally examine the energy storage and heat transfer mechanisms of the module. This work will also aim to develop analytical models of the transport within the module. The results will be used to determine optimal module configurations, PCM materials, working fluids, and thermal control techniques for typical storage applications.

To assess the viability of the module concept and investigate thermal transport within it, a fully instrumented laboratory-scale module has been designed. In this prototype module, encapsulated Glauber's salt is used as the PCM, and R-11 fluorocarbon as the working fluid. This salt changes phase at 89°F. At this temperature, the vapor pressure of R-11 is about 19 psia, so the test module will operate at just above atmospheric pressure.

ACCOMPLISHMENTS DURING FY 1985

During 1985, the prototype thermal storage module was fabricated in the shop, instrumented, and testing was started. Compatibility studies indicated that the encapsulating resin used to make the pellets slowly breaks down when exposed to R-11. Consequently, testing with these pellets in the module could be conducted only for limited time periods.

Transient tests conducted in the spring of 1985 demonstrated the feasibility of the storage module concept. In addition to documenting the energy storage and retrieval modes, the heat transfer process during the heat input mode was studied in detail. The heat input process was observed to consist of three stages. During the initial stage of heat input, the temperature and pressure rise within the module, storing heat sensibly. When the temperature inside exceeds the melting temperature of the PCM by a slight amount, the PCM begins to melt and energy is stored in its latent heat. The temperature and pressure within the module remain about constant during this process. As initially hoped, this storage process is very efficient, requiring only a very small temperature difference to transfer the heat.

When the PCM is completely melted, the temperature and pressure in the module again begin to rise. An analytical model of the transient two-phase heat transfer during the input process when the PCM melts has also been developed. The predictions of this model agree well with the experimental results. This work is summarized in Ref. 1.

PLANNED ACTIVITIES FOR FY 1986

Further work is needed to experimentally determine the two-phase transport behavior during the heat extraction process, and to develop an analytical model for it. However, it appears that reduced funding support will make it impossible to achieve these objectives.

REFERENCES

1. Do, M.T. (1985), "An Experimental and Theoretical Study of Heat Transfer in a Constant-Volume Three-Phase Thermal Storage Module," M.S. Report, Department of Mechanical Engineering, Univ. of California at Berkeley.

*This work was supported by the Assistant Secretary for Conservation and Renewable Energy, Office of Energy Storage and Distribution of the U.S. Department of Energy under Contract No. DE-AC03-76SF00098.

LAWRENCE BERKELEY LABORATORY
TECHNICAL INFORMATION DEPARTMENT
UNIVERSITY OF CALIFORNIA
BERKELEY, CALIFORNIA 94720